

AMERICAN UNIVERSITY OF BEIRUT

MINIMAL MODEL OF ACTIVE MATTER WITH
ATTRACTION: PHASE BEHAVIOR AND
KINETICS

by
KAFA ABDALLAH ALAMEH

A thesis
submitted in partial fulfillment of the requirements
for the degree of Master of Science
to the Department of Physics
of the Faculty of Arts and Sciences
at the American University of Beirut

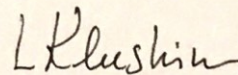
Beirut, Lebanon
July 2020

AMERICAN UNIVERSITY OF BEIRUT

MINIMAL MODEL OF ACTIVE MATTER WITH
ATTRACTION: PHASE BEHAVIOR AND
KINETICS

by
KAFA ABDALLAH ALAMEH

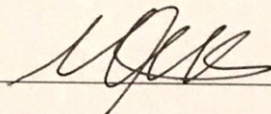
Approved by:



Dr. Leonid I. Klushin, Professor

Advisor

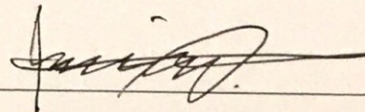
Physics



Dr. Michel J. Kazan, Associate Professor

Member of Committee

Physics



Dr. Jihad R. Touma, Professor

Member of Committee

Physics

Date of thesis defense: July 3, 2020

AMERICAN UNIVERSITY OF BEIRUT

THESIS, DISSERTATION, PROJECT RELEASE FORM

Student Name: Adameh Kafa Abdallah
Last First Middle

Master's Thesis Master's Project Doctoral Dissertation

I authorize the American University of Beirut to: (a) reproduce hard or electronic copies of my thesis, dissertation, or project; (b) include such copies in the archives and digital repositories of the University; and (c) make freely available such copies to third parties for research or educational purposes.

I authorize the American University of Beirut, to: (a) reproduce hard or electronic copies of it; (b) include such copies in the archives and digital repositories of the University; and (c) make freely available such copies to third parties for research or educational purposes after:

One ___ year from the date of submission of my thesis, dissertation or project.

Two ___ years from the date of submission of my thesis, dissertation or project.

Three ___ years from the date of submission of my thesis, dissertation or project.

Ap 7/7/2020
Signature Date

This form is signed when submitting the thesis, dissertation, or project to the University Libraries

Dedication

To my mother, brother, and uncle,
To my father, I wish you were here..

Acknowledgements

I would start by thanking my thesis advisor Prof. Leonid Klushin for embarking with me on this adventure of studying active matter. Countless hours were spent with him thinking and discussing these systems. I am thankful for his guidance, confidence to allow me to explore freely, and all the knowledge I acquired from our discussions.

A big thank your for my thesis committee members. Prof. Michel Kazan for always having his door open for us when we have a problem. You are a great graduate advisor. Most of my courses, on a graduate and undergraduate level, were taught by Prof. Jihad Touma. It goes without saying that I am grateful for being taught by him and inspired by his style of teaching.

I had constant support throughout my thesis work by the professors and staff in the Physics Department. I especially appreciate the support given by Prof. Khalil Bitar and Prof. Sara Najem. I would also like to thank our administrative officer Jumana Abi Falah for her support and always reminding me of important deadlines.

I am also thankful for my colleagues, in particular Rodrique Badr. I appreciate his help in shaping up my thesis with his comments on the numerics and algorithms involved in my work. Fruitful discussions with Carmen Al Masri and Wassim Sleiman are also appreciated.

I would also like to thank the support of my colleagues in the graduate room, especially Alaa Akkush, Nourhan Barakat, Marwa Dakik, Ghina Al Atat, Rola Dbouk, and Ahmad Lalti. Additionally, I want to thank my friends Saly El Wazze and Stephan. I am truly thankful for always having time to hear my nagging and for all the fun times we shared together.

Lastly, it goes without saying, that I am thankful for my family and parents for their unconditional support.

An Abstract of the Thesis of

Kafa Abdallah Alameh for Master of Science
Major: Physics

Title: Minimal Model of Active Matter with Attraction: Phase Behavior and Kinetics

Physicists' fascination of the phenomena of collective motion/behavior that we often see in nature on many scales (from fish to bacteria and down to intra-cellular units) has led to the emergence of the field of active matter. An active system is a collection of many interacting self-driven active particles capable of converting stored energy into systematic movement. They are out-of-equilibrium systems characterized by the interplay of noise, activity, and interactions which give rise to a wealth of novel phases. The simplest model consisting of self-propelled disks with purely repulsive interactions, exhibits surprising behavior; it phase separates into a dense fluid phase and a gas phase. This phenomena of phase separation in the absence of attractive interactions is termed motility-induced phase separation (MIPS). It is controlled by the Péclet number (Pe), which characterizes the persistence of self-propelled motion. Recent advances in understanding the novel phases of active matter are based on the concept of swim or active pressure that measures the strength of propulsive forces. Another contribution is termed passive pressure which measures the direct contribution of interaction forces. In this thesis, we add a layer of complexity by studying the phase behavior of active particles with attraction. When the attraction strength is much larger than the self-propulsion, this results in clustering of particles. We study the kinetics of cluster-cluster aggregation by measuring the time-evolution of the domain size and the number of particles in a cluster as a function of time. We identify three regimes: in the first low Pe regime attraction forces dominates leading to clustering. An intermediate regime in which neither of the two forces is strong enough to produce macroscopic phase separation. And a high Pe regime where phase separation is expected. Finally, we attempt at characterizing the reentrant behavior through a pressure equation of state calculation.

Contents

Dedication	v
Acknowledgements	vi
Abstract	vii
1 Introduction to Active Matter	1
1.1 What is Active Matter?	1
1.2 Examples of Active Matter	2
1.2.1 Biological Systems	2
1.2.1.1 Bacterial Suspensions	2
1.2.1.2 Cytoskeletal Filaments and Molecular Motors	2
1.2.2 Macroscopic Systems	4
1.2.2.1 Vibrated Granular Rods	4
1.2.2.2 Flocking of Birds	4
1.2.3 Synthetic Systems	5
1.3 Scope of Thesis	6
2 Passive vs. Active Matter - Phenomenological Differences	8
2.1 Passive Brownian Particles	8
2.2 Active Brownian Particles	10
2.2.1 Methods of Simulating Active Matter	10
2.2.1.1 Active Brownian Particles in a Solvent	10
2.2.1.2 Dry Active Matter	11
2.2.1.3 Interacting ABPs	12
2.2.2 Simple Simulation Approaches to Active Matter	13
2.2.2.1 Flocking Transition in the Vicsek Model	13
2.2.2.2 Motility Induced Phase Separation of Self-Propelled Disks	16
2.3 Towards a Statistical and Thermodynamic Description of Active Matter .	20
2.3.1 Temperature	20
2.3.2 Pressure	20
2.3.2.1 Stress in Active Matter: Swim Pressure	21
2.3.2.2 Phenomenological Hydrodynamic Description of Motility Induced Phase Separation	22
2.3.3 Chemical Potential	24
3 Attractive Active Brownian Particles	25
3.1 Introduction	25
3.2 Clustering and Kinetics	25

3.2.1	Model	25
3.2.2	Computational Approach Throughout the Thesis	28
3.2.3	Mean Squared Displacement	32
3.2.4	Giant Number Fluctuations	33
3.2.5	Long Time Behavior Configurations	35
3.2.6	Kinetics of Cluster-Cluster Aggregation	36
3.3	Reentrant Phase Behavior	41
3.3.1	Model	41
3.3.2	Attraction Strength = 0.005	43
3.3.3	Attraction Strength = 0.0025	43
3.3.4	Attraction Strength = 0.00125	43
3.3.5	Attraction Strength = 0.0008	43
3.3.6	Attraction Strength = 0.000625	43
3.3.7	Attraction Strength = 0.0005	43
4	Pressure of Active Matter	55
4.1	Introduction	55
4.2	Methods	56
4.2.1	Model: MIPS Revisited	56
4.2.2	Hydrodynamic Description	57
4.2.3	Generalized Pressure and Equation of State	59
4.3	Passive and Active Pressure	60
4.3.1	Linear Force	60
4.3.2	Lennard-Jones Potential	62
4.3.3	Adding Attraction	63
5	Conclusion	64
A	Abbreviations	65

List of Figures

1.1	Bacterial Suspension	3
1.2	a. Kinesin–streptavidin construct moving simultaneously along two microtubules. b. A self-organized aster observed by dark-field microscopy.	3
1.3	Giant number fluctuations in active granular rods	5
2.1	Schematic representation of an active particle	12
2.2	Schematic representation of the Vicsek model phase diagram	15
2.3	Snapshots of the Vicsek model in four regions of phase space. a. Homogeneous State b. Groups of particles moving coherently in random directions for small densities and noise. c. Particles moving randomly with some correlations at high densities and noise. d. Ordered motion at higher densities and small noise.	16
2.4	An active particle leaves a cluster after a time proportional to the reorientation time-scale	18
2.5	Snapshots of repulsive active particles. a. Homogeneous fluid at low self-propulsion speed below close packing. b. Phase separated state below close packing, consisting of high density liquid surrounded by a gas of active particles. c. Phase separated state above close packing, consisting of a hole filled by a gas of active particles surrounded by a high density liquid. d. Homogeneous liquid above close packing. e. Glassy phase.	19
3.1	Schematic representation of a self-propelled particle	26
3.2	A plot of the force of interaction between attractive active particles	27
3.3	Diagram summarizing the numerical integration algorithm	30
3.4	The Verlet list: particle i interacts with particles within the interaction radius r_c . The Verlet list contains all particles within a radius $r_v > r_c$	32
3.5	Mean square displacement for $\tilde{\nu}_r = 0.0005$, $\phi = 0.1$ for various values of Pe . The dashed lines correspond to the theoretical MSD that a single particle performs. At short time, the dashed lines correspond to slope of 2 (ballistic) and at large times, the dashed lines correspond to slope of 1 (diffusive).	33
3.6	Number fluctuations for $\tilde{\nu}_r = 0.0005$, $\tilde{\nu} = 0.1$ corresponding to $Pe = 200$, for various values of ϕ . The dashed lines correspond to slopes 1 (black) and 2 (red). Inset: the values of β obtained by the power-law fit $\Delta N^2(N_s) \sim N_s^\beta$ for the data at large N_s	34
3.7	Phase diagram of active particles as function of Péclet and packing fraction at t_f	35
3.8	Structure factor at tf for $\tilde{\nu}_r = 0.0005$, $\phi = 0.1$, and $Pe = 2$	37
3.9	Structure factor at tf for $\tilde{\nu}_r = 0.0005$, $\phi = 0.2$, and $Pe = 2$	37

3.10	Number of particles in a cluster as a function of time for $\tilde{\nu}_r = 0.0005$, $\phi = 0.2$, and $Pe = 8$. The dashed line corresponds to a slope of 0.5	38
3.11	Number of particles in a cluster as a function of time for $\tilde{\nu}_r = 0.0005$, $\phi = 0.2$, and $Pe = 10$. The dashed line corresponds to a slope of 0.5	38
3.12	Number of particles in a cluster as a function of time for $\tilde{\nu}_r = 0.0005$, $\phi = 0.2$, and $Pe = 20$. The dashed line corresponds to a slope of 0.5	39
3.13	Time-dependent domain length $\mathcal{L}(t)$ for $\tilde{\nu}_r = 0.0005$, $\phi = 0.1$, and $Pe = 100$. The dashed line corresponds to a slope of 0.25	40
3.14	Time-dependent domain length $\mathcal{L}(t)$ for $\tilde{\nu}_r = 0.0005$, $\phi = 0.2$, and $Pe = 100$. The dashed line corresponds to a slope of 0.25	41
3.15	Plot of the quadratic attractive force for various δ	42
3.16	Particles configurations corresponding to an Attraction Strength = 0.005, $\tilde{\nu}_r = 0.0005$ at t_f for several Péclet numbers.	44
3.17	Particles configurations corresponding to an Attraction Strength = 0.0025, $\tilde{\nu}_r = 0.0005$ at t_f for several Péclet numbers.	45
3.18	Number fluctuations for $\tilde{\nu}_r = 0.0005$ for various self-propulsion, for an Attraction Strength = 0.0025. The dashed lines correspond to slopes 1 (black) and 2 (red). Inset: the values of β obtained by the power-law fit $\Delta N^2(N_s) \sim N_s^\beta$ for the data at large N_s	46
3.19	Mean square displacement for $\tilde{\nu}_r = 0.0005$ for various self-propulsion, for an Attraction Strength = 0.0025. The dashed lines correspond to the theoretical MSD that a single particle performs. At short time, the dashed lines correspond to slope of 2 (ballistic) and at large times, the dashed lines correspond to slope of 1 (diffusive)	46
3.20	Particles configurations corresponding to an Attraction Strength = 0.00125, $\tilde{\nu}_r = 0.0005$ at t_f for several Péclet numbers.	47
3.21	Number fluctuations for $\tilde{\nu}_r = 0.0005$ for various self-propulsion, for an Attraction Strength = 0.00125. The dashed lines correspond to slopes 1 (black) and 2 (red). Inset: the values of β obtained by the power-law fit $\Delta N^2(N_s) \sim N_s^\beta$ for the data at large N_s	48
3.22	Mean square displacement for $\tilde{\nu}_r = 0.0005$ for various self-propulsion, for an Attraction Strength = 0.00125. The dashed lines correspond to the theoretical MSD that a single particle performs. At short time, the dashed lines correspond to slope of 2 (ballistic) and at large times, the dashed lines correspond to slope of 1 (diffusive)	48
3.23	Particles configurations corresponding to an Attraction Strength = 0.0008, $\tilde{\nu}_r = 0.0005$ at t_f for several Péclet numbers.	49
3.24	Number fluctuations for $\tilde{\nu}_r = 0.0005$ for various self-propulsion, for an Attraction Strength = 0.0008. The dashed lines correspond to slopes 1 (black) and 2 (red). Inset: the values of β obtained by the power-law fit $\Delta N^2(N_s) \sim N_s^\beta$ for the data at large N_s	50
3.25	Mean square displacement for $\tilde{\nu}_r = 0.0005$ for various self-propulsion, for an Attraction Strength = 0.0008. The dashed lines correspond to the theoretical MSD that a single particle performs. At short time, the dashed lines correspond to slope of 2 (ballistic) and at large times, the dashed lines correspond to slope of 1 (diffusive)	50
3.26	Particles configurations corresponding to an Attraction Strength = 0.000625, $\tilde{\nu}_r = 0.0005$ at t_f for several Péclet numbers.	51

3.27	Number fluctuations for $\tilde{\nu}_r = 0.0005$ for various self-propulsion, for an Attraction Strength = 0.000625. The dashed lines correspond to slopes 1 (black) and 2 (red). Inset: the values of β obtained by the power-law fit $\Delta N^2(N_s) \sim N_s^\beta$ for the data at large N_s	52
3.28	Mean square displacement for $\tilde{\nu}_r = 0.0005$ for various self-propulsion, for an Attraction Strength = 0.000625. The dashed lines correspond to the theoretical MSD that a single particle performs. At short time, the dashed lines correspond to slope of 2 (ballistic) and at large times, the dashed lines correspond to slope of 1 (diffusive)	52
3.29	Particles configurations corresponding to an Attraction Strength = 0.0005, $\tilde{\nu}_r = 0.0005$ at t_f for several Péclet numbers.	53
3.30	Number fluctuations for $\tilde{\nu}_r = 0.0005$ for various self-propulsion, for an Attraction Strength = 0.0005. The dashed lines correspond to slopes 1 (black) and 2 (red). Inset: the values of β obtained by the power-law fit $\Delta N^2(N_s) \sim N_s^\beta$ for the data at large N_s	54
3.31	Mean square displacement for $\tilde{\nu}_r = 0.0005$ for various self-propulsion, for an Attraction Strength = 0.0005. The dashed lines correspond to the theoretical MSD that a single particle performs. At short time, the dashed lines correspond to slope of 2 (ballistic) and at large times, the dashed lines correspond to slope of 1 (diffusive)	54
4.1	A plot of the potential and force of interaction given by LJ	57
4.2	Passive pressure for a fixed self-propulsion $v_0 = 0.2$ for two different rotational diffusion values $\tilde{\nu}_r = 0.02$ and $\tilde{\nu}_r = 0.01$ corresponding to $Pe = 10$ and $Pe = 20$, respectively. Solid lines are guide for the eye.	61
4.3	Active pressure at fixed $\tilde{\nu}_r = 0.0005$ for $v_0 = 0.01$ and $v_0 = 0.02$ corresponding to $Pe = 20$ and $Pe = 40$, respectively. Solid lines are guide for the eye.	62
4.4	Construction of the equation of state. Active and passive pressure at a fixed $v_0 = 24$. Solid lines are guide for the eye.	63

List of Tables

Chapter 1

Introduction to Active Matter

How can the events in space and time which take place within the spatial boundary of a living organism be accounted for by physics and chemistry?

Erwin Schrödinger

1.1 What is Active Matter?

Cells migrate, birds fly, fish swim. Have you admired the intricate coordinated dynamics of these systems? Motivated by such complex systems spanning macroscopic (flocking of birds) to microscopic scales (crawling of cells, swimming of bacteria), scientists study “active matter.” Often, they are interested by how do individual self-driven units, such as starlings, can generate large scale complex dynamical pattern, such as ordering? What type of physical principles underlie the behavior of such systems? How can we elucidate their balletic maneuvers? Which state of matter do they generate? What parameter should we tune to go from one state to another? And finally, how can we classify their behavior and identify their properties?

Describing these systems as self-propelled particle systems whose individual units have their own propulsion mechanism which evolve via update rules and/or while interacting with each other, provides a way to study the physical principles governing their collective behavior.

Active matter systems are out of equilibrium systems that differ from other class of systems that are driven out of equilibrium by shear flow, forces at the boundaries, temperature gradients, imposed fields, etc. The former are driven out of equilibrium by a drive that acts on each individual unit. This drive can be internally generated by transforming chemical energy into motion. In addition, the state of the particle is depicted by the direction in which each particle moves and not the direction of the external field. In addition, these systems exhibit interesting behavior absent in systems in thermal equilibrium. Orientational order is thus a crucial characteristic of active matter. An example of an ordered state that is obtained in thermal equilibrium is the nematic liquid crystal

in which anisotropic particles align along a common axis. It is important to differentiate between “self-propelled particles” and “active nematics.” The former occurs in the description of “swimmers” in a fluid, while the latter is used in describing “living liquid crystals” of orientationally ordered states of active matter [1].

Thus, the term “active matter” describes a discrete or continuum systems, whose individual units are driven out of equilibrium through an internal (or external) energy reservoir into kinetic work. These systems are characterized by the emergence of coherently moving, large scale spatial patterns, such as clusters and swirls.

Living matter in which active units interact, reproduce, and adapt, such as animal flocks, motile microorganisms, biofilaments, molecular motor, are a paradigmatic example of active matter. These systems are characterized by a wide variety of active agents and behavior which renders having a comprehensive theoretical description of their complex nature challenging.

In this thesis, we differentiate between two classes of active matter: dry and wet and we focus on the former. Dry active matter systems are systems in which hydrodynamic interactions are absent. Thus, momentum is not conserved due to the presence of friction caused by the background fluid. Examples of such systems are the bacteria or granular beads gliding on a frictional surface.

1.2 Examples of Active Matter

1.2.1 Biological Systems

1.2.1.1 Bacterial Suspensions

Some experimental realization of a bacterial suspension includes studying the velocity fields prompt by bacterial motion of sessile and pendent drops containing the bacterium *B. subtilis* [2].

Fig. 1.1 shows bacterial flows in a sessile drop. The image is viewed from below through the bottom of a petri dish. The horizontal white line at the top of the image is the air-water-plastic contact line and gravity is perpendicular to the plane of the picture. The frame rate is 1/30 seconds is not enough to capture the collective motion, which resulted in a low resolution image. The scale bar is $35 \mu m$.

These fields highlight how a concentration gradient of bioconvective plumes down a slanted meniscus in order to concentrate cells at the drop edge or bottom. This effect is mediated by the interchange between buoyancy effects and bacterial chemotaxis. This concentration results in interesting motion exhibited by groups of bacteria such as vortical structures and other complex patterns. From a model point of view, Dombrowski et. al. proposes a mechanism to explain the resulting large scale coherent structures using hydrodynamics interactions between swimming cells. Consequently, these experiments are crucial in highlighting the role of hydrodynamic interactions, along with the motion of individual swimmers, in understanding the process of the generation of self-organized, large-scale dynamical structures in the constituent fluid.

1.2.1.2 Cytoskeletal Filaments and Molecular Motors

Starting from an initially disordered state of a mixture of cytoskeletal and molecular motors elements (such as kinesis complexes, ATP, and microtubules) in a two-dimensional

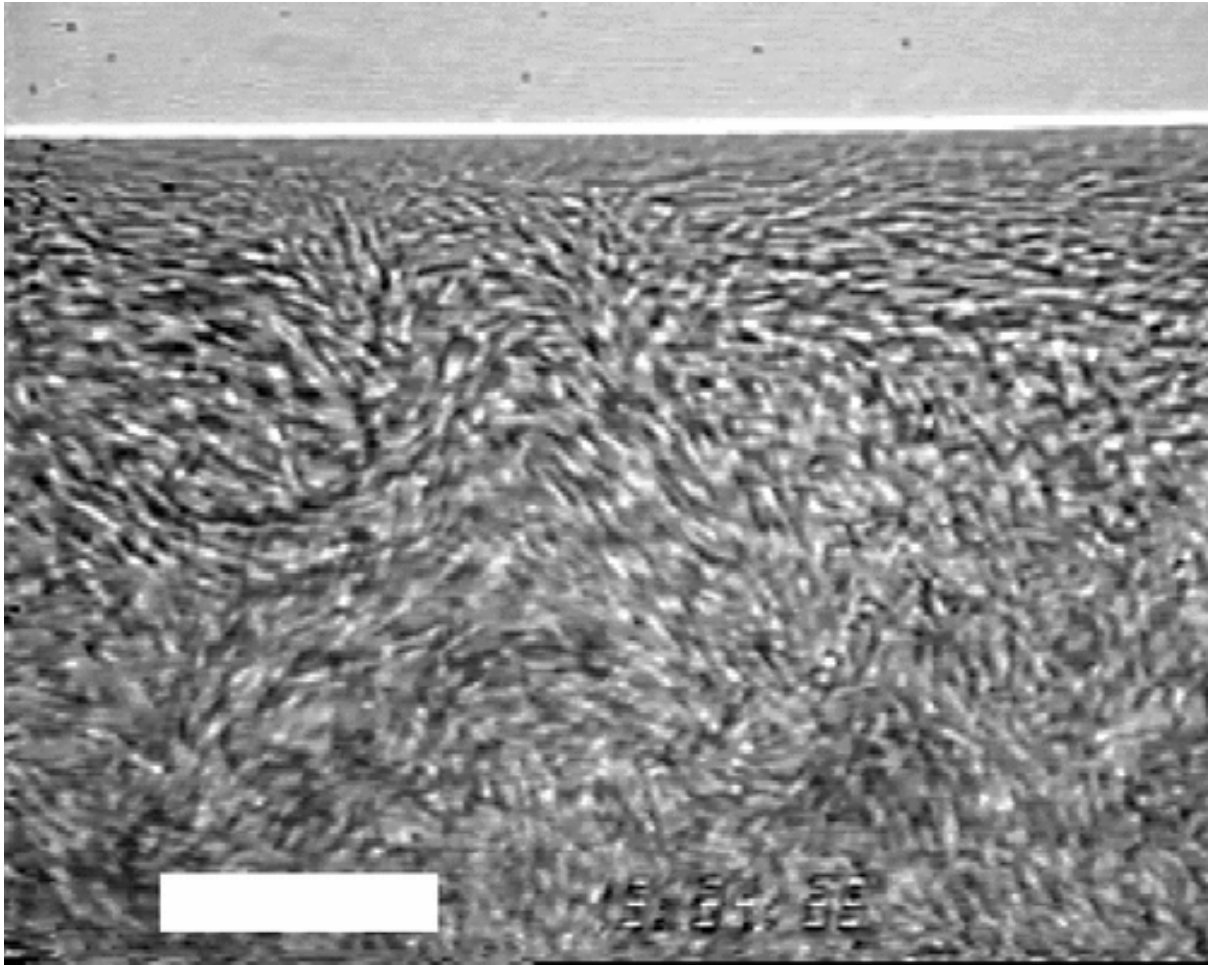


Figure 1.1: Bacterial Suspension

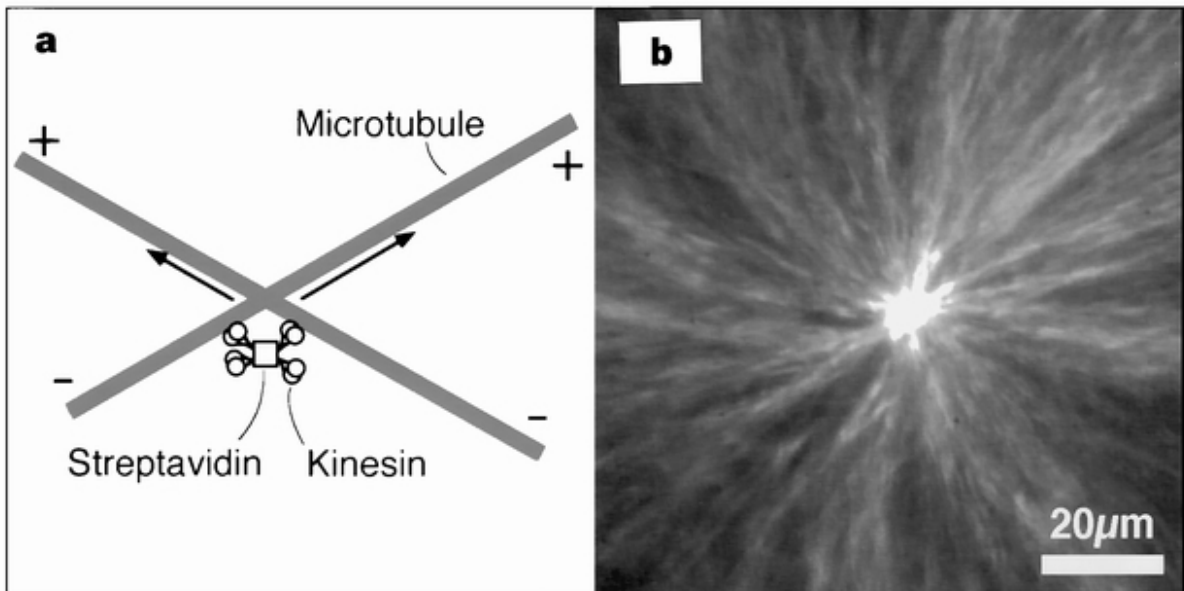


Figure 1.2: **a.** Kinesin–streptavidin construct moving simultaneously along two microtubules. **b.** A self-organized aster observed by dark-field microscopy.

geometry in vitro, Nedelec et. al. find self-organized states [3]. By carrying the concentration of the components of the model, they observe the formation of asters and vortices. Fig. 1.2 **b** shows an image of the experiment carried in [3]. A self-organized aster formed by mixing polymerized and taxol-stabilized microtubules were mixed with motor constructs and ATP.

Dynamic asters are found in mitotic and meiotic spindles, thus the usage of microtubules is essential for the understanding of cellular structures. The formation of such large-scale structures is a non-equilibrium process since it is mediated by the presence of ATP. Hydrodynamical theories of these models have been proposed. The theory and experiments are summarized in [4].

1.2.2 Macroscopic Systems

1.2.2.1 Vibrated Granular Rods

Using a system of a fluidized monolayer of macroscopic rods in the nematic liquid crystalline phase in a two-dimensional cell, Narayanan et. al. [5], study the collective behavior of the elongated rods by vertically shaking the system.

Fig. 1.3 is a snapshot from the experiment. We can observe a sparse region between 10 and 11 o'clock showing a large density fluctuation.

The shaking is essential in maintaining the system out of equilibrium. They observe long-lived fluctuations in the dynamical regions. These fluctuations mimic the flocking, coherent motion observed in moving flocks of birds. These experiments provide insights on the giant number fluctuations in non-equilibrium systems, which deviates from the known equilibrium central limit prediction of the behavior of the number fluctuations as function of the number of particles N . Details on number fluctuations will be presented in Chapter 3.

1.2.2.2 Flocking of Birds

The literature includes several numerical models inspired by biological systems [6] and physics [7] aiming to understand the emergence of collective behavior. These models include simple rules of interaction among the constituent elements of the system that produce collective behavior. However, these models lack the precise nature of interaction between the individuals. Ballerini et. al. [8] use novel stereometric and computer vision techniques to measure the number of individual birds positions in a flock of up to 2600 starlings. They find that, contrary to what have been previous expected, birds adjust their motion in the flock by measuring the behavior of topologically, rather than metrically, neighboring birds. Hence, at each instant in time, each bird would compare its instantaneous position and velocity to their neighboring birds (found to be around 5 to 7). By making such adjustment, birds maintain coherent flocks. This result thus highlights that topological interaction is more robust than a metric interaction. The former has the same strength regardless of the density of the system. However, the latter is less robust in the sense that when inter-individual distance becomes larger than the metric range, the interaction between birds will vanish, and cohesion would be lost.

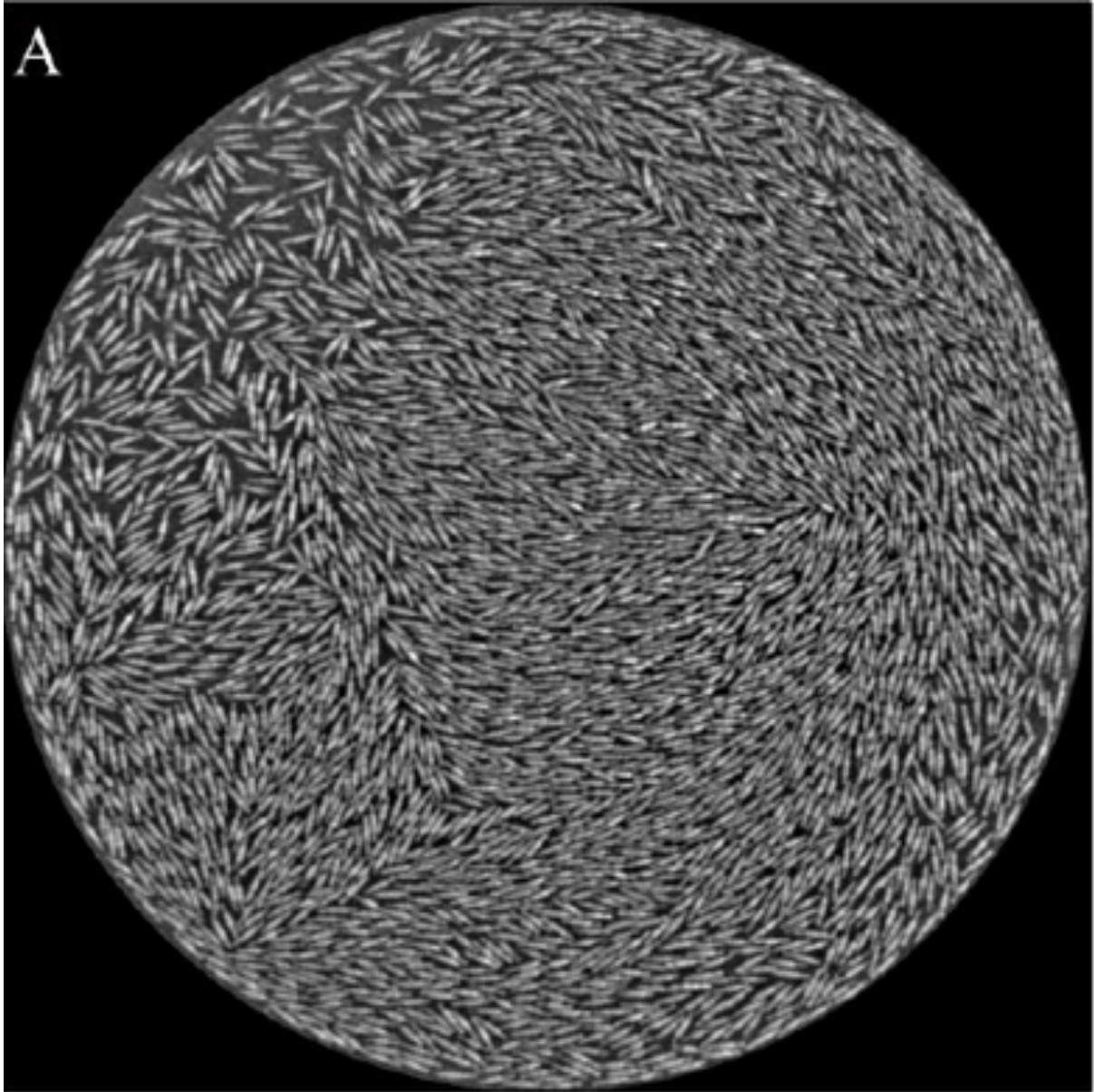


Figure 1.3: Giant number fluctuations in active granular rods

1.2.3 Synthetic Systems

During the last decade, diverse artificial active agents have been synthesized. Bechinger et. al. present a summary of these systems in [9]. These active motors range from tens of nanometers to micrometers and exploit various propulsion mechanisms. Experimental realizations include thermophoresis such as thermal gradients, diffusiophoresis such as concentration gradients, and inhomogeneous charge distribution of electrolytes using electrophoresis. By synthesizing micro and nano machines, we will have a better quantitative understanding of non-equilibrium phenomena, in addition to the design of novel propulsion mechanisms, crucial for novel technological applications.

1.3 Scope of Thesis

Two phenomena are commonly occurring in equilibrium behavior of passive matter: phase separation at intermediate densities and glassification (jamming) near the dense packing limit. Recent simulations explored extensively the effects of self-propulsion in active matter on these two phenomena. In particular, it was demonstrated that self-propulsion shifts the boundary between the fluid and jammed regimes. It was also shown that phase separation emerges even in the case of purely repulsive interaction between active colloidal particles. This phenomena, termed motility-induced phase separation (MIPS) will be revised in Chapter 2. However, the literature lacks some work on the phase behavior of active particles interacting through attractive interactions. Redner et. al. [10] study a system of self-propelled colloids interacting through short range attraction and found that the phase diagram is reentrant as a function of activity. In the presence of attractive interactions, one may intuitively think that including attraction in the potential will promote phase separation. However, phase separation may be suppressed depending on the activity level. So self-propulsion can either enhance or suppress phase separation by either acting cooperatively or competing with inter-particle attractions. Attractive active particles show a reentrant phase behavior in which phase separation occurs at a certain Péclet number. Phase separation is then suppressed as we increase the Péclet number and phase separation appears again for higher Péclet numbers. Péclet number is a dimensionless parameter, which will be defined in Chapter 3. Péclet number is proportional to the persistence length. The phase diagram studied by Redner et. al. is a function of attraction strength and Péclet numbers, at a fixed density. In this thesis, we investigate the phase behavior of attractive active particles, in the density-Péclet number plane, at a fixed attraction strength, which is much larger than the scale of self-propulsion. We make use of these simulations to study the kinetics of cluster-cluster aggregation and the time-evolution of the domain size of our system. We then move to investigate the reentrant behavior at a fixed density and fixed attraction strength, and we take limiting values of the self-propulsion, in such a way that we explore the phase behavior of the system for self-propulsion less than, equal to, and larger than the attraction strength. In other words, we study the reentrant phase behavior as we vary the strength of attraction and self-propulsion, simultaneously. Lastly, recently there has been a lot of interest in characterizing the pressure of active systems. It was shown that these systems have a unique contribution to pressure, termed swim or active pressure. Due to their self-propulsion motion, active particles exert a pressure that measures the strength of propulsive forces across a bulk plane. Significant progress in theoretical efforts to understand phase behavior of active matter was achieved very recently by introducing the notion of active pressure and eventually lead to a formulation of generalized thermodynamics of active matter [11]. Numerical exploration of active colloids with purely repulsive interactions supports the theory. Whether the generalized thermodynamics is applicable to a broader class of interactions including attraction remains an open question. We investigate the applicability of the recent thermodynamic formulation of active matter by measuring, from simulation, active and passive pressure. Passive pressure measures the direct transmission of interaction forces across a bulk plane. When phase separation takes place, we observe a suppression in active pressure which leads to the non-monotonic behavior of the full equation of state (active and passive pressure). This usually happens at high densities. This instability is captured in MIPS and in our system. It describes a system transitioning from a homogeneous to an in-homogeneous state. This is controlled by the

suppression of active pressure. However, in systems depicting reentrant behavior, the first instability is not trivial to obtain and it describes the transition from a phase separated state to a homogeneous state by the breaking down of clustering due to attraction. We did not observe this instability in our pressure calculations and it raises the question to whether one can measure, from simulations, passive pressure due to attraction. In chapter 4, we revisit the pressure equation of state calculation found in MIPS and we highlight our unsuccessful attempt in passive pressure calculation for active systems with attraction.

Chapter 2

Passive vs. Active Matter - Phenomenological Differences

We cannot, indeed, without the most careful scrutiny, decide whether the movements of our minutest organisms are intrinsically ‘vital’ (in the sense of being beyond a physical mechanism, or working model) or not.

D’Arcy Thompson

2.1 Passive Brownian Particles

Active matter such as migrating cells and motile bacteria are systems performing their motion in a liquid environment. They are out of equilibrium systems whose constituent elements convert harvested or internal energy into kinetic motion. These systems are subject to viscous forces which oppose their velocity. Additionally, since they are immersed in a fluid, they are also subject to thermal noise due to the collision between fluid molecules and molecules constituting the active system.

Via numerical integration, Molecular Dynamics (MD) simulations solve Newton’s equations of motion:

$$m\ddot{\mathbf{x}}_i(t) = -\nabla_i U(\mathbf{x}_i) \quad (2.1)$$

We are often interested in the time evolution of the particle’s positions $\dot{\mathbf{x}}_i(\mathbf{t})$ and velocities $\dot{\mathbf{v}}_i(\mathbf{t})$. Since the ergodicity hypothesis allows us to compute the time average as the ensemble average of quantities of interest, we can compute the latter by averaging over the time evolution of particles positions $\dot{\mathbf{x}}_i(\mathbf{t})$ and velocities $\dot{\mathbf{v}}_i(\mathbf{t})$ of all particles in the system.

Nonetheless, we are often interested in studying some degrees of freedom in our system such as particles suspended in a liquid. More specifically, we are interested in the behavior of the suspended particles rather than the dynamics of the liquid’s molecules. However, taking account of the liquid’s molecules mean that we need to tune our integration time step to the fast dynamics of the molecules in the liquid, which would result in keeping

track of all the liquid molecules positions and velocities. This is computationally expensive and thus, unfeasible. Since the solvent affects the dynamics of the suspended particles, we cannot completely drop the liquid out of the picture. Instead, we treat the solvent's molecules stochastically and we focus on studying the trajectories (and velocities) of the suspended particles.

The suspended particles interact with the molecules constituting the fluid. These collisions result in a slow down in the velocities of the suspended particles. This slow down is modeled by a friction term. An additional term, called fluctuation force, will be added to the equation. This term is due to the fluctuation in the movement of particles' due to collisions. The influence on the suspended particles is caused by collisions with the solvent's atoms or molecules. On average, this slows down the velocity of the suspended particles which can be modeled by a friction term. Nonetheless, there are additional fluctuations of the particles' movements due to the collisions, which results in the need for a stochastic force. This treatment gives rise to a second order ordinary stochastic differential equation, called the Langevin equation:

$$m\ddot{\mathbf{x}}_i(t) = -\gamma m\dot{\mathbf{x}}_i(t) + \boldsymbol{\xi}_i(t) \quad (2.2)$$

$$\langle \boldsymbol{\xi}_i(t) \rangle = 0 \quad (2.3)$$

$$\langle \boldsymbol{\xi}(t_1)\boldsymbol{\xi}(t_2) \rangle = g\delta(t_1 - t_2) \quad (2.4)$$

where $\boldsymbol{\xi}_i(t)$ is a stochastic random force giving the effect of background noise due to the fluid on the particles. The random force has zero mean and variance $g = 2\gamma mk_B T$ where k_B is the Boltzmann's constant and T is the absolute temperature. g is a measure of the fluctuating force and the delta function means that there is no correlation between the impacts. In other words, any memory between collisions at different times will be lost due to collisions. The fluctuating force has a Gaussian distribution determined by these moments. The randomness of Brownian noise is fully determined by the initial state of the heat bath. In other words, the results of any calculation are expected to be independent of the initial state and to involve only the statistical distribution of the noise. There are three timescales involved in such systems. A short atomic timescale $\tau_s \sim 10^{-12}s$, a Brownian timescale for the relaxation of the particles velocity $\tau_B \sim \frac{m}{\gamma}$, and a relaxation time for the Brownian particle τ_r , which is the time needed for a particle to diffuse its own radius. In general, we have $\tau_s \ll \tau_B \ll \tau_r$.

Let us assume we have a transparent silica particle of mass $m = 10^{-14} \text{ kg}$ and of diameter $3 \mu\text{m}$ floating in a water solution, deposited on a microscopic glass slide. Using a microscope, we can watch the erratic motion of the particle. We can also track the particle's displacement by measuring its position between different time intervals Δt . We will find that the particle's motion is purely diffusive with a diffusion coefficient given by:

$$D_t = \frac{k_B T}{\gamma} \quad (2.5)$$

This is Einstein's fluctuation-dissipation relation. Note that in the bulk of the liquid solution, the friction coefficient is given by $\gamma = 6\pi\eta R$, where η is the viscosity of the fluid and R is the radius of the particle.

Often, the particles have a tiny mass and thus inertia can be neglected. Moreover, inertial forces acting on such particles suspended at low Reynolds numbers are negligible compared to viscous forces caused by the liquid. This is the overdamped limit. In addition, the relaxation timescale needed to forget the inertial effects, termed τ_B , is of

order of $0.1 \mu s$ for silica particles. Comparing this relaxation time to the time intervals for sampling in experiments, which is of order of ms for an acquisition via a standard CMOS camera, this relaxation time is much smaller [12]. Therefore, equation (2.2) can be simplified to the overdamped Langevin equation:

$$\dot{\mathbf{x}}_i(t) = \boldsymbol{\xi}_i(t) \quad (2.6)$$

2.2 Active Brownian Particles

2.2.1 Methods of Simulating Active Matter

In the introduction, we discussed a non-exhaustive review of some experimental realization of active matter. They included activating particles using different propulsion mechanisms, designing particles with different properties, in addition to carrying the experiments in different environments. When it comes to mimicking the behavior of such systems in a computer simulation, we need a theoretical description capturing the inter particle interaction, the propulsion mechanism, such as a fixed propulsive speed, the environment in which the particles are embedded, such as a fluid, and finally a comprehension of how these parameters affect each other.

In the following, we will discuss two eminent techniques to account for the propulsion mechanism of active matter.

2.2.1.1 Active Brownian Particles in a Solvent

Imagine you have a swimmer flowing in a fluid. In order to swim, the swimmer must generate a flow. This will result in a long range hydrodynamic interaction between the swimmers and the constituent particles of the fluid. A brute force approach to the problem is to take into account the inter-particle interaction between the swimmers and its surrounding fluid molecule, and to fully integrate the full equations of motion using Newton's 2^{nd} law. Taking into account of all of the above is computationally expensive since we are interested in simulating a large number of active particles.

In order to overcome this difficulty, we can coarse-grain the solvent. This is doable since we are interested in the behavior of active matter rather than the surrounding fluid. Different simulation techniques adapt this idea.

In the following simulation techniques, one has to assume some constant momentum transfer from the solvent to the swimmers or a velocity profile of the fluid on the boundaries of the active particles. This will result in the conservation of linear and angular momentum of the system. Such active systems are termed wet active matter. One simulation technique, called multi-particle collision dynamics (MPCD), explicitly takes into account a small number of the fluid molecules by solving modified equation of motion [13]. A second approach is obtaining the flow of the solvent through solving discrete Boltzmann equation. This is the lattice Boltzmann (LB) technique [14]. A third procedure involves calculating, for each swimmer, the modes of velocity and force fields, by solving Stokes equations [15].

In the following, we will discuss another class of systems called dry active matter in which linear and angular momentum of the system is not conserved. This results from modeling the activity mechanism through an explicit force or torque that acts on the active particle. In [16], Hagen et. al. argued that modeling self-propulsion using forces

and torques can be also be made for anisotropic particles and in the presence of external fields. However, it is still an open question whether this simplification can be used in the limit where hydrodynamics effects are dominant.

2.2.1.2 Dry Active Matter

Another route of coarse-graining includes writing an effective equation of motion for each swimmer and completely ignoring the hydrodynamics between the colloidal particles and the solvent. In the absence of inter-particle interaction, the equation of motion should recover the limit of Brownian motion. Such a stochastic differential equation was introduced in 1908 by Paul Langevin [17]. Throughout this thesis, the Langevin equation will be used. Consequently, in the following a detailed description of the equation is presented.

We describe, using the following Langevin equation, the motion of a colloidal particle i suspended in a solvent whose constituent elements have a size much smaller than the colloidal particle. Time is denoted by t and the particle's position is given by the vector \mathbf{r}_i

$$m \frac{d^2 \mathbf{r}_i}{dt^2} = -\eta \frac{d\mathbf{r}_i}{dt} + \sqrt{\frac{2\eta}{\beta_s}} \boldsymbol{\xi}_i^{tr} \quad (2.7)$$

$$\langle \boldsymbol{\xi}_i^{tr}(t) \rangle = 0 \quad (2.8)$$

$$\langle \boldsymbol{\xi}_i^{tr}(t) \boldsymbol{\xi}_j^{tr}(t') \rangle = \mathbb{I}_d \delta_{ij} \delta(t - t') \quad (2.9)$$

m is the particle's mass, η is the particle's damping coefficient which is a measure of the viscosity of the solvent. The temperature of the solvent (and not that of the whole system) is given by T_s which is given by $\beta_s = 1/k_B T_s$, where k_B is the Boltzmann constant. We have introduced two forces to account for the collisions between the molecules of the solvent and the colloidal particles.

On the right-hand side of (2.7), the first term, from the left side, is the drag force, and the second term is the noise term describing a stochastic force.

Eq. (2.8) shows that the vector $\boldsymbol{\xi}_i^{tr}$ is a unit-variance random vector with 0 mean. Eq. (2.9) dictates that the vector $\boldsymbol{\xi}_i^{tr}$ has delta correlations in time, where \mathbb{I}_d is the unit matrix in d dimensions, and δ_{ij} and $\delta(t)$ are the Kronecker and Dirac deltas, respectively. The brackets in (2.8) and (2.9) denote an average over noise realizations of the stochastic components of random vectors from a Gaussian probability distribution.

If we follow the particle's trajectory, we would find that the particle undergoes Brownian motion. On average, the particle's displacement is 0, and its mean squared displacement (MSD) is given by the following

$$\langle \mathbf{r}_i(t) - \mathbf{r}_i(0) \rangle = 0 \quad (2.10)$$

$$\langle (\mathbf{r}_i(t) - \mathbf{r}_i(0))^2 \rangle = \frac{2dt}{\beta_s \eta} \quad (2.11)$$

The particle, hence, undergoes Brownian motion with a diffusion coefficient

$$D_{tr} = \frac{1}{\beta_s \eta} \quad (2.12)$$

which coincides with the Einstein-Smoluchowski relation [18].

2.2.1.3 Interacting ABPs

Now we wish to include a set of interacting particles via a pairwise potential $U(r)$. We proceed by modifying the Langevin equation. We make the colloidal particles active by introducing a self-propelling force, of constant magnitude f_0 . We assume that the particles self-propel along their body-axis via a d -dimensional unit vector \mathbf{u}_i . In other words, this unit vector describes the direction of motion of the particle. The modified Langeving equation is given by

$$m \frac{d^2 \mathbf{r}_i}{dt^2} = - \sum_{j \neq i} \frac{\partial U(\mathbf{r}_{ij})}{\partial \mathbf{r}_i} - \eta \frac{d\mathbf{r}_i}{dt} + f_0 \mathbf{u}_i + \sqrt{\frac{2\eta}{\beta_s}} \boldsymbol{\xi}_i^{tr} \quad (2.13)$$

where $\mathbf{r}_{ij} = \mathbf{r}_j - \mathbf{r}_i$ is the interparticle separation.

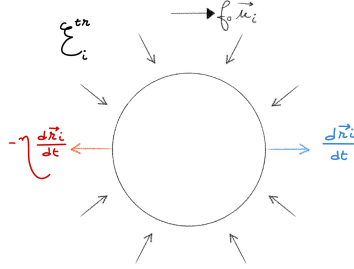


Figure 2.1: Schematic representation of an active particle

Fig. 2.1 is a schematic representation of an active particle modeled by Eq. (2.13). On the right hand side of Eq. (2.13), the first term, from the left side, is the force of interaction between the particles, the second term is the previous drag fore, the third term is the self-propulsive force, and the forth term is the previously introduced stochastic force. As we have previously mentioned, the absence of an explicit solvent and the presence of self-propulsion violate conservation of momentum in the system.

To further simplify the description of a swimmer, we compare the strength of viscous forces and inertial forces. It turns out that the latter are negligible with respect to the former [19]. The ratio of inertial forces to viscous forces is called Reynolds number. Colloidal systems have a low Reynolds number so that we can neglect the inertial term on the left hand side of Eq. (2.13). This is the overdamped Langevin equation

$$\frac{d\mathbf{r}_i}{dt} = - \frac{1}{\eta} \sum_{j \neq i} \frac{\partial U(\mathbf{r}_{ij})}{\partial \mathbf{r}_i} + v_0 \mathbf{u}_i + \sqrt{2D_{tr}} \boldsymbol{\xi}_i^{tr} \quad (2.14)$$

where we have defined a self-propulsion speed as

$$v_0 = \frac{f_0}{\eta} \quad (2.15)$$

Thus we will refer to Eq. (2.13) as the underdamped Langeving equation and to Eq. (2.14) as the overdamped Langevin equation. We will proceed by only considering the

overdamped equation. This equation describes the translational motion of the particles. However, one should also take into consideration the rotational motion of the particles. Thus, we will write an overdamped rotation Langevin equation for particles that do not exert any torques on each other as

$$\frac{d\mathbf{u}_i}{dt} = \sqrt{2D_r}(\mathbf{u}_i \times \boldsymbol{\xi}_i^r) \quad (2.16)$$

where the unit-variance random vector $\boldsymbol{\xi}_i^r$ satisfies relations similar to Eqs. (2.8) and (2.9).

Rotational diffusion is an important parameter in active matter systems. Experimentally, its importance was shown in different systems subject to athermal rotational diffusion, such as bacterial colonies [20]. For this reason, different models in the literature take into account rotational diffusion by treating it as an independent parameter that can be varied in order to explore the different behavior of the system [21].

The systems we described in this section are referred to in the literature as Active Brownian Particles (ABP). They are colloidal particles immersed in a solvent. The equations described in this section can be slightly modified to describe dry active matter, in which the solvent is absent. To do so, the friction term is dropped from the equation of motion. In addition, translational noise can be ignored due to the fact that thermal fluctuations is absent in dry active matter systems [22]. Furthermore, it was shown in simulations of active matter systems that the phase behavior is independent of translational noise [23, 24].

2.2.2 Simple Simulation Approaches to Active Matter

In this section, we present a literature review of two prominent models of active matter that we investigated before delving into our model which we will present in Chapter 3. These are the Vicsek model [7], and the model of self-propelled, purely repulsive disks [24]. They present novel types of behavior and phases acquired by active matter systems. We proceed by concisely reviewing their phase behavior.

2.2.2.1 Flocking Transition in the Vicsek Model

The simplest model of collective motion was introduced by Vicsek et. al [7] in 1995. The model describes the behavior of a two-dimensional point-particles system on a square shaped lattice of size L with periodic boundary conditions. The simulation is carried as follow: at time $t = 0$, N particles were randomly distributed in an area $L \times L$. All particles have the same self-propulsion velocity v_0 and a randomly distributed direction θ . At each time step, $\Delta t = 1$, the position \mathbf{r}_i of particle i is updated using the following discretized update equation

$$\mathbf{r}_i(t + \Delta t) = \mathbf{r}_i(t) + v_0 \mathbf{u}_i \Delta t \quad (2.17)$$

where \mathbf{u}_i denotes the direction of self-propulsion of particle i along its predefined axis, and is given by

$$\mathbf{u}_i = (\cos(\theta_i), \sin(\theta_i)) \quad (2.18)$$

The update equation of the direction of self-propulsion of particle i is given by

$$\theta_i(t + \Delta t) = \langle \theta_i(t) \rangle_r + \Delta \theta_i \quad (2.19)$$

where $\langle \theta_i(t) \rangle_r$ denotes the average direction of velocities of particles, including particle i , within a circle of radius $r = 1$ surrounding particle i . The term $\Delta\theta_i$ represents noise. It is a random number chosen from a uniform probability distribution from the interval $[-\frac{\eta}{2}, \frac{\eta}{2}]$.

The free parameters considered by Vicsek et. al are the noise strength η , the self-propulsion speed v_0 , and the density of the system defined by

$$\rho = \frac{N}{L^2} \quad (2.20)$$

Even though the update equation of the system does not include any explicit interaction term, on the right hand side of equation (2.19), the first term from the right tend to align the direction of particles, and hence act as an attractive term.

The interesting behavior of this model appears when we vary the strength of noise and density, at a fixed self-propulsion speed. The particles do not move in the limit of $v_0 \rightarrow 0$ and hence the system becomes similar to the well-known XY model. In the limit of $v \rightarrow \infty$, the particles are always completely mixed. This is the limit of the mean-field behavior of a ferromagnet. Accordingly, we use a value of v_0 for which we ensure that the particles always interact with their neighbors and that the configuration of particles would change after some time updates.

Small groups of coherently moving particles is formed at small densities and noise. However, particles move randomly with some correlation at higher densities and noise. The novel behavior appears for small noise and large densities; this is when the particles order their motion and move together in a randomly selected direction as a flock. This suggests that the system transitions from a homogeneous state in which correlation between the positions and velocities of the particles is absent (isotropic, disordered regime), to an ordered state in which all particles move collectively in the same direction (polar, ordered regime). Hence, as we decrease noise or increase the density, the system transitions from a homogeneous phase to an ordered polar phase. Fig. 2.2 illustrates the Vicsek model phase diagram in the (ρ, η) plane. The transition can be explained by the following: small groups of particle moving coherently is formed initially due to alignment interaction. As the system evolves in time, different particles cluster will collide with each other leading to an exchange of velocities between those clusters, and hence driving the system to an ordered state. However, it was shown in [25] that the phase diagram has a central region of coexisting phases in which liquid domains are observed in a disordered background. Fig. 2.3 shows snapshots of the model in different states.

It is beneficial to highlight the similarities and differences between the Vicsek model update equations and the previously introduced overdamped Langevin equations for ABP. If we ignore the interaction term and translational noise term in Eq. (2.14), Eq. (2.17) is the integration of Eq. (2.14) using the Euler method. However, the update equation for the angles in Eq. (2.19) include an alignment interaction term and the noise results from a uniform probability distribution, in contrast to a Gaussian probability distribution in Eq. (2.16).

Despite the simplicity of the Vicsek model, it is one of the first models of active matter systems and contributed to the emergence of several new models including hydrodynamics, steric repulsion in addition to translational and rotational noise, and mean field theories models of active matter [26–29].

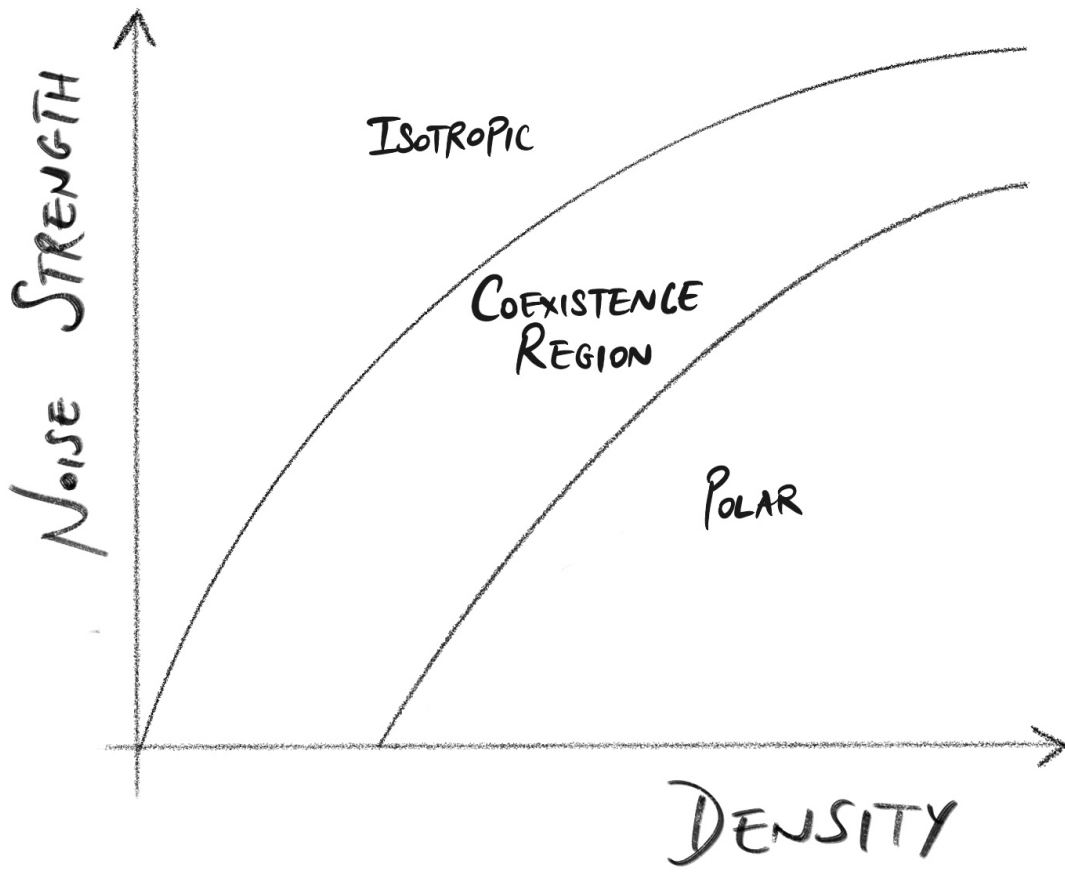


Figure 2.2: Schematic representation of the Vicsek model phase diagram

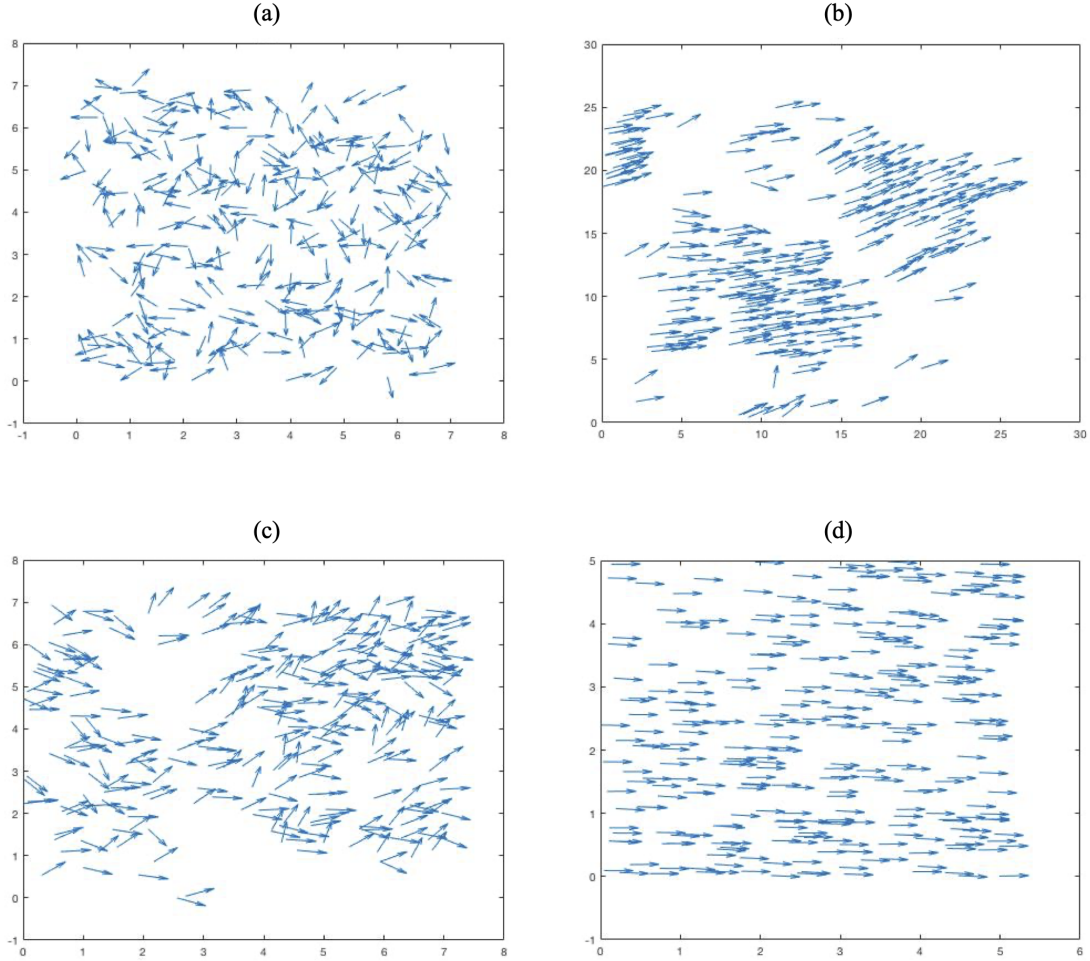


Figure 2.3: Snapshots of the Vicsek model in four regions of phase space. **a.** Homogeneous State **b.** Groups of particles moving coherently in random directions for small densities and noise. **c.** Particles moving randomly with some correlations at high densities and noise. **d.** Ordered motion at higher densities and small noise.

2.2.2.2 Motility Induced Phase Separation of Self-Propelled Disks

Novel type of phases in active matter systems were reported first in 2012, by Fily et. al. in [24], and later in 2014 by the same authors [23]. In the following, we highlight the results obtained in these two papers as well as other literature inspired by these results. Fily et. al. study a model of N purely repulsive discs in a box of size L with periodic boundary conditions. Their equations of motions are overdamped Langevin equations similar to those introduced previously in Eqs. (2.14) and (2.16). However, in their numerical simulations, in order to highlight the importance of orientational noise, they set the translational noise term to zero.

The particles interact through short ranged soft repulsive forces given by the following

$$\mathbf{F}_{ij} = \begin{cases} k(2a - r_{ij})\hat{\mathbf{r}}_{ij} & \text{if } r_{ij} < 2a \\ \mathbf{0} & \text{otherwise} \end{cases} \quad (2.21)$$

where $a = 1$ is the particle radius and k is the strength of interaction. After fixing the values of rotational noise and interaction strength, the remaining free parameters are the

self-propulsion speed v_0 and the density or packing fraction of the system defined as

$$\phi = \frac{N\pi a^2}{L^2} \quad (2.22)$$

Despite the fact that the model include only repulsive interaction between the particle, the system shows phase separation in an intermediate range of packing fractions and activity (self-propulsion). We obtain a high density cluster surrounded by a gas at packing fractions below close packing, and a hole of gas phase inside a dense packed liquid at packing fractions above close packing. This suggests that the system undergoes a phase transition, as the self-propulsion speed v_0 is varied, from a homogeneous state to a phase separated state, at high densities. Equivalently, as the density of the system is increased, the system undergoes a phase transition from a homogeneous state to a phase separated state for high self-propulsion speed v_0 .

Fig 2.5 shows a series of the phase behavior of a system of repulsive hard disks. As we increase the self-propulsion speed from 0.001 to 0.1 at a fixed packing fraction of $\phi = 0.5$ (from figure **a** to **b**), the system goes from a homogeneous state to a phase separated state. Phase separation remains as we increase the packing fraction from 0.5 to 0.9 at a fixed $v_0 = 0.1$. However, at high densities we obtain a gas of active particles surrounding a high density liquid (figure **b**), whereas at low densities we obtain a gas of active particles surrounded by a liquid (figure **c**).

The mechanism by which we observe this change in behavior of active particles is novel and different than the flocking transition of the Vicsek model driven by alignment interaction. As particles start colliding together, they form small clusters. The particles in the cluster need some time proportional to the reorientational timescale set by the simulation before they can turn their direction of motion and escape from the cluster. Fig. 2.4 illustrates this process. Before this happens, particle from the dilute phase may bump into the clusters and consequently slow down. For high density and self-propulsion of the particles, this will lead to a positive feedback which allow the cluster to grow in size and hence, we will obtain a phase separated state.

This phenomena of phase separation with only repulsive interactions between the active colloids is referred to in the literature as motility induced phase separation (MIPS) [30]. The idea of MIPS is the following: self-propelled particles tend to accumulate where they move more slowly. This slow down creates a positive feedback which induced MIPS. The accumulation of active particles where they move more slowly lead to the formulation of density dependent propulsion speed: the speed of the active particles decreases as their local density increases. A comprehensive review of MIPS can be found in [31] by Cates et. al.

Redner et. al. study a similar model of active colloidal self-propelled particles [32] and report that the phase diagram of MIPS can be mapped onto an equilibrium phase diagram, despite the non-equilibrium transition found in MIPS. This suggests that we need an extended theory of thermodynamics and statistical mechanics in order to understand active matter systems. In fact, extensive theoretical studies on repulsive active matter systems involve numerical simulations, field theories, and continuum models [33–35]. Moreover, as we will discuss in the next section, attempts to describe active matter from thermodynamic and statistical mechanics perspective are being extensively studied in the literature.

As a final remark on MIPS, it was shown in the literature that MIPS takes place regardless of the interaction potential form as long as it has a repulsive core and for a variety

of particle shapes. However, the shape of active particles affects the collective behavior of the system and hence allow the emergence of an ordered state [36–38]. In this thesis, we modify the force of interaction presented in this section to study the phase behavior of a system of active particles with attractive interactions.

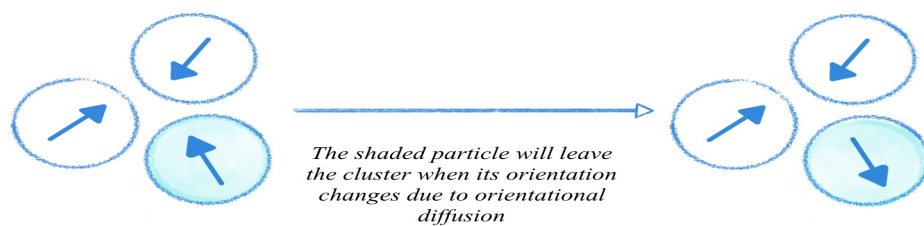


Figure 2.4: An active particle leaves a cluster after a time proportional to the reorientation time-scale

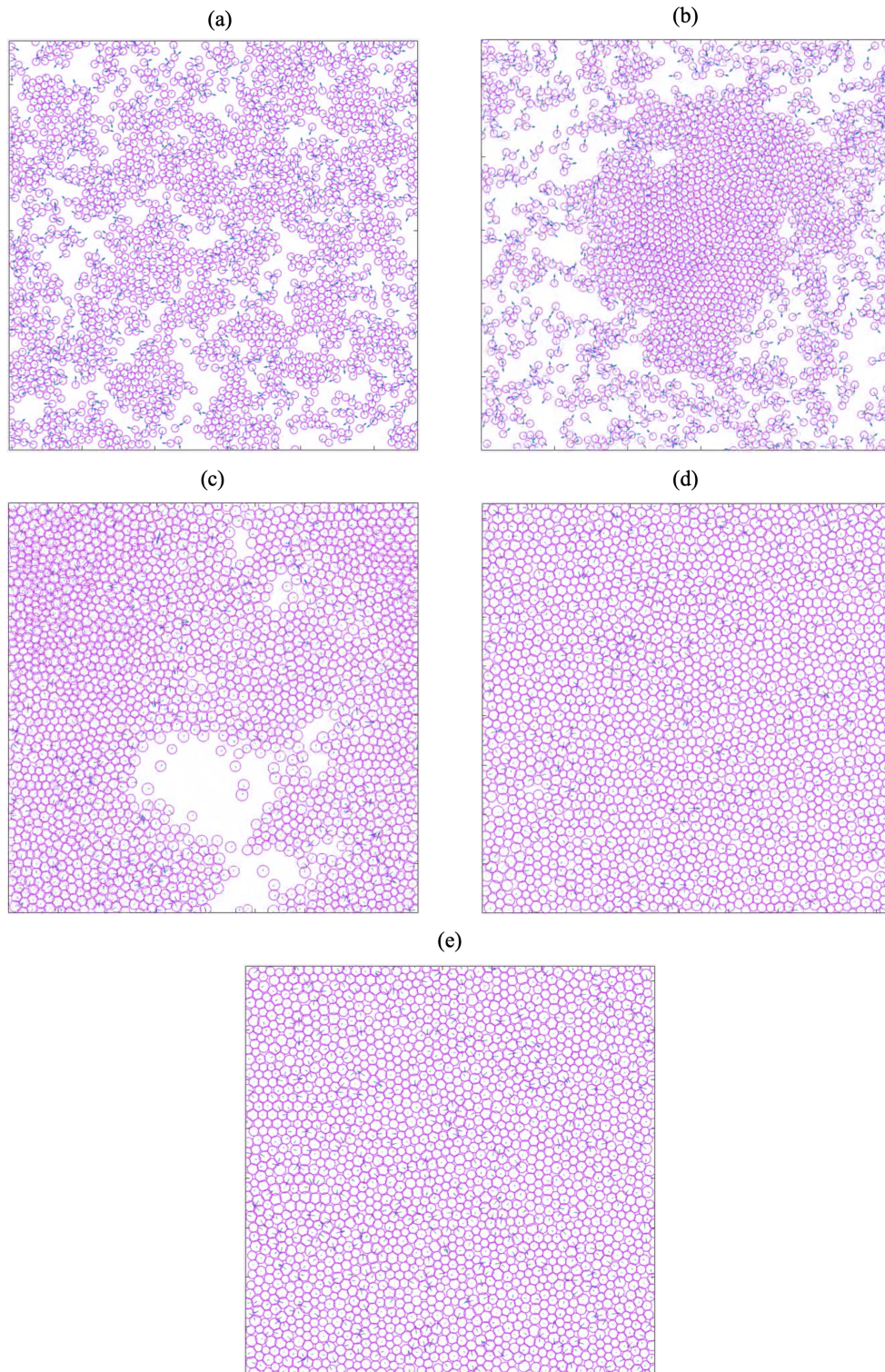


Figure 2.5: Snapshots of repulsive active particles. **a.** Homogeneous fluid at low self-propulsion speed below close packing. **b.** Phase separated state below close packing, consisting of high density liquid surrounded by a gas of active particles. **c.** Phase separated state above close packing, consisting of a hole filled by a gas of active particles surrounded by a high density liquid. **d.** Homogeneous liquid above close packing. **e.** Glassy phase.

2.3 Towards a Statistical and Thermodynamic Description of Active Matter

Statistical mechanics was established by Ludwig Boltzmann towards the end of the 19th century. Further development of thermodynamics and statistical mechanics was formulated by Josiah Willard Gibbs and James Clerk Maxwell in the early 20th century. Classical statistical mechanics and thermodynamics describe the theory behind thermal equilibrium systems such as passive matter. Thermodynamics theories describe systems containing a large number of particles, using macroscopic observables, such as pressure and temperature. Hence, as a result of many-particle statistics, we need to link the macroscopic behavior of the system to its microscopic properties using mathematical constructions that are offered by statistical mechanics, such as the free energy and the partition function. In addition, statistical mechanics sets the needed machinery to study the stability of systems and explains the physics behind phase transitions using the notions of minimizing free energy or maximizing entropy. As a result, thermodynamics defines state quantities characterizing the macrostate, and relate these quantities using universal equations such as the equation of state and the laws of thermodynamics [39].

We have previously described that the novel phases observed in active matter systems arise from their out of equilibrium behavior. Consequently, we cannot directly apply the notions of equilibrium statistical mechanics. Nevertheless, in recent years, intense research has been done on the relevance of some statistical mechanics notions such as pressure, temperature, entropy, and surface tension to active matter systems [11, 30, 40–43].

What we will discuss below is still an active area of research among scientists with different approaches to the exciting ideas that arise from the behavior of active matter systems.

2.3.1 Temperature

Systems in thermal equilibrium, such as a colloidal suspension, have a well defined thermal energy $k_B T$, where T denotes the temperature of the system, that describes the particles kinetic energy. However, for active matter systems, the notion of temperature is still a debatable topic among scientists. Studies of active matter systems in a thermal bath find that a newly defined effective temperature, of the whole system, take a value higher than the temperature of the thermostat [44]. In addition, an experimental work, by Palacci et. al., study chemically activated colloidal particles and define an effective temperature as a function of the activity level of the particles [45]. Using this effective temperature, they map the equation of state of chemically activated colloids onto an equilibrium equation of state. However, MIPS is not captured by an effective temperature because as we have mentioned before, fluctuations in the system described by translational noise does not affect the phase behavior of active matter undergoing MIPS.

2.3.2 Pressure

In recent years, the notion of pressure for active matter systems, specifically dry active matter, has been an intensive field of study. Takatori et. al. [46] introduced the notion of

swim pressure using the following arguments. Given that active matter systems generate their self-motion using self-propulsion, such systems have a unique pressure, called active or swim pressure, that is athermal in origin.

2.3.2.1 Stress in Active Matter: Swim Pressure

In the following, we motivate the definition of swim pressure as it was introduced by Takatori in [46]. In general, we obtain an equation for the stress $\boldsymbol{\sigma}$ (or pressure) on a system, using the virial theorem, in terms of the forces acting on the system. The stress is given by

$$\boldsymbol{\sigma} = -\frac{1}{V} \left\langle \sum_i^N \mathbf{x}_i \mathbf{F}_i \right\rangle \quad (2.23)$$

where \mathbf{F}_i are the forces acting on the particle i , \mathbf{x}_i is the position of particle i , and V is the volume of the system. Suppose we have a particle in a fluid. We write the overdamped Langevin Equation as

$$-\zeta \mathbf{V}(t) + \mathbf{F}(t) = \mathbf{0} \quad (2.24)$$

where the drag is given by ζ , the particle velocity is \mathbf{V} , and \mathbf{F} is any force acting on the system. We write the position of the particle at time t as

$$\mathbf{x}(t) = \int \mathbf{V}(t') dt' \quad (2.25)$$

so that we can write the stress on a particle as

$$\boldsymbol{\sigma} = -n \langle \mathbf{x} \mathbf{F} \rangle = -n \zeta \int \left\langle \mathbf{V}(t') \mathbf{V}(t) \right\rangle dt' = -n \zeta D \quad (2.26)$$

where $n = N/V$ denotes the number density and the time integral of the velocity auto-correlation is the diffusivity of the particle, D . This shows that any particle undergoing any type of random motion exerts a pressure $\Pi = -tr \boldsymbol{\sigma} / 2 = n \zeta D$. This applies to any source of random motion and to particles of arbitrary shape. As an example, the source of random motion for Brownian motion is thermal energy, and we write the diffusivity as $D = k_B T$, and we recover the ideal-gas (Brownian osmotic) pressure law $\Pi^B = n k_B T$. This can be interpreted as a mechanical pressure resulting from the fluctuated motion of the solvent.

Similarly, this applies to active matter with diffusivity given by

$$D^{swim} = \frac{v_0^2 \tau_r}{6} \quad (2.27)$$

and we arrive to an swim pressure similar to an ideal-gas as

$$\Pi^{swim}(\phi \rightarrow 0) = \frac{n \zeta v_0^2 \tau_r}{6} \quad (2.28)$$

Now we define the swim stress using the virial theorem as

$$\boldsymbol{\sigma}^{swim} = -n \langle \mathbf{x} \mathbf{F}^{swim} \rangle \quad (2.29)$$

where we have taken the forces \mathbf{F}_i to be the swim force \mathbf{F}^{swim} , and the swim pressure is the trace of the swim stress. Eq. 2.29 defines the swim stress using the self-propulsive

force of a particle and the position of this particle. This is a crucial interpretation of swim force that gives a single-particle self contribution to stress, unlike the familiar inter-particle interactions of passive systems $-\langle \mathbf{x}_{ij} \mathbf{F}_{ij} \rangle$.

Additional recent work on the pressure of active systems include efforts by Solon et. al. [47]. They studied the mechanical pressure as a function of density for a system of spherical ABP. They show that the pressure is a state function and two terms contribute to it: the first is called passive or direct contribution to pressure known from passive systems and is given by Irving and Kirkwood stress tensor, and the other is a newly defined pressure term which is due to the slow down of particles that drive MIPS. In addition, they show that the pressure is independent from the particle-wall interaction. Moreover, Bialké et. al. use this definition of mechanical pressure to measure a negative interfacial tension associated with MIPS between two coexisting phases [42].

We now review a work presented by Solon et. al. [11] in 2018 which is crucial for our results in Chapter 4.

2.3.2.2 Phenomenological Hydrodynamic Description of Motility Induced Phase Separation

We describe a continuum description of non-aligning active particles interacting through isotropic interactions. The hydrodynamic description does not include the degrees of freedom corresponding to the particle orientations since they are fast. Thus we define the conserved density field $\rho(\mathbf{r}, t)$, obeying $\dot{\rho} = -\nabla \cdot \mathbf{J}$. The current \mathbf{J} vanishes in homogeneous phases, by symmetry. The gradients expansions of the current in density involves only odd terms under space reversal. We use at third order the following

$$\dot{\rho} = \nabla \cdot (M \nabla g[\rho]) \quad (2.30)$$

where $g[\rho]$ is given by

$$g[\rho] = g_0(\rho) + g_1[\rho] \quad \text{where} \quad g_1 = \lambda(\rho)(\nabla \rho)^2 - \kappa(\rho)\Delta \rho \quad (2.31)$$

Note that $g[\rho]$ cannot be written as a derivative of a free energy for general $\kappa(\rho)$ and $\lambda(\rho)$. Equations 2.30 and 2.31 present a simple generalization of the Cahn-Hilliard equation out of equilibrium. This generalization has been relevant for the phase separation of active particles. The free energy structure breaks down for generic functions $\lambda(\rho)$ and $\kappa(\rho)$, which do not satisfy $2\lambda(\rho) + \kappa'(\rho) = 0$. The gradient terms in g , thus, cannot be written as a functional derivative as follows

$$g_1[\rho] = \lambda(\rho)(\nabla \rho)^2 - \kappa(\rho)\Delta \rho \neq \frac{\delta F}{\delta \rho} \quad (2.32)$$

Correct coexisting densities are then not obtained from the common tangent construction on a free energy density defined through $f'(\rho) = g_0(\rho)$. However, one can write g as a functional derivative of a generalized free energy G with respect to a new non-trivial variable denoted by R , which depends on the functional forms of κ and λ . We define a one-to-one mapping $R(\rho)$ defined by

$$\kappa R'' = -(2\lambda + \kappa')R'c \quad (2.33)$$

g can now be written as a functional derivative with respect to R as

$$g = \frac{\delta G}{\delta R} \quad (2.34)$$

with

$$G = \int d\mathbf{r} G[\mathbf{R}] \equiv \int d\mathbf{r} \left[\phi(R) + \frac{\kappa}{2R'} (\nabla R)^2 \right] \quad (2.35)$$

where we have defined a generalized free energy density $\phi(R)$ such that

$$\frac{d\phi}{dR} = g_0 \quad \text{or alternatively} \quad \phi = \int^\rho g_0(\hat{\rho}) R'(\hat{\rho}) d\hat{\rho} \quad (2.36)$$

We can now write the dynamics of ρ as the derivative of a generalized free energy functional

$$\dot{\rho} = \nabla \cdot \left[M[\rho] \nabla \frac{\delta G}{\delta R} \right] \quad (2.37)$$

The structure of Eq. 2.37 is different from the equilibrium case since the functional derivative is taken with respect to R rather than ρ . Moreover, we can say that the dynamics is driven by gradients of a generalized chemical potential given by

$$g = \frac{\delta G}{\delta R} \quad (2.38)$$

We can also write the dynamics in 2.37 as to appear driven by the divergence of a generalized stress tensor, so that we can write the current \mathbf{J} as

$$\mathbf{J} = -M \nabla g = \frac{M}{R} \nabla \cdot \boldsymbol{\sigma} \quad (2.39)$$

and the tensor in Cartesian coordinates is given by

$$\sigma_{\alpha\beta} = - \left[h_0 + R g_1 - \frac{\kappa R'}{2} (\nabla \rho)^2 \right] \delta_{\alpha\beta} - \kappa R' (\partial_\alpha \rho) (\partial_\beta \rho) \quad (2.40)$$

where we have defined

$$h_0 = R \frac{d\phi}{dR} - \phi \quad (2.41)$$

Finally, we identify the diagonal coefficients of $\boldsymbol{\sigma}$, the normal stresses, with generalized pressures. We split $h = \sigma_{xx}$ into two contributions, one as a local function and the other as interfacial contribution

$$h = h_0(\rho) + h_1[\rho] \quad \text{where} \quad h_1 = R g_1 - \frac{\kappa R'}{2} (\nabla \rho)^2 + \kappa R' (\partial_x \rho)^2 \quad (2.42)$$

Note that $\boldsymbol{\sigma}$ and h here do not have any connection to momentum transfer and mechanics.

As a final remark, we can recover the equilibrium limit by setting $2\lambda + \kappa' = 0$ and Eq. 2.33 then shows that $R = \rho$ up to additive and multiplicative constants that do not play any role in phase equilibria and can thus be discarded. Hence, all the generalized quantities reduce to their equilibrium counterparts.

2.3.3 Chemical Potential

Lastly, some work has been done on the notion chemical potential in active matter systems. Takatori et. al. [40] describe an out of equilibrium definition of chemical potential by using mechanical arguments based on the swim pressure. This was done by generating a phase diagram with a spinodal and binodal. This attempt hints that we need a generalized thermodynamics in order to describe non-equilibrium systems and to predict phase coexistence. Additionally, Solon et. al. in 2018 [11] use a generalized thermodynamic description of the free energy to account for the binodal cure of MIPS. In Chapter 4, we use the formalism presented in [11] to test the definition of active pressure in our system.

As a final note, we have briefly reviewed some of the different approaches to the thermodynamics of active matter systems. In the literature, there is a plethora of different, sometimes contradicting, results on the definition and applicability of the presented thermodynamic variables. However, it is evident that it is an exciting route of research that will continue to grow and attract attention in the coming years.

Chapter 3

Attractive Active Brownian Particles

Essentially, all models are wrong,
but some are useful.

George E. P. Box

3.1 Introduction

Motivated by prominent literature of active systems with purely repulsive interactions, we add a layer of complexity by introducing attractive interactions between active particles. We study the phase behavior and kinetics using two different approaches. The first method is by setting a strength of attraction much larger than the strength of self-propulsion. This will result in clustering of particles. This phenomena is similar to clustering of particles found in some experiments [48]. Additionally, we try to make use of this model to study the kinetic of cluster-cluster aggregation. Our second approach in studying active matter with attraction is more fruitful, qualitatively, at least! We study the phase behavior of active particles with attraction for various strengths of attraction and we show that the phase behavior is reentrant as a function of activity as reported by [10].

3.2 Clustering and Kinetics

3.2.1 Model

In this section, we study the phase behavior of a well established minimal model of a two-dimensional system of N self-propelled particles modeled as disks in an area $L \times L$ with periodic boundary conditions. We identify the particles by the position vector \mathbf{r}_i of its center and a unit vector $\hat{\mathbf{n}}_i = (\cos(\theta_i), \sin(\theta_i))$ defining the the axis of self-propulsion, where θ_i is the orientation of the polar axis. We follow the model introduced by Fily et. al in [23] and modify the interaction forces to account for attractive interactions.

The dynamics is overdamped and is governed by the following equations

$$\partial_t \mathbf{r}_i = v_0 \hat{\mathbf{n}}_i + \mu \sum_{j \neq i} \mathbf{F}_{ij} \quad (3.1)$$

$$\partial_t \theta_i = \eta_i(t) \quad (3.2)$$

where v_0 denotes the single-particles self-propulsion speed and μ the mobility.

On the right hand side of Eq. (3.1), the first term, from the left side, is the self-propulsive force term, and the second term is the force of interaction between the particles. For simplicity, we neglect translational noise in Eq. (3.1). The angular dynamics is described in Eq. (3.2) and is controlled by Gaussian rotational noise $\eta_i(t)$ with zero mean and delta correlations in time

$$\langle \eta_i(t) \rangle = 0 \quad (3.3)$$

$$\langle \eta_i(t) \eta_j(t') \rangle = 2\nu_r \delta_{ij} \delta(t - t') \quad (3.4)$$

where ν_r denotes the rotational diffusion rate. The brackets in (4.7) and (4.8) denote an average over noise realizations of the stochastic components of random vectors from a Gaussian probability distribution.

Each disk i has a radius a_i , uniformly distributed with mean $a = 1$ from the interval $[0.8, 1.2]$. Fig. 3.1 illustrates a schematic representation of a self-propelled particle. The

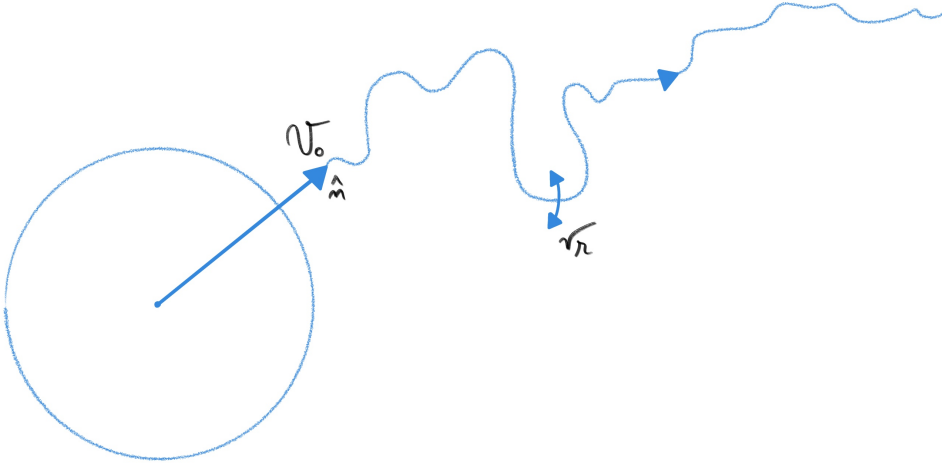


Figure 3.1: Schematic representation of a self-propelled particle

particles interact through the a modified repulsive forces introduced in Eq. (2.21)

$$\mathbf{F}_{ij} = \begin{cases} k(a_i + a_j - r_{ij})\hat{\mathbf{r}}_{ij} & \text{if } r_{ij} < 1.2 \times (a_i + a_j) \\ \mathbf{0} & \text{otherwise} \end{cases} \quad (3.5)$$

where we have extended the range of the force by extending the range of interaction from $a_i + a_j$ to $1.2 \times (a_i + a_j)$. Fig 3.2 shows a plot of the force of interaction between active particles.

In Eq. (3.5), $\hat{\mathbf{r}}_{ij} = (\mathbf{r}_i - \mathbf{r}_j)/r_{ij}$, where $r_{ij} = |\mathbf{r}_i - \mathbf{r}_j|$. We simulate the system in a square box of area L^2 with periodic boundary conditions. We adjust the size of the box L to obtain the desired packing fraction given by

$$\phi = \frac{\sum_i \pi a_i^2}{L^2} \quad (3.6)$$

In the following, we explain how we make the equations of motion dimensionless. We write the equation of motion in its x-component to illustrate the steps taken.

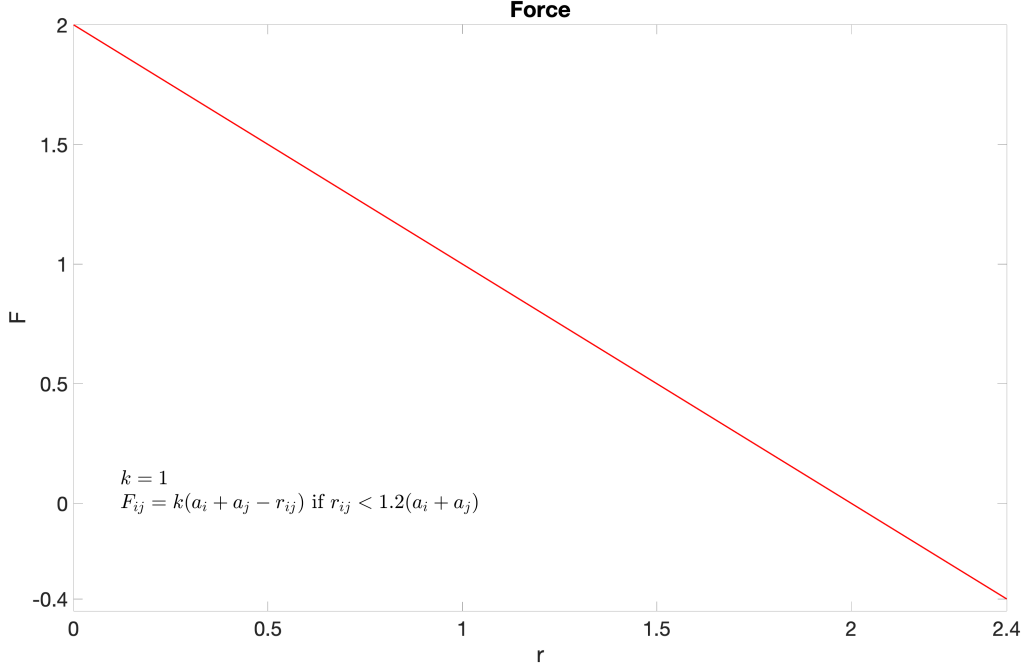


Figure 3.2: A plot of the force of interaction between attractive active particles

Starting from the following equation

$$\partial_t x_i = v_0 \cos(\theta_i) + \mu \sum_{j \neq i} k(a_i + a_j - r_{ij}) \left(\frac{x_i - x_j}{r_{ij}} \right) \quad (3.7)$$

- We use $a = 1$ and $(\mu k)^{-1} = 1$ as units of length and time, respectively
- We denote the new dimensionless variables with a prime
- $x' = \frac{x}{a} \Rightarrow x = ax'$
- $t' = \mu kt \Rightarrow t = \frac{t'}{\mu k}$

The equation becomes

$$a\mu k \times \partial_{t'} x'_i = a\mu k \times v_0 \cos(\theta_i) + a\mu k \times \sum_{j \neq i} \left(2 - \frac{ar'_{ij}}{a} \right) \left(\frac{x'_i - x'_j}{r'_{ij}} \right) \quad (3.8)$$

Accordingly, we define the scaled single-particle propulsion speed, which controls the overlap due to activity, as

$$\tilde{v} \equiv \frac{v_0}{a\mu k} \quad (3.9)$$

and the scaled rotational diffusion constant as

$$\tilde{\nu}_r \equiv \frac{\nu_r}{\mu k} \quad (3.10)$$

Furthermore, we define an important dimensionless parameter, called the Péclet number. The distance traveled by a free particle before it loses its orientation is denoted by Pe and is given by

$$Pe = \frac{v_0}{a\nu_r} = \frac{\tilde{v}}{\tilde{\nu}_r} \quad (3.11)$$

The following are the three time-scales contained in the model

- $\frac{a}{v_0}$ is the time needed for a particle to travel its own radius
- $\tau_r \equiv \frac{1}{\nu_r}$ is the orientation correlation time
- $\frac{1}{\mu k}$ is the elastic time scale

In the following, we will explain the computational approach used to integrate the equations of motion numerically.

3.2.2 Computational Approach Throughout the Thesis

We often encounter the following ordinary differential equation (ODE) when we simulate dynamical systems

$$\frac{dx}{dt} = f(t, x) \quad (3.12)$$

where we define a function f with arguments time t and state x . Note that in our model, the function f is independent of time. However, we proceed by keeping time for generality. In order to solve the differential equation, we need to specify some initial conditions, *i.e.* $x(t = 0)$ and propagate x forward in time at a fixed time interval, which we denote by Δt . Hence, we need to update the current position $x(t)$ to $x(t + \Delta t)$.

Doing a Taylor expansion on $f(t, x)$, we get

$$\begin{aligned} f(t + \Delta t, x + \Delta x) = & f(t, x) + \frac{\partial f}{\partial t} \Delta t + \frac{\partial f}{\partial x} \Delta x + \frac{1}{2!} \frac{\partial^2 f}{\partial t^2} \Delta t^2 \\ & + \frac{1}{2!} \frac{\partial^2 f}{\partial t \partial x} \Delta t \Delta x + \frac{1}{2!} \frac{\partial^2 f}{\partial x \partial t} \Delta x \Delta t + \frac{1}{2!} \frac{\partial^2 f}{\partial x^2} \Delta x^2 + \dots \end{aligned} \quad (3.13)$$

The simplest method to solve an ODE is the forward *Euler* method. It is given by looking at the the right hand side of Eq. (3.13) and picking only the first two terms from the left. Hence writing the forward method in terms of x gives

$$x(t + \Delta t) = x(t) + \frac{dx}{dt} \Delta t = x(t) + f \Delta t \quad (3.14)$$

The forward *Euler* method neglect high order terms (Δt^2 and above). Hence it is first order accurate.

We use this formula to integrate the rotational dynamics Eq. (3.2) as

$$\theta(t + \Delta t) = \theta(t) + \sqrt{2\nu_r} \times \text{Gaussian Distribution} \times \sqrt{\Delta t} \quad (3.15)$$

To solve the overdamped Langevin equation, Eq. (3.1), we implement a second order *Runge-Kutta* method given by

$$\begin{aligned} k_1 &= \Delta t f \\ k_2 &= \Delta t f(t + \Delta t/2, x(t) + k_1/2) \\ x(t + \Delta t) &= x(t) + k_2 \end{aligned} \quad (3.16)$$

Note however that in our Langevin equation, f is independent of time t and depends on the two-dimensional coordinates x and y .

By using a second order *Runge-Kutta* method, we obtain a second order accuracy because we include terms of order two. We prove it by showing that the coefficient k_2 is approximated using a Taylor series

$$\begin{aligned} x(t + \Delta t) &= x(t) + \Delta t f + \Delta t^2 \left[\frac{\partial f}{\partial t} + \frac{\partial f}{\partial x} f + \dots \right] \\ &= x(t) + \Delta t \frac{dx}{dt} + \frac{\Delta t^2}{2} \frac{d^2x}{dt^2} + \dots \end{aligned} \quad (3.17)$$

Hence we can write k_2 as

$$\begin{aligned} k_2 &= \Delta t f(t + \Delta t/2, x + k_1/2) \\ &= \Delta t \left[f + \frac{\Delta t}{2} \frac{\partial f}{\partial t} + \frac{k_1}{2} \frac{\partial f}{\partial x} + \dots \right] \\ &= \Delta t \left[f + \frac{\Delta t}{2} \frac{\partial f}{\partial t} + \frac{\Delta t}{2} \frac{\partial f}{\partial x} f + \dots \right] \end{aligned} \quad (3.18)$$

So in this way we can see that second order terms are captured in a second order *Runge-Kutta* method.

As a final note, in our integration scheme, we treat self-propulsion as a constant and do not evolve its value in time. A first order correction would be by implementing the following update equation:

$$\int_t^{t+\Delta t} v_{0,i}(t) dt = \frac{v_{0,i}(t) + v_{0,i}(t + \Delta t)}{2} \Delta t \quad (3.19)$$

The diagram in Fig. 3.3 summarizes the algorithm for integrating the equations of motion.

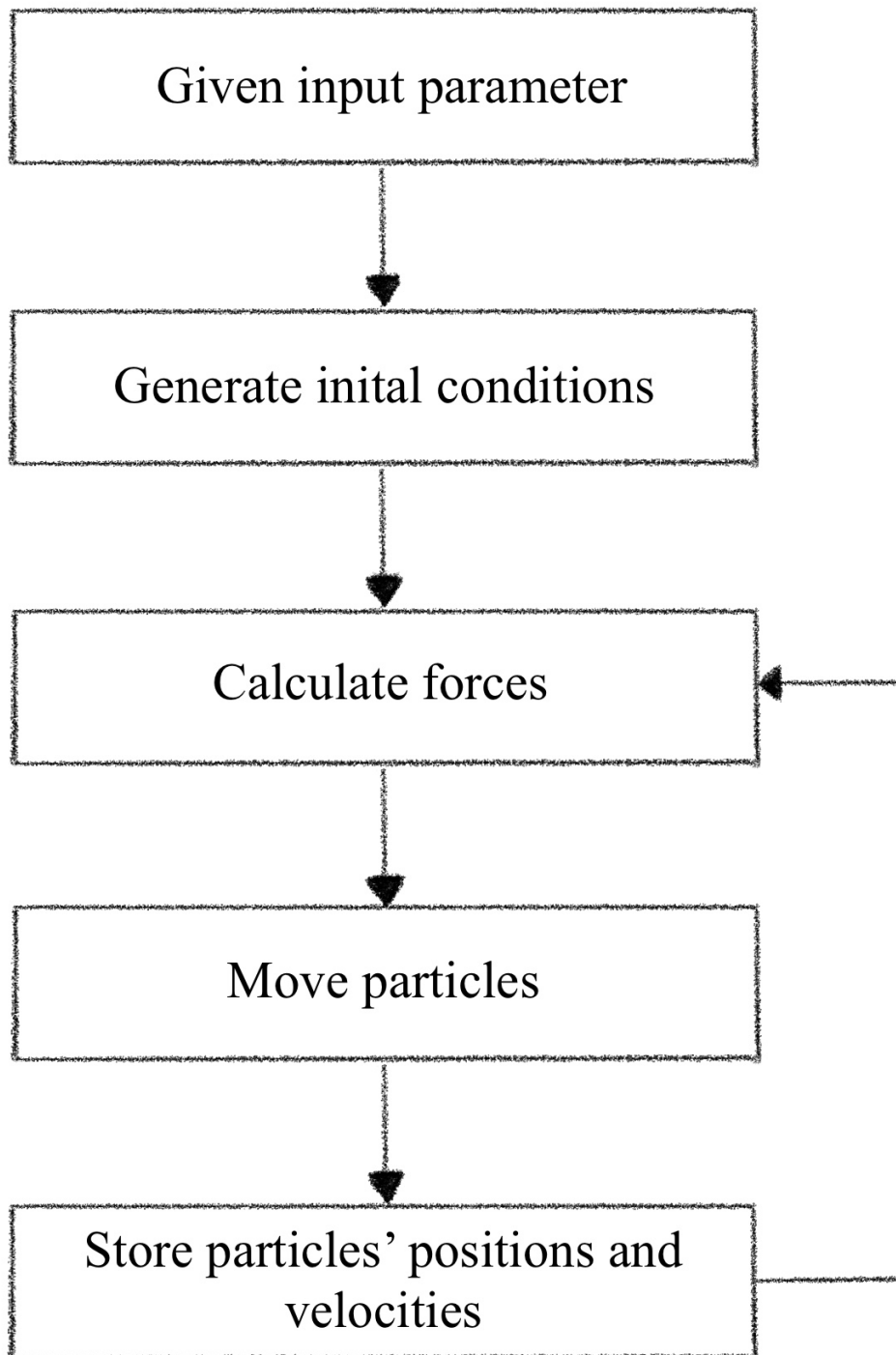


Figure 3.3: Diagram summarizing the numerical integration algorithm

The most time-consuming part of our simulation is the force calculation. In a typical pairwise additive forces interactions, in order to compute forces of interactions, to calcu-

late the force on particle i , we need to consider the contribution to the force from all its neighbors. This means we have to compute $N(N-1)/2$ pair distances. This suggests that if we do not optimize our algorithm, the evaluation of forces time scales as N^2 . Several efficient techniques exist to speed up this calculation in such a way that the time scales as $N^{3/2}$ [49]. Some of the techniques are

1. Verlet list
2. Cell of linked list
3. Combination of Verlet and cell lists

In our simulations, we use the Verlet list method to speed up our calculations. Given a simulation of some system, by using a cutoff that is smaller than the simulation box, while calculating the force on a particle i , several particles will not contribute to this force. Hence, it is crucial not to include particles that do not interact with particle i from the force calculation. For this reason, we use a Verlet list or neighbor list, which is illustrated in Fig. 3.4. We introduce a second cutoff radius denoted by r_v , which is greater than the interaction radius r_c . Before doing the force calculation, we make a list of all the neighboring particles of particle i , within a radius r_v . In the next calculation, only the particles in the Verlet list have to be considered for calculating the interaction forces. So far we have not saved any CPU time. We gain the time when we calculate the next interactions. We next calculate the displacement of particles, if the maximum displacement is less than $r_v - r_c$, then we only consider the particles in the Verlet list of particle i . Once any particle is displaced more than $r_v - r_c$, we need to update the Verlet list. This update operation is of order N^2 . However, this step is not performed each time. Hence, the use of the Verlet list in our simulation is important to reduce the computing time scale from N^2 to $N^{3/2}$.

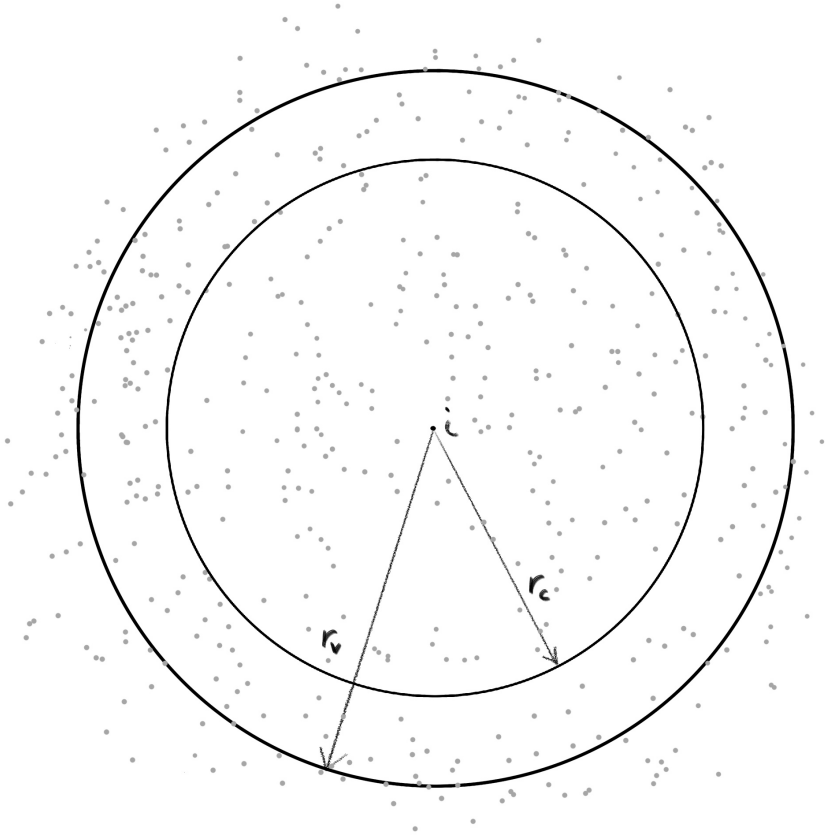


Figure 3.4: The Verlet list: particle i interacts with particles within the interaction radius r_c . The Verlet list contains all particles within a radius $r_v > r_c$

The free parameters in our system are the following: the scaled rotational diffusion constant $\tilde{\nu}_r$, the scaled single-particle propulsion speed \tilde{v} , and the packing fraction ϕ . We study the phase behavior of our system by fixing the value to $\tilde{\nu}_r = 5 \times 10^{-4}$ and vary the self-propulsion speed and the packing fraction. In the simulations of this model, we set $N = 2000$ particles and we run our simulations to $t_f \gg \tau_r$, where $\tau_r = \tilde{\nu}_r^{-1} = 2000$ is the rotational relaxation time. We choose our integration time step in such a way that it is much smaller than \tilde{v} . Quantities of interest are averaged over N and over time for the mean squared displacement and for the number fluctuation calculations, respectively.

3.2.3 Mean Squared Displacement

In order to quantify the phase behavior of active particles, it is constructive to evaluate numerically the mean squared displacement (MSD), in the center of mass frame, defined as:

$$\langle [\Delta r(t)]^2 \rangle = \frac{1}{N} \sum_i [\mathbf{r}_i(t) - \mathbf{r}_i(0)]^2 \quad (3.20)$$

Since momentum is not conserved, the center of mass is not fixed and moves with a drifting velocity \mathbf{v}_{CM} . We subtract this contribution from the MSD by calculating it in the center of mass frame. We can write the MSD of a single self-propelled particle

performing a random walk. The MSD is given by:

$$\langle [\Delta r(t)]^2 \rangle = 4D_0 \left[t + \frac{e^{-\nu_r t} - 1}{\nu_r} \right] \quad (3.21)$$

where $D_0 = \frac{v_0^2}{2\nu_r}$ is the diffusion coefficient. At short time scales, the MSD is ballistic and it grows as t^2 . At larger time scales such as $t \gg \tilde{\nu}_r^{-1}$, the MSD is diffusive and $\langle [\Delta r(t)]^2 \rangle \sim 4D_0 t$.

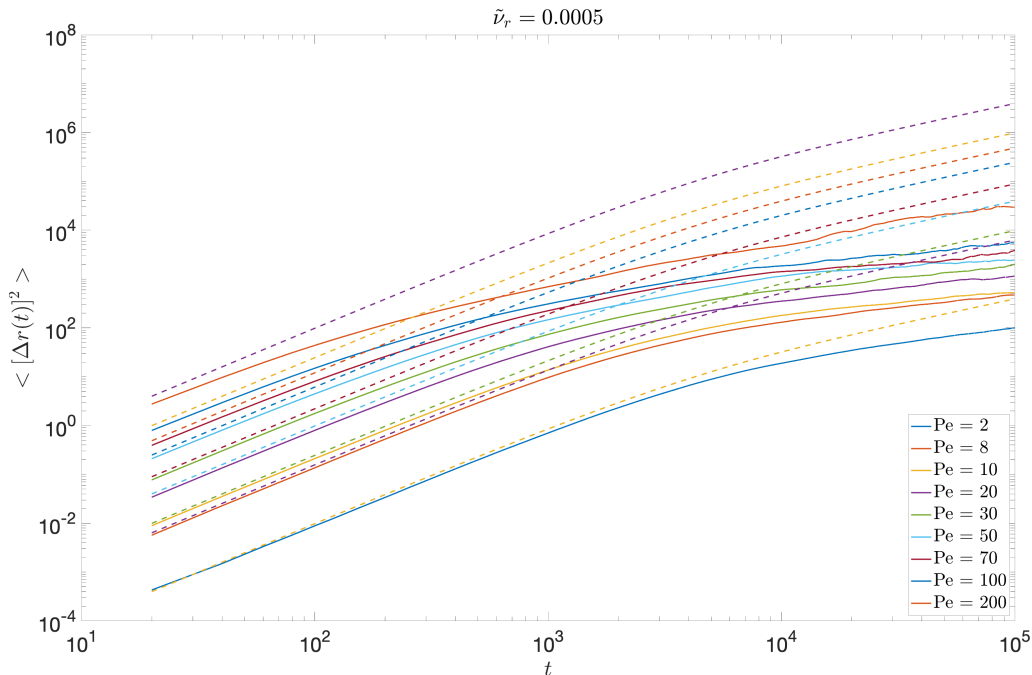


Figure 3.5: Mean square displacement for $\tilde{\nu}_r = 0.0005$, $\phi = 0.1$ for various values of Pe . The dashed lines correspond to the theoretical MSD that a single particle performs. At short time, the dashed lines correspond to slope of 2 (ballistic) and at large times, the dashed lines correspond to slope of 1 (diffusive).

Fig. 3.5 is a loglog plot of the MSD as a function of time, a fixed packing fraction $\phi = 0.1$, for various Pe . The phase behavior of the particles is shown in the first column of Fig. 3.7. In the MSD plot, the dashed lines correspond to the MSD performed by a single self-propelled particle using Eq. 3.21. The simulations data show ballistic show time behavior. However, the long time behavior is slowed down due to clustering of particles that move with $\mathbf{v}_{CM} = \frac{1}{N} \sum_i \tilde{\mathbf{v}}$.

3.2.4 Giant Number Fluctuations

In order to identify phase separation in our simulations, we measure the number fluctuations $\langle [\Delta N^2] \rangle$, which is the spatial variance of the number of particles in a sub-box as a function of the average N_s of particles in the sub-box. We divide our quadratic domain of size L into b^2 sub-domains (or boxes) of size $\frac{L}{b}$. We calculate the average number of particles $\langle N \rangle$ and the standard deviation for each size. The spatial variance is given by:

$$\langle [\Delta N]^2 \rangle = \langle N^2 \rangle - \langle N \rangle^2 \quad (3.22)$$

A power law given by

$$\langle[\Delta N^2]\rangle = N_s^\beta \quad (3.23)$$

is observed for large sub-domains, with $\beta = 1$ corresponds to the equilibrium (ideal gas) limit and $\beta > 1$ corresponds to phase separated regions.

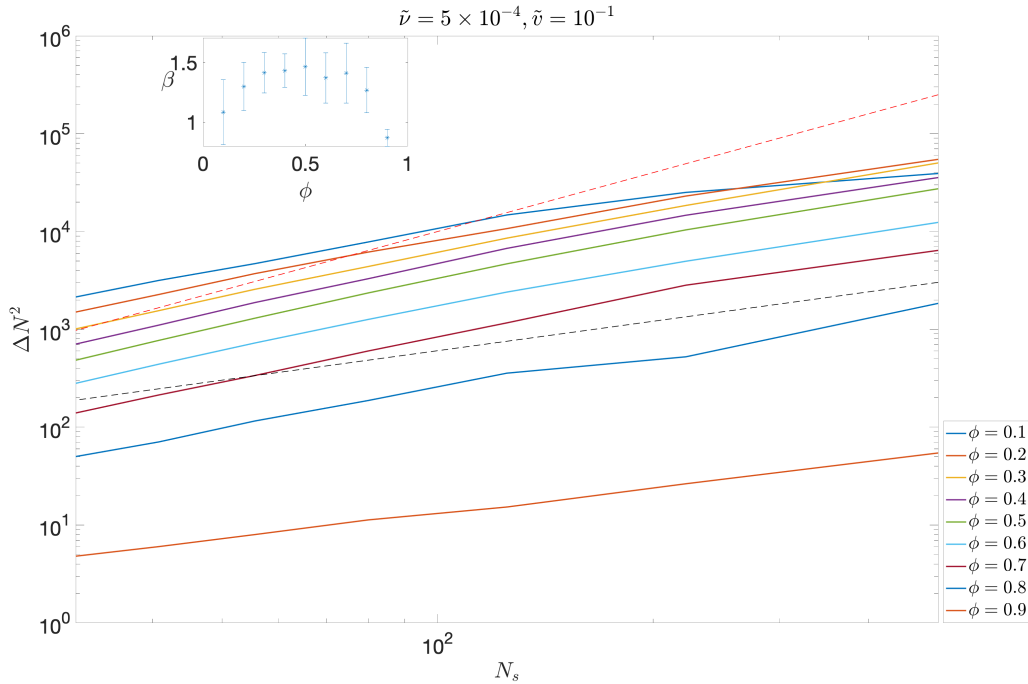


Figure 3.6: Number fluctuations for $\tilde{\nu}_r = 0.0005$, $\tilde{\nu} = 0.1$ corresponding to $Pe = 200$, for various values of ϕ . The dashed lines correspond to slopes 1 (black) and 2 (red). Inset: the values of β obtained by the power-law fit $\Delta N^2(N_s) \sim N_s^\beta$ for the data at large N_s .

Fig. 3.6 show the results of a loglog plot of the number fluctuations calculations for various packing fractions, at fixed $Pe = 200$ corresponding to $\tilde{\nu}_r = 0.0005$ and $\tilde{\nu} = 0.1$. The dashed lines correspond to slopes 1 (ideal gas) and 2 (phase separated). The inset shows the value of β obtained by the power law fit of Eq. 3.23 of the data. Error bars are obtained as the error on the slope. Phase separating regions show large number fluctuations corresponding to $\beta > 1$, as shown in the inset. The t_f particle configurations are shown in the phase diagram in Fig. 3.7. The first row from above ($Pe = 200$) correspond to the various packing fractions ($\phi = 0.1 - 0.6$) of the number fluctuations calculations.

3.2.5 Long Time Behavior Configurations

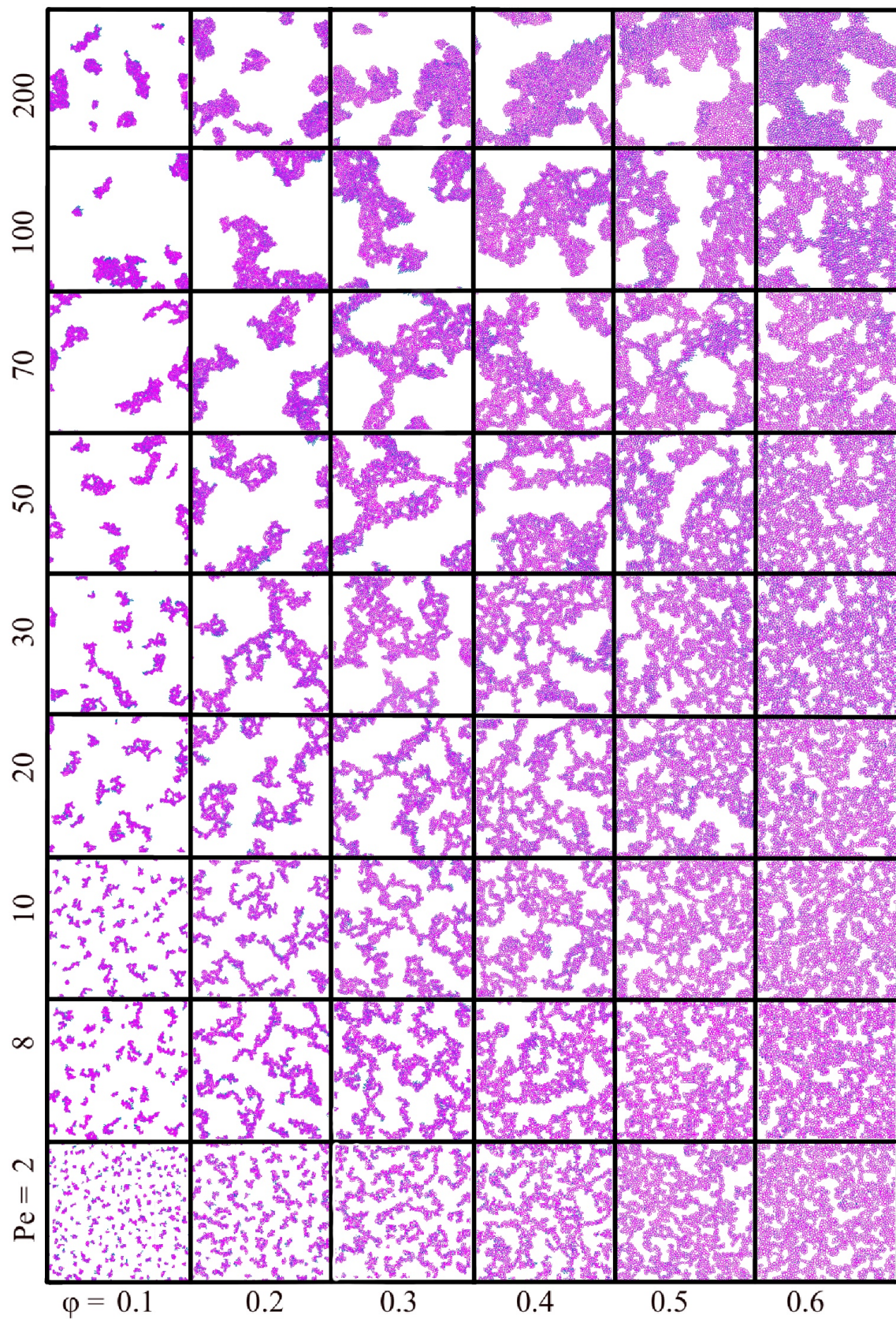


Figure 3.7: Phase diagram of active particles as function of Péclet and packing fraction at t_f

3.2.6 Kinetics of Cluster-Cluster Aggregation

In order to gain some knowledge about the structure and kinetics of our clusters, we measure, at low packing fractions, the structure factor, which is given by [50]:

$$S(q) = \frac{1}{N} \left\langle \sum_{j,k=1}^N e^{-i\vec{q} \cdot (\vec{r}_j - \vec{r}_k)} \right\rangle \quad (3.24)$$

where \vec{q} denotes the wave vector, which is an integer multiple of $\frac{2\pi}{L}$. The density fluctuations probed by $S(q)$ have a wave vector \vec{q} . Angular brackets represents an average over non-equilibrium stationary state. In general, the wave vector \vec{q} is on a square grid and takes positive and negative values. Since our system is inherently disordered, we take the limit of an infinite system and assume we have rotational symmetry. We then expect the structure factor to be a function of the modulus of the scattering vector. By angular averaging over the complex exponential, we obtain the Debye scattering function. Averaging over different directions gives the Bessel function of the first kind. The structure factor as function of the scalar $q > 0$ simplifies to:

$$S(q) = \frac{1}{N} \sum_{j,k} J(0, qr_{jk}) \quad (3.25)$$

where r_{ij} is the scalar distance between particle j and particle k , $|\mathbf{r}_j - \mathbf{r}_k|$ and $J(0, z)$ is the Bessel function of the first kind evaluated at $z = qr_{jk}$.

As a note on our calculation scheme, we assumed spherical symmetry, which is a crude assumption. The proper way of calculating the structure factor is by averaging over wave vectors in the x and y directions.

Since we set our radius $a = 1$, our diameter is 2. So the position of the first peak in $S(q)$ reflecting interparticle distance that usually occurs at $q_* = 2\pi$ will occur in our system at $q_* = \pi$. The sharpness of the peak indicates how pronounced ordering is. For phase separation due to clustering, we expect the intensity of the peak to grow with time. We make use of the static structure to estimate some properties of our clusters. For instance, the position of the peak indicates the separation between clusters. Moreover, we make a crude assumption that the intensity of the peak gives us the number of particles in a cluster. In this way, we measure the maximum number of particles in a cluster over time, and we compare our results to a previously established theory on cluster-cluster aggregation [51]. We define $M(t)$ to be the average number of particles in a cluster as a function of time. Following [51], we write $M(t) = t^\gamma$, with $\gamma = 0.5$. Note that we will stick to cluster aggregation at low packing fractions because aggregation is harder to characterize when we have a percolating cluster at high packing fractions.

In the following, we present some of our results from the structure factor calculation.

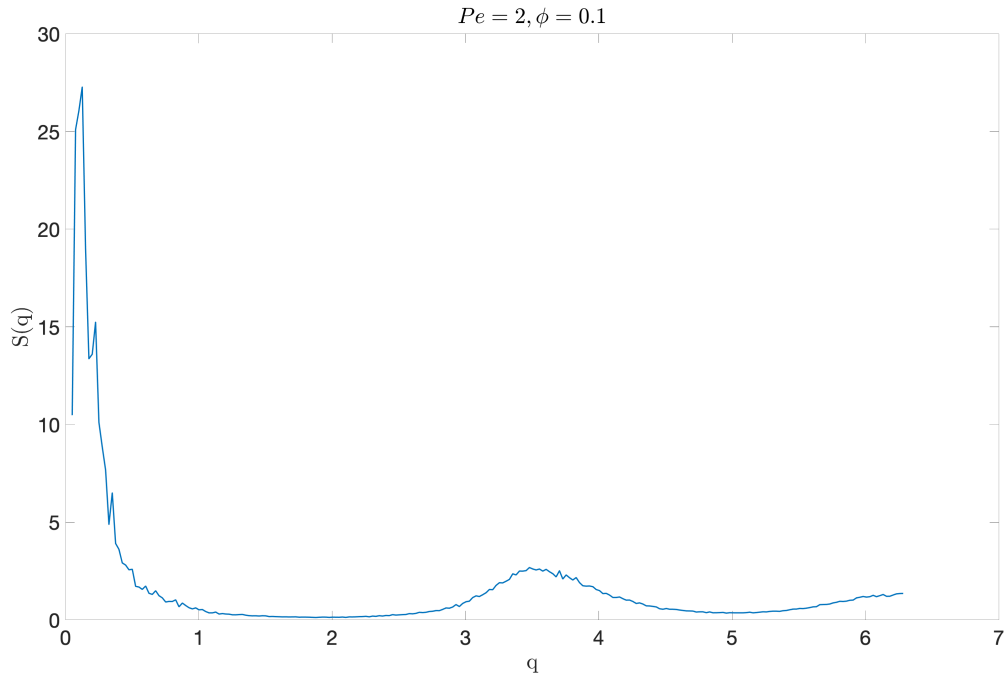


Figure 3.8: Structure factor at t_f for $\tilde{\nu}_r = 0.0005$, $\phi = 0.1$, and $Pe = 2$.

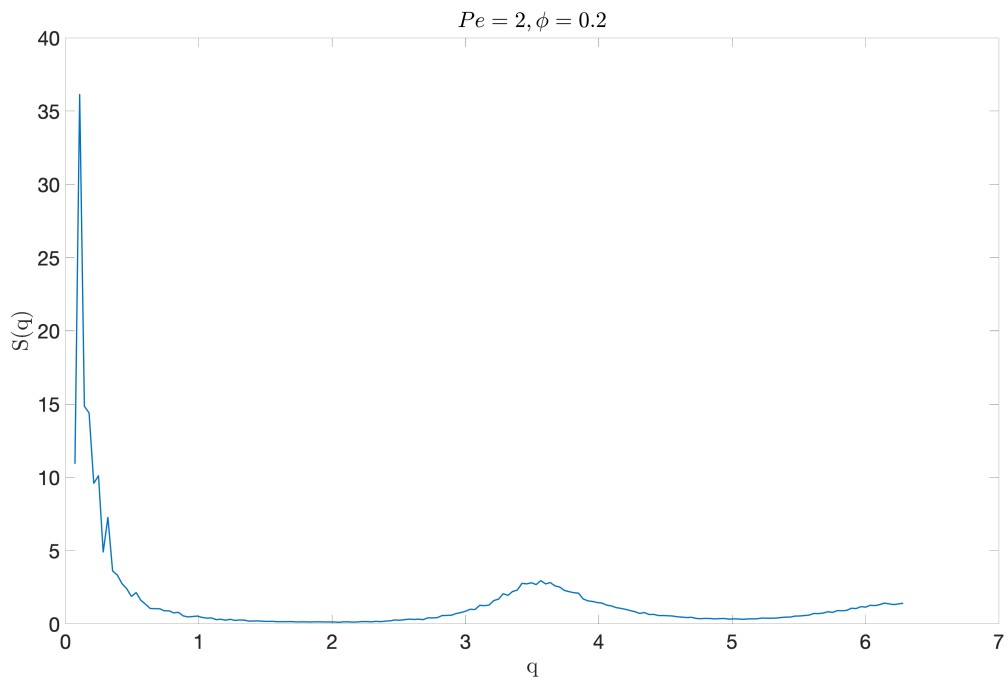


Figure 3.9: Structure factor at t_f for $\tilde{\nu}_r = 0.0005$, $\phi = 0.2$, and $Pe = 2$.

Figures 3.8 and 3.9 show the structure factor, at t_f and $Pe = 2$, for packing fractions 0.1 and 0.2, respectively. The graphs show that the intensity of the highest peak is larger at $\phi = 0.2$ than at $\phi = 0.1$. This is expected as we expect bigger cluster sizes at higher densities.

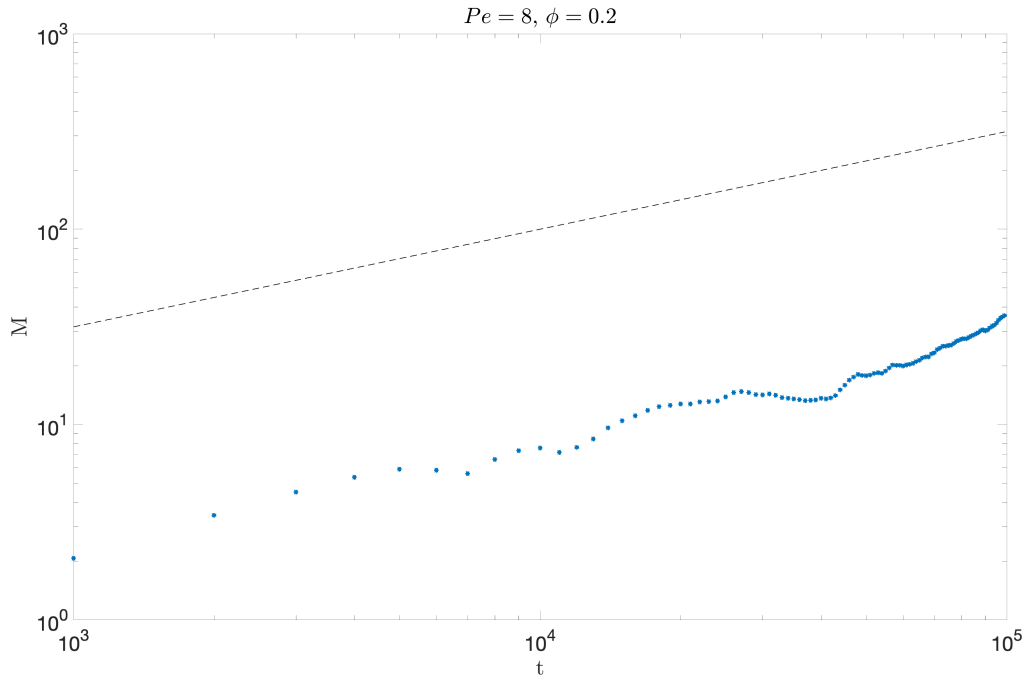


Figure 3.10: Number of particles in a cluster as a function of time for $\tilde{\nu}_r = 0.0005$, $\phi = 0.2$, and $Pe = 8$. The dashed line corresponds to a slope of 0.5

Fig. 3.10 is a loglog plot of the number of particles in a cluster as a function of time. A power fit gives an exponent $\gamma = 0.576 \pm 0.025$.

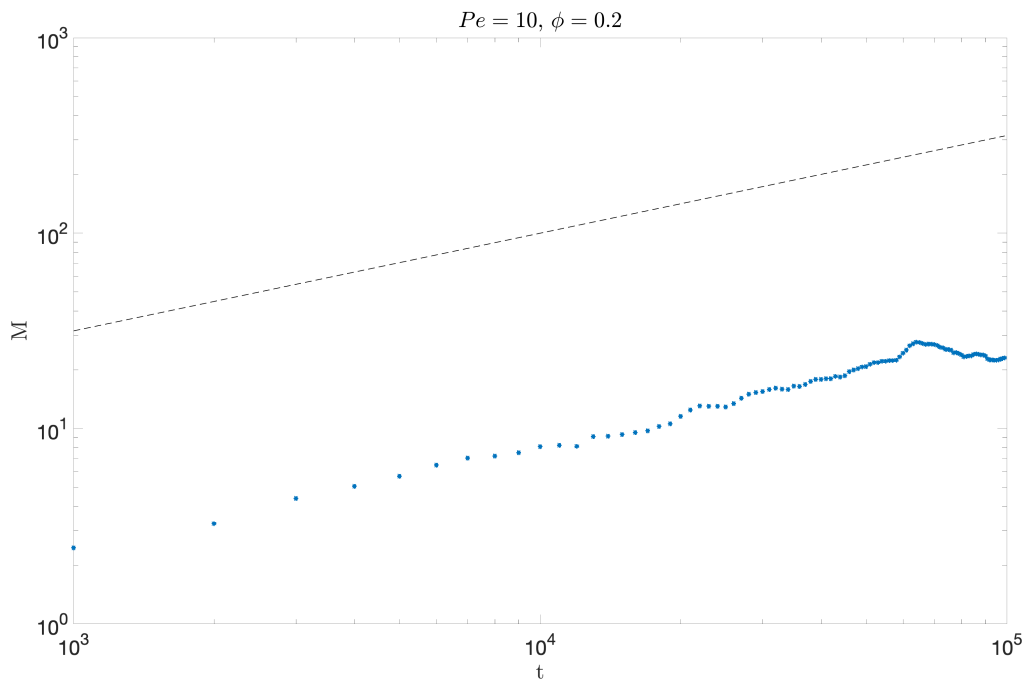


Figure 3.11: Number of particles in a cluster as a function of time for $\tilde{\nu}_r = 0.0005$, $\phi = 0.2$, and $Pe = 10$. The dashed line corresponds to a slope of 0.5

Fig. 3.11 is a loglog plot of the number of particles in a cluster as a function of time

for $\phi = 0.2$, and $Pe = 10$. A power law fit gives an exponent $\gamma = 0.534 \pm 0.022$.

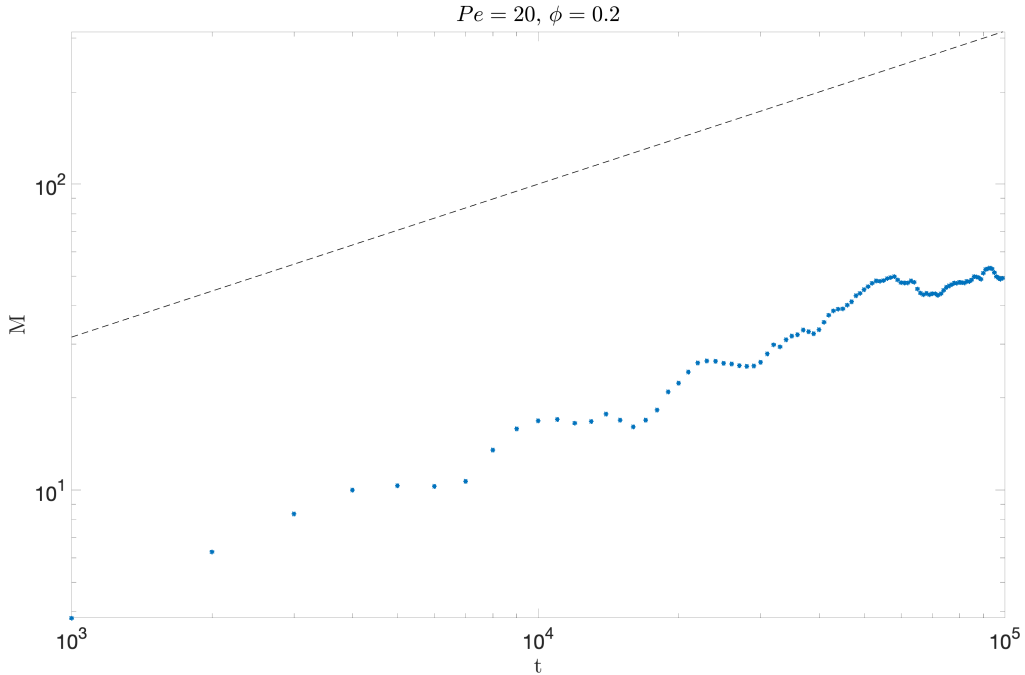


Figure 3.12: Number of particles in a cluster as a function of time for $\tilde{\nu}_r = 0.0005$, $\phi = 0.2$, and $Pe = 20$. The dashed line corresponds to a slope of 0.5

Fig. 3.12 is a loglog plot of the number of particles in a cluster as a function of time for $\phi = 0.2$, and $Pe = 20$. A power law fit gives an exponent $\gamma = 0.571 \pm 0.021$.

Another important calculation that can be deduced from the structure factor is the time evolution of the characteristic domain size $\mathcal{L}(t)$, which can be obtained from the inverse of the first moment of the structure factor as follows [30]:

$$\mathcal{L}(t) = 2\pi \left[\frac{\int_{\frac{2\pi}{L}}^{q_{cut}} q S(q, t) dq}{\int_{\frac{2\pi}{L}}^{q_{cut}} S(q, t) dq} \right]^{-1} \quad (3.26)$$

where L and q_{cut} denote the size of the box and the upper cut-off taken to be the minimum in $S(q)$, respectively. $\mathcal{L}(t) \sim t^\alpha$ is a power-law growth of the domain size, which is expected from classical models of phase separation kinetics. In general, the exponent is dependent on the transport mechanism of the system. An exponent of $1/3$ is expected for phase separating diffusive systems neglecting hydrodynamics [52]. We will next show that we obtain an exponent $\alpha < 1/3$.

The velocity of the center of mass of the cluster is given by:

$$\mathbf{v}_{CM} = \frac{1}{M} \sum_{i=1}^M \tilde{\mathbf{v}}_i \quad (3.27)$$

So that we can write

$$\langle v_{CM}^2 \rangle = \frac{1}{M^2} M \tilde{v}^2 = \frac{\tilde{v}^2}{M} \quad (3.28)$$

Recall that the diffusion coefficient for a single particle is given by:

$$D_0 = \frac{v_0}{2\nu_r} \quad (3.29)$$

So that we can write the effective diffusion coefficient for a cluster as:

$$D_{eff} = \frac{\tilde{v}_{CM}^2}{2\nu_r} = \frac{\tilde{v}^2}{2\nu_r M} \quad (3.30)$$

The size of a compact cluster grows with the size of the box, $M \sim L^2 \equiv \mathcal{L}$. Hence when we have $M(t) = t^{0.5}$, we predict

$$\mathcal{L}(t) = t^{0.25} \quad (3.31)$$

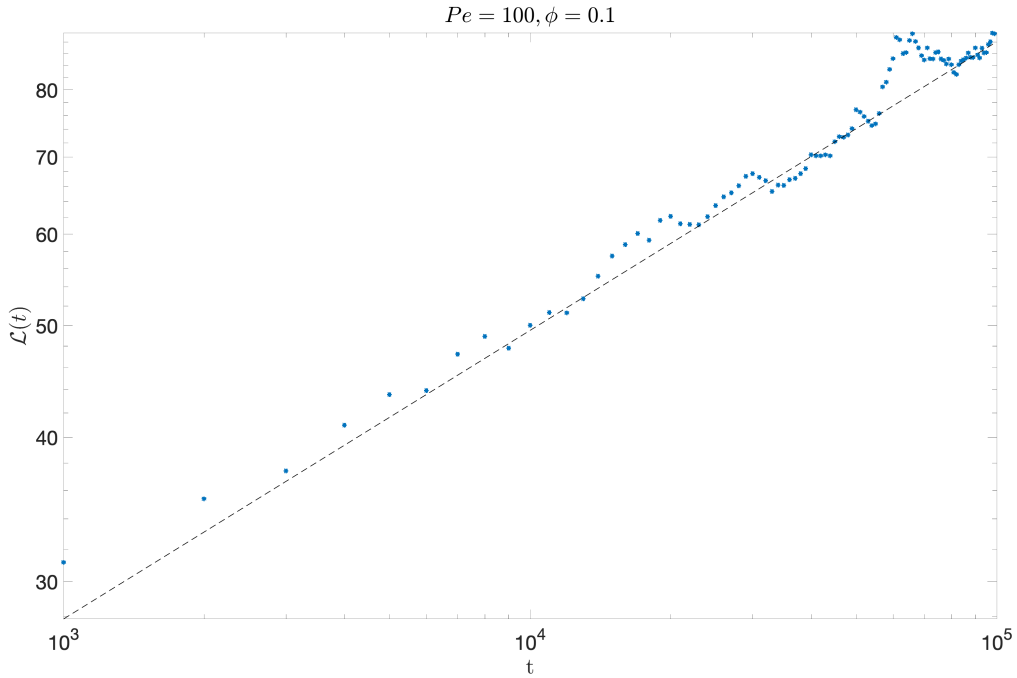


Figure 3.13: Time-dependent domain length $\mathcal{L}(t)$ for $\tilde{\nu}_r = 0.0005$, $\phi = 0.1$, and $Pe = 100$. The dashed line corresponds to a slope of 0.25

Fig. 3.13 is a loglog plot of the domain length as a function of time for $\phi = 0.1$, and $Pe = 100$. A power law fit gives an exponent $\alpha = 0.246 \pm 0.008$.

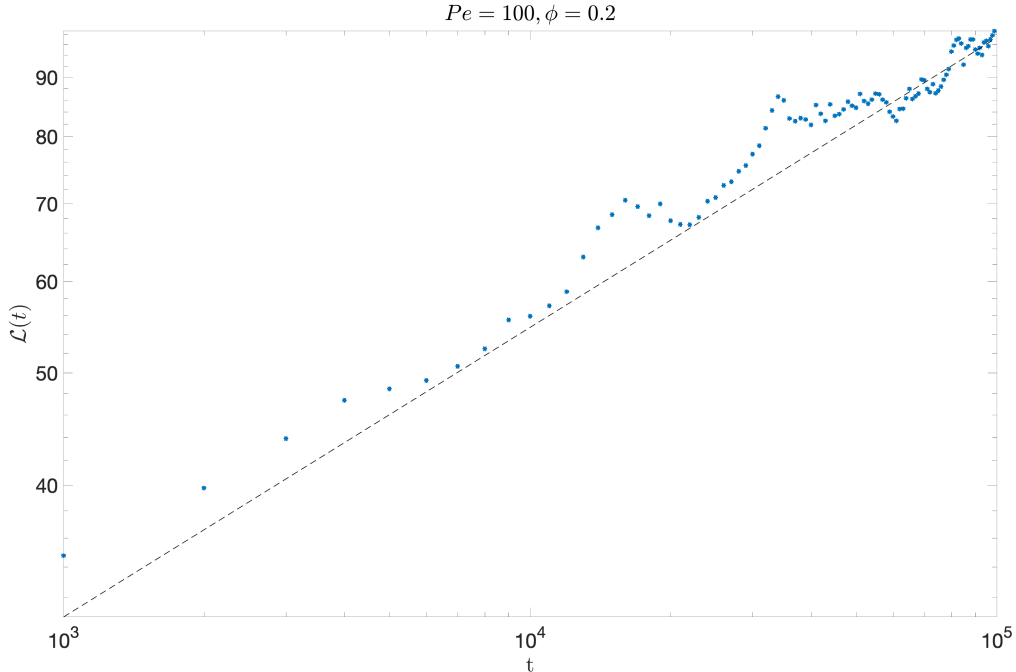


Figure 3.14: Time-dependent domain length $\mathcal{L}(t)$ for $\tilde{\nu}_r = 0.0005$, $\phi = 0.2$, and $Pe = 100$. The dashed line corresponds to a slope of 0.25

Fig. 3.14 is a loglog plot of the domain length as a function of time for $\phi = 0.2$, and $Pe = 100$. A power law fit gives an exponent $\alpha = 0.226 \pm 0.008$.

As a final note, by looking at the phase diagram in Fig. 3.7, it is evident that the t_f configurations at low Pe correspond to the configurations we obtain at small time scales for large Pe . In other words, if we run the small Pe regime for longer simulation times, we expect to see a kinetically evolving cluster similar to what is shown in Fig. 3.7 for large Pe .

3.3 Reentrant Phase Behavior

3.3.1 Model

In this section, we study the phase behavior of a minimal model of N self-propelled particles modeled as disks in an area $L \times L$ with periodic boundary conditions. We follow the definition of the model introduced in Subsection 3.2.1 and we use the same overdamped Langevin Eqs. 3.1 and 3.2. Redner et. al. showed in [10] that the phase behavior of active particles experiencing short-range attraction is reentrant as a function of activity. In other words, a homogeneous fluid exists between two phase separating regions that occur at low and high activity regimes. For simplicity, they use the standard Lennard-Jones (LJ) potential. However, we investigate this reentrance behavior using the following force:

$$\mathbf{F}_{ij} = \begin{cases} k(a_i + a_j - r_{ij})\hat{\mathbf{r}}_{ij} & \text{if } r_{ij} < a_i + a_j \\ (2 - r_{ij})(1 + \frac{2-r_{ij}}{\delta})\hat{\mathbf{r}}_{ij} & \text{if } r_{ij} > a_i + a_j \text{ and } r_{ij} < a_i + a_j + \delta \end{cases} \quad (3.32)$$

where a_i and δ denote the radius of particle i and the width of the potential, respectively. The force $F_{ij} = 0$ otherwise. The particles in this model are monodispersed, each having

a size $a = 1$. δ sets our attraction strength, which we define as $\frac{\delta}{4}$. Fig. 3.15 shows the attractive force, for various δ . The depth of the force sets our attraction strength.

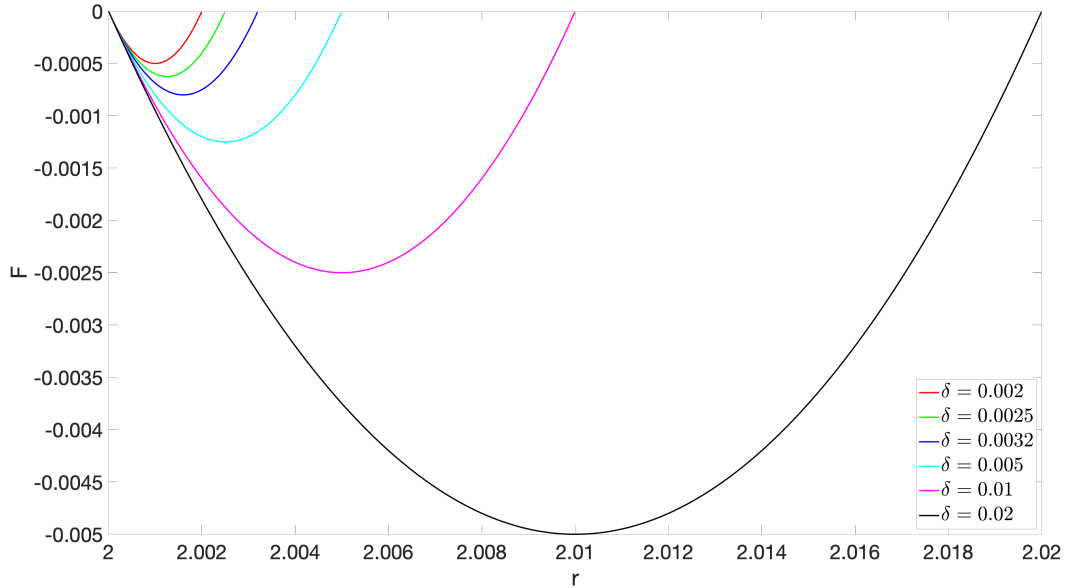


Figure 3.15: Plot of the quadratic attractive force for various δ

In our simulations, we fix $N = 815$ and L in such a way to obtain a packing fraction $\phi = 0.4$ as in [10]. At this density, for high enough Pe , a system of purely repulsive self-propelled particles undergo athermal phase separation. We set rotational diffusion $\tilde{\nu}_r = 0.0005$. For each strength of attraction, we explore the phase diagram by varying $\tilde{\nu}$, which sets our Pe . We choose the values of self-propulsion in such a way that we scan the range of $\tilde{\nu} \ll$ attraction strength, $\tilde{\nu} \sim$ attraction strength, and $\tilde{\nu} \gg$ attraction strength. In the following, we show particle configurations at t_f for various Pe and attraction strength. To identify the intermediate homogeneous phases, we measure the number fluctuations and report that homogeneous states have $\beta \sim 1$, while phase separated regions have $\beta > 1$. Note that since we are only using $N = 815$ particles, this resulted in poor averaging of the number fluctuations. As a consequence, while fitting ΔN^2 to a power law, we excluded anomalous points from our fitting, which resulted in large error bars for some exponents. It will be evident from the particles phases, that phase separated regions at low Pe correspond to phase separation due to attractive interactions since $\tilde{\nu} \ll$ attraction strength. This results in phase separation due to clustering. Particles form percolating clusters and need much longer simulation time to form one big cluster. This is due to slow kinetics caused by small self-propulsion. However, phase separation at large Pe occurs for $\tilde{\nu} \gg$ attraction strength. The resulting phase separation is then similar to the one induced by MIPS. Further attempts to characterize the dynamics of reentrance were using MSD calculations. However, these calculations were not very informative; they just show a cross-over from ballistic to diffusive behavior. Hence, we switched to structure factor calculations to study the kinetics of reentrance. Nevertheless, we do not show the corresponding results and we leave it for future work. Note that in the MSD results shown below have an anomalous behavior at short times for small Pe . We have investigated the cause of this behavior. It is just the left over of initial relaxation time due to particle overlaps from initial conditions. Since the low Pe limit in this model

correspond to very small \tilde{v} , we need to run the simulations for longer times than the previous model for particles to relax. A faster way of getting rid of this anomaly is by calculating MSD from a different moment in time. In other words, instead of measuring MSD from $t(0)$, we measure it from a later time, say $t(5)$.

3.3.2 Attraction Strength = 0.005

Particles configurations for various Pe are shown in Fig. 3.16. This strength of attraction resulted in clustering and phase separation for all the Pe numbers we have investigated.

3.3.3 Attraction Strength = 0.0025

Particles configurations for various Pe are shown in Fig. 3.17. Number fluctuations calculations in Fig. 3.18 show an exponent $\beta = 0.97 \pm 0.14$ at $Pe = 40$.

3.3.4 Attraction Strength = 0.00125

Particles configurations for various Pe are shown in Fig. 3.20. Number fluctuations calculations in Fig. 3.21 show an exponent $\beta = 0.99 \pm 0.18$ at $Pe = 20$.

3.3.5 Attraction Strength = 0.0008

Particles configurations for various Pe are shown in Fig. 3.23. Number fluctuations calculations in Fig. 3.24 show an exponent $\beta = 0.93 \pm 0.17$ at $Pe = 11.2$.

3.3.6 Attraction Strength = 0.000625

Particles configurations for various Pe are shown in Fig. 3.26. Number fluctuations calculations in Fig. 3.27 show an exponent $\beta = 0.89 \pm 0.15, 0.91 \pm 0.17, 0.96 \pm 0.14, 0.95 \pm 0.12, 0.95 \pm 0.08, 0.96 \pm 0.08, 0.85 \pm 0.12$ for $Pe = 5, 6.25, 7.5, 8.75, 10, 11.25, 12.5$, respectively.

3.3.7 Attraction Strength = 0.0005

Particles configurations for various Pe are shown in Fig. 3.29. Number fluctuations calculations in Fig. 3.30 show an exponent $\beta = 0.98 \pm 0.14, 0.83 \pm 0.27$ for $Pe = 8, 9$, respectively.

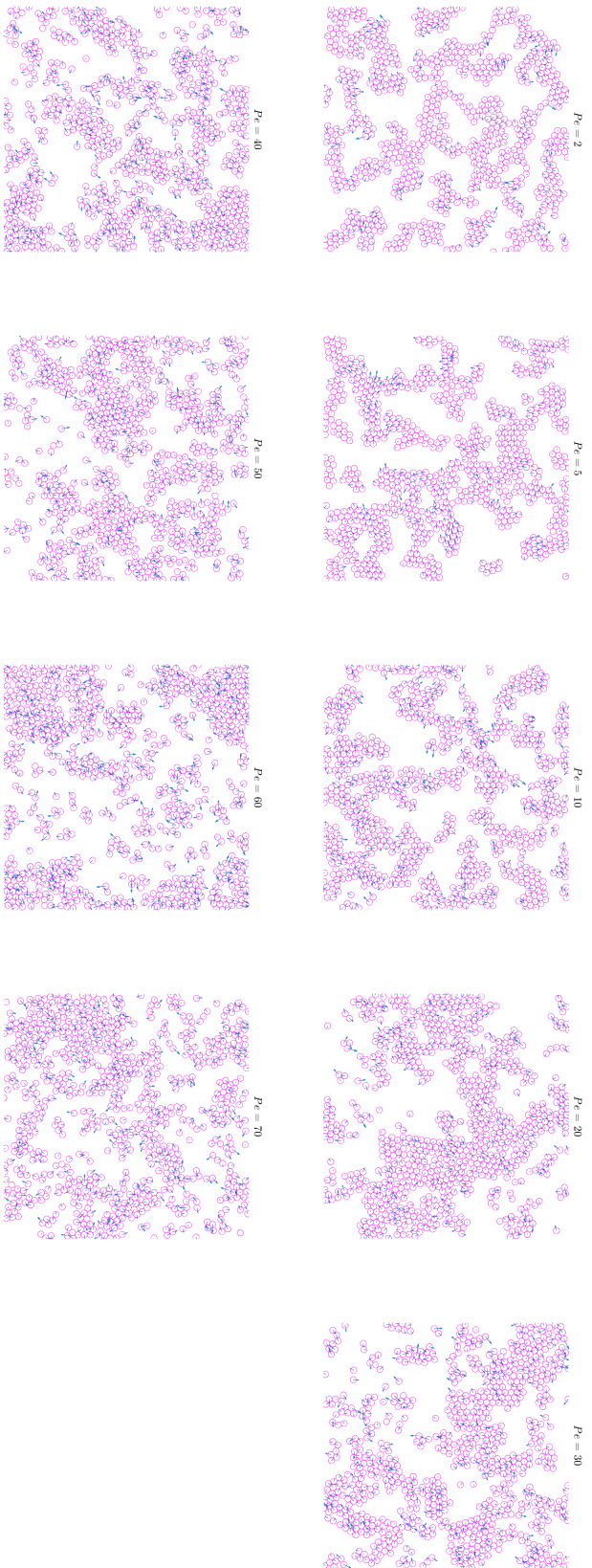


Figure 3.16: Particles configurations corresponding to an Attraction Strength = 0.005, $\tilde{v}_r = 0.0005$ at t_f for several Péclet numbers.

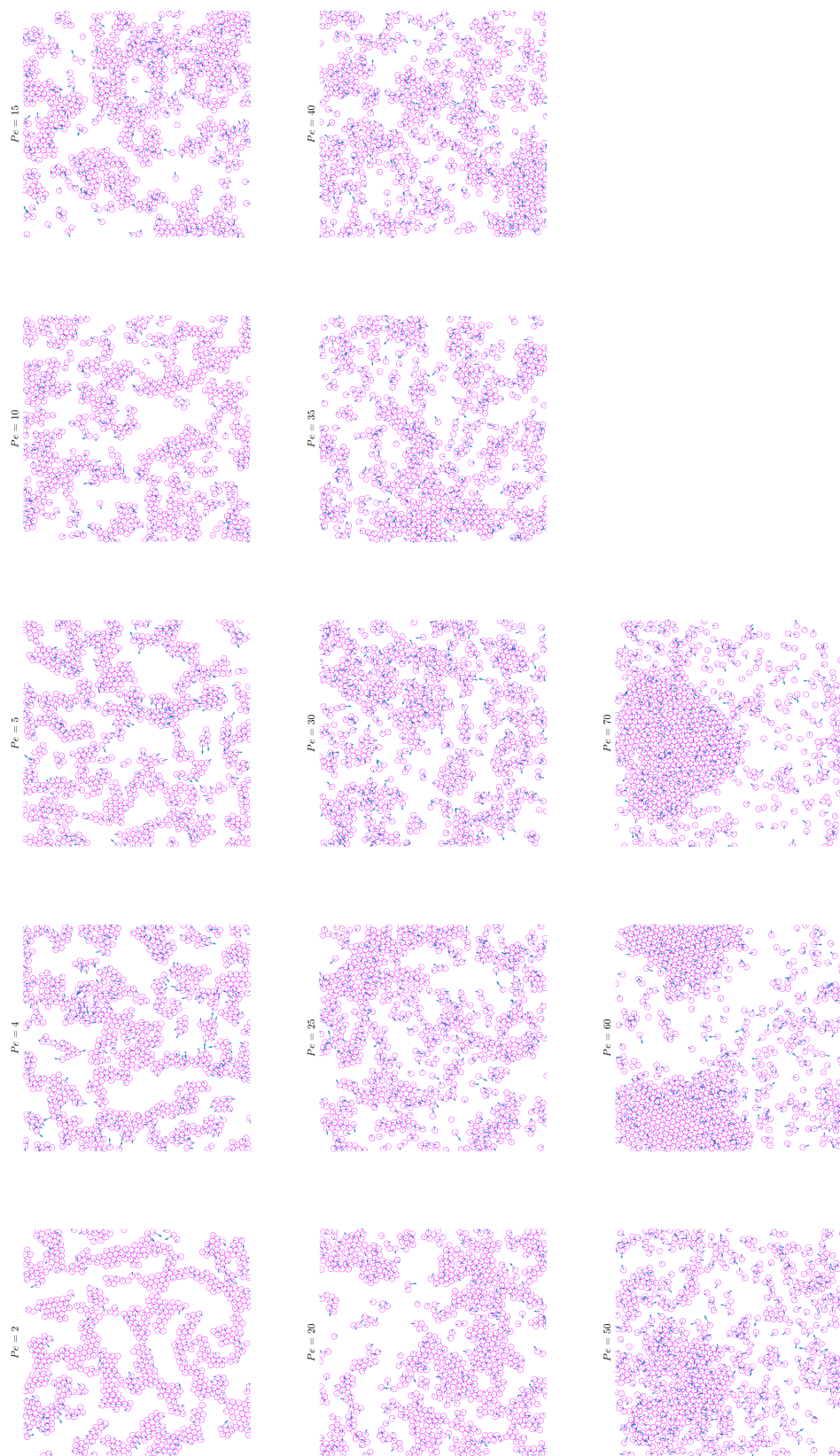


Figure 3.17: Particles configurations corresponding to an Attraction Strength = 0.0025, $\tilde{u}_i = 0.0005$ at t_f for several Péclet numbers.

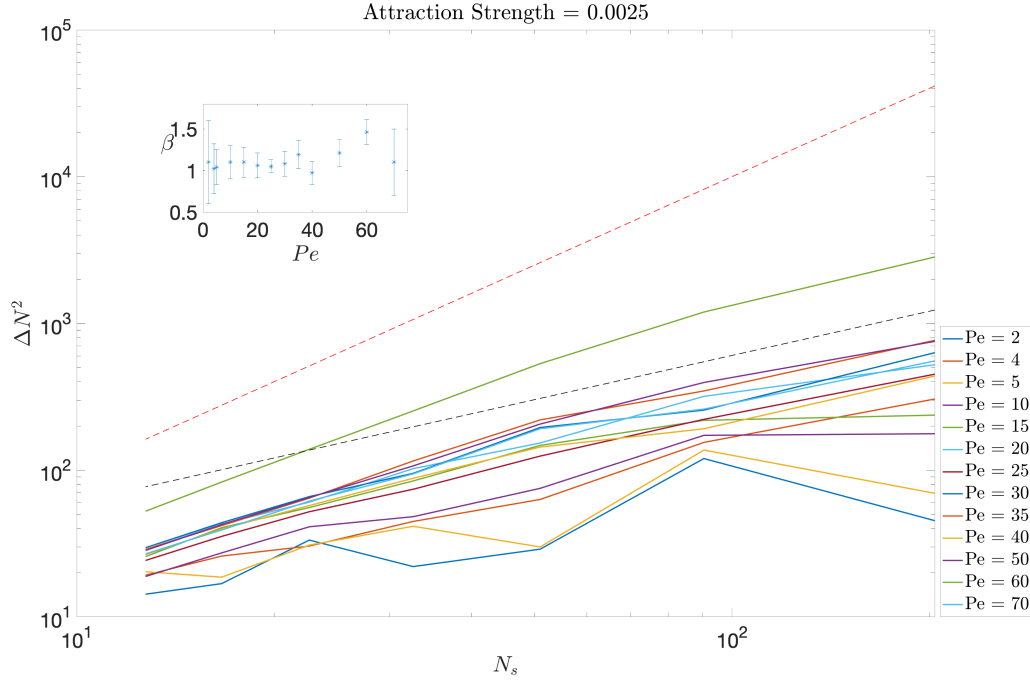


Figure 3.18: Number fluctuations for $\tilde{\nu}_r = 0.0005$ for various self-propulsion, for an Attraction Strength = 0.0025. The dashed lines correspond to slopes 1 (black) and 2 (red). Inset: the values of β obtained by the power-law fit $\Delta N^2(N_s) \sim N_s^\beta$ for the data at large N_s .

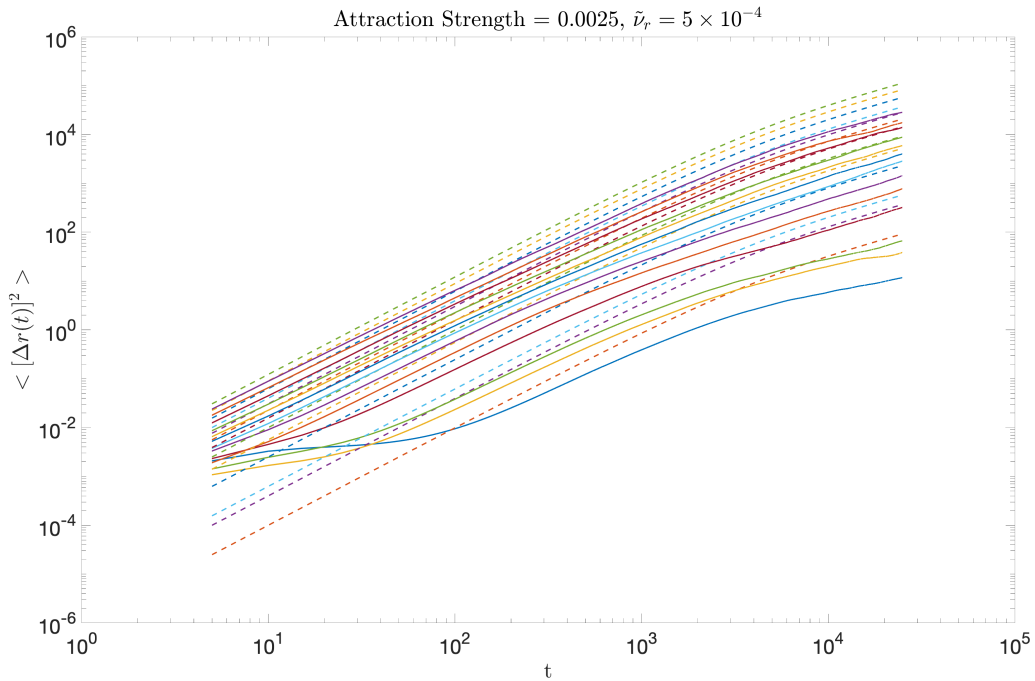


Figure 3.19: Mean square displacement for $\tilde{\nu}_r = 0.0005$ for various self-propulsion, for an Attraction Strength = 0.0025. The dashed lines correspond to the theoretical MSD that a single particle performs. At short time, the dashed lines correspond to slope of 2 (ballistic) and at large times, the dashed lines correspond to slope of 1 (diffusive)

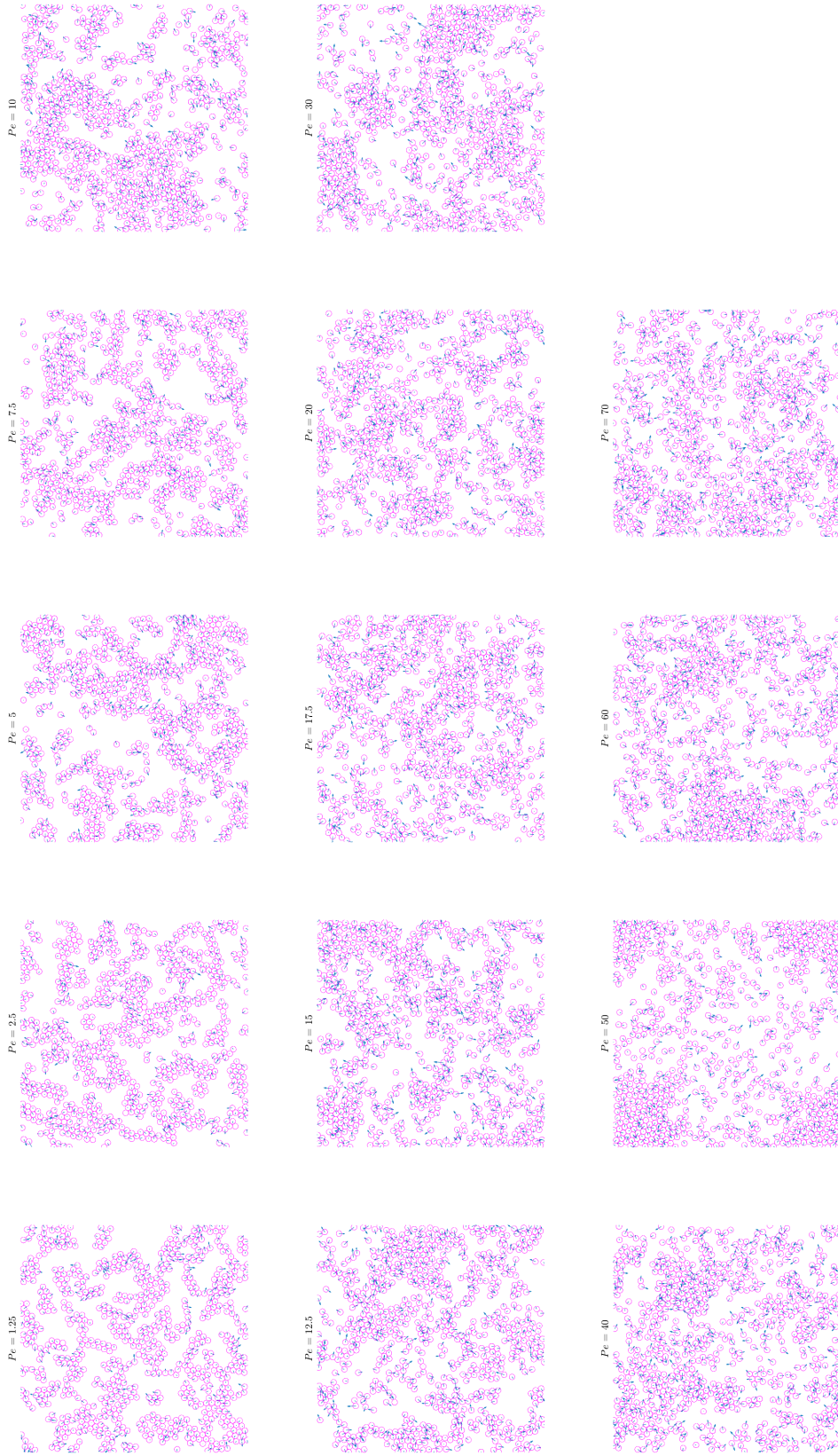


Figure 3.20: Particles configurations corresponding to an Attraction Strength = 0.00125, $\tilde{\nu}_r = 0.0005$ at t_f for several Péclet numbers.

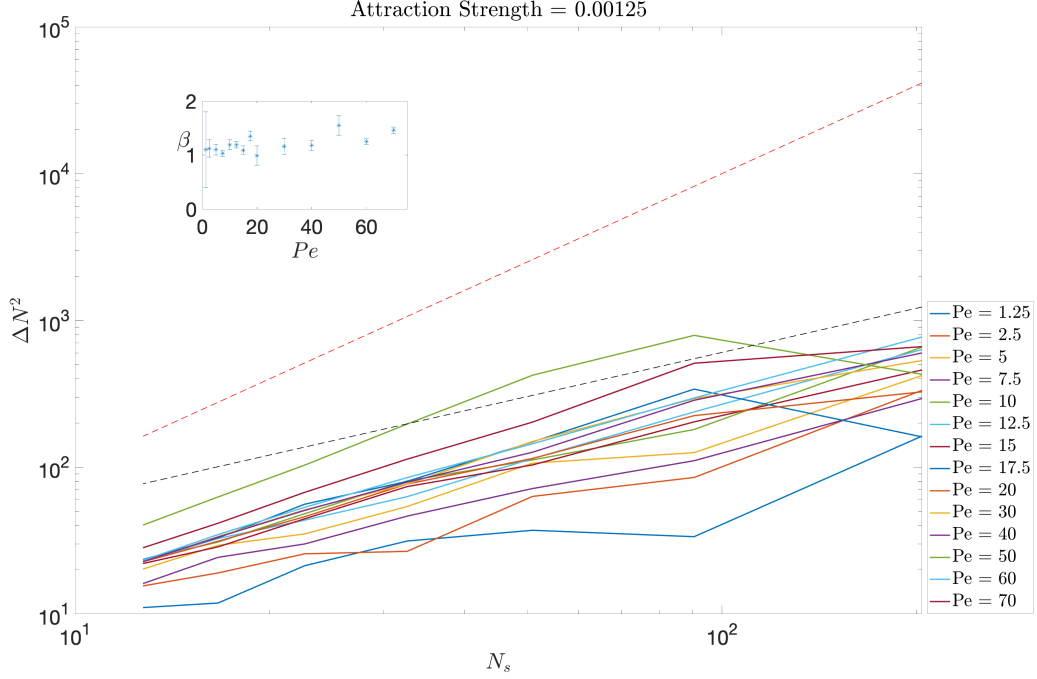


Figure 3.21: Number fluctuations for $\tilde{\nu}_r = 0.0005$ for various self-propulsion, for an Attraction Strength = 0.00125. The dashed lines correspond to slopes 1 (black) and 2 (red). Inset: the values of β obtained by the power-law fit $\Delta N^2(N_s) \sim N_s^\beta$ for the data at large N_s .

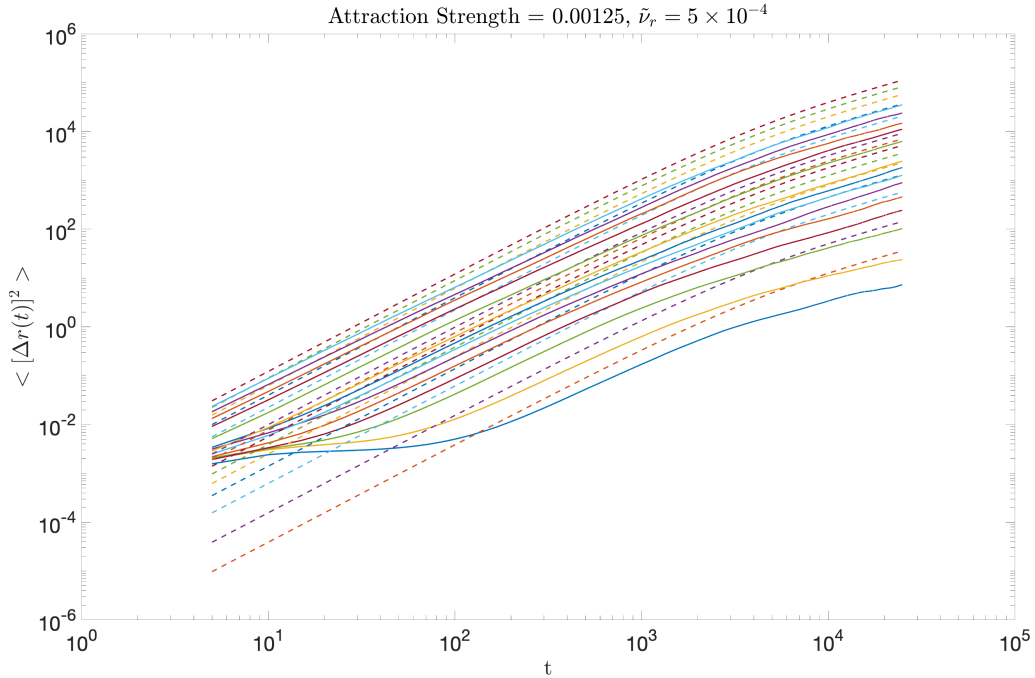


Figure 3.22: Mean square displacement for $\tilde{\nu}_r = 0.0005$ for various self-propulsion, for an Attraction Strength = 0.00125. The dashed lines correspond to the theoretical MSD that a single particle performs. At short time, the dashed lines correspond to slope of 2 (ballistic) and at large times, the dashed lines correspond to slope of 1 (diffusive)

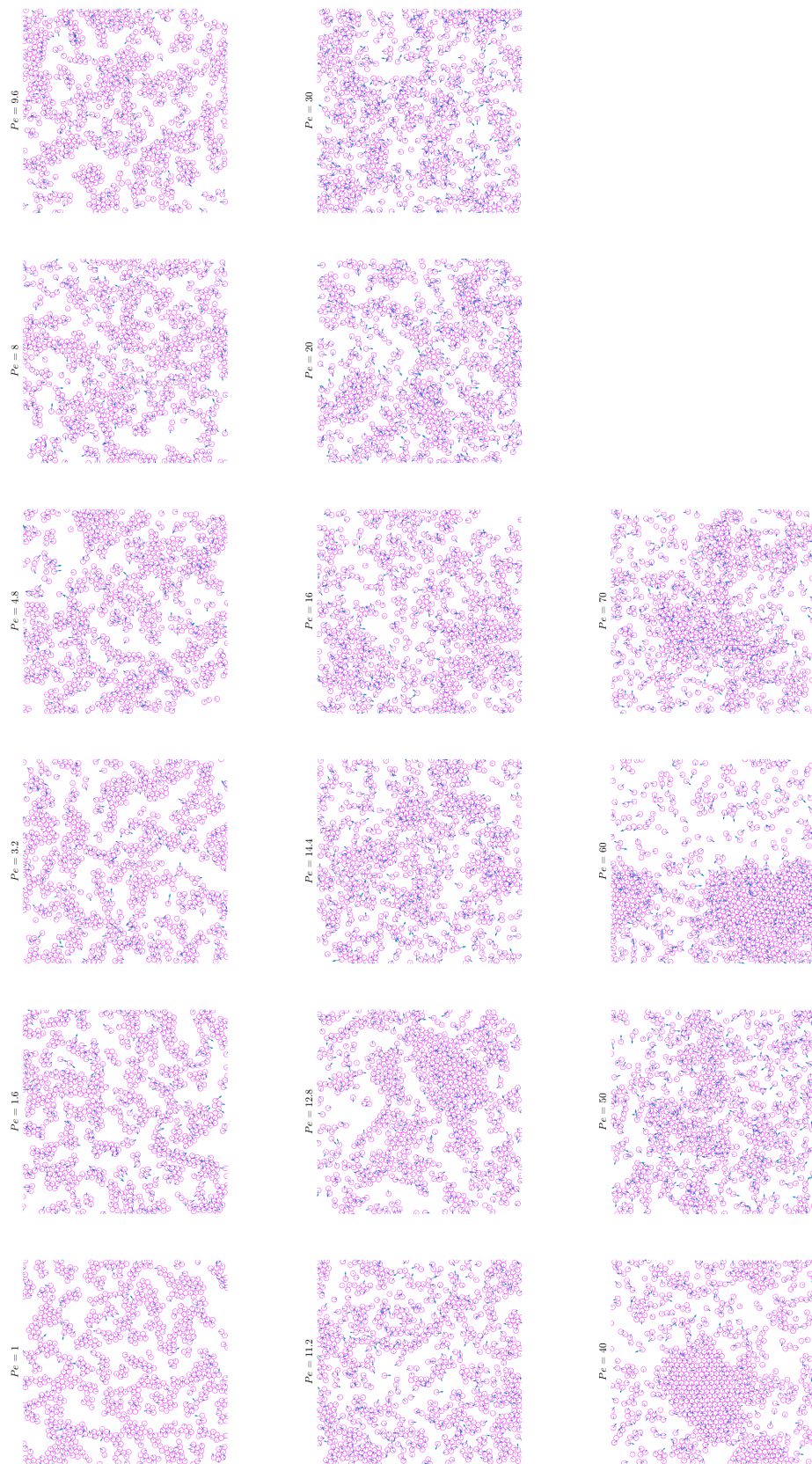


Figure 3.23: Particles configurations corresponding to an Attraction Strength = 0.0008, $\tilde{u}_r = 0.0005$ at t_f for several Péclet numbers.

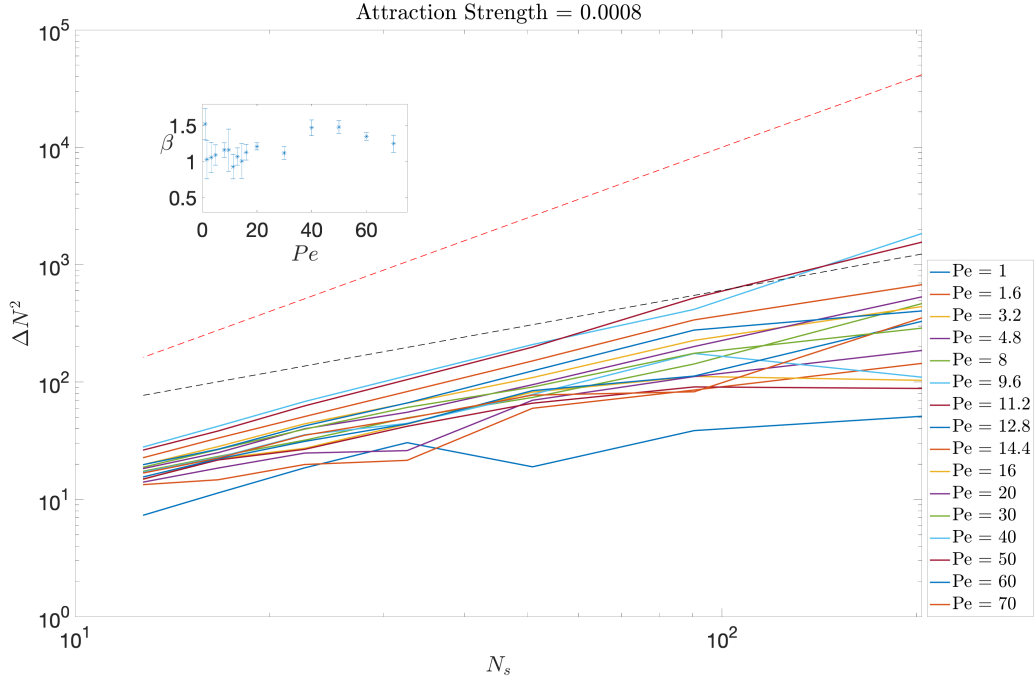


Figure 3.24: Number fluctuations for $\tilde{\nu}_r = 0.0005$ for various self-propulsion, for an Attraction Strength = 0.0008. The dashed lines correspond to slopes 1 (black) and 2 (red). Inset: the values of β obtained by the power-law fit $\Delta N^2(N_s) \sim N_s^\beta$ for the data at large N_s .

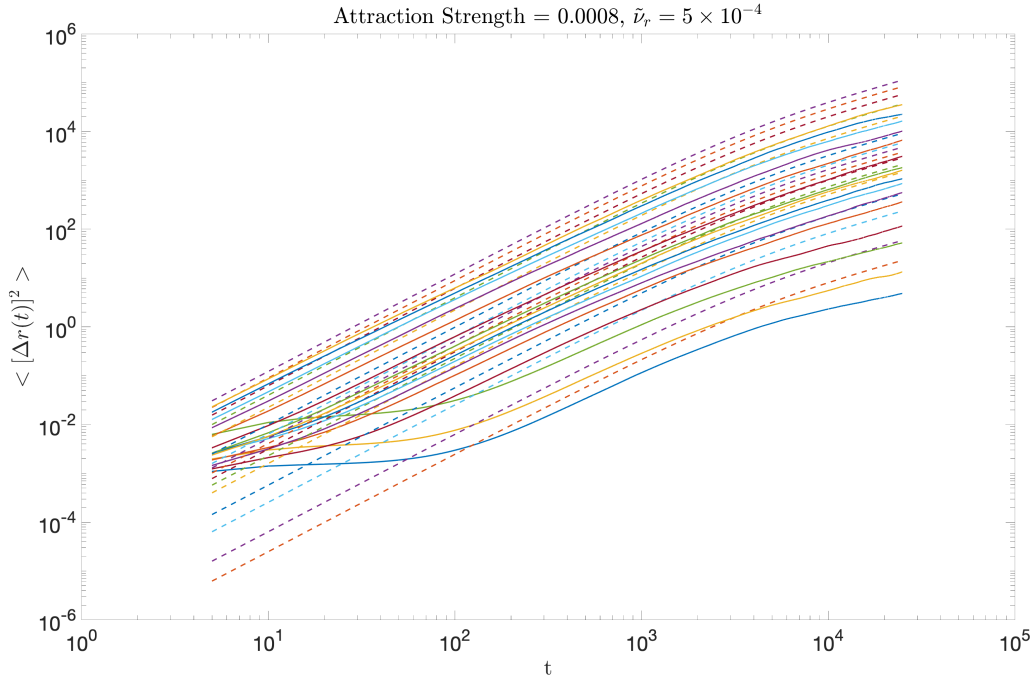


Figure 3.25: Mean square displacement for $\tilde{\nu}_r = 0.0005$ for various self-propulsion, for an Attraction Strength = 0.0008. The dashed lines correspond to the theoretical MSD that a single particle performs. At short time, the dashed lines correspond to slope of 2 (ballistic) and at large times, the dashed lines correspond to slope of 1 (diffusive)

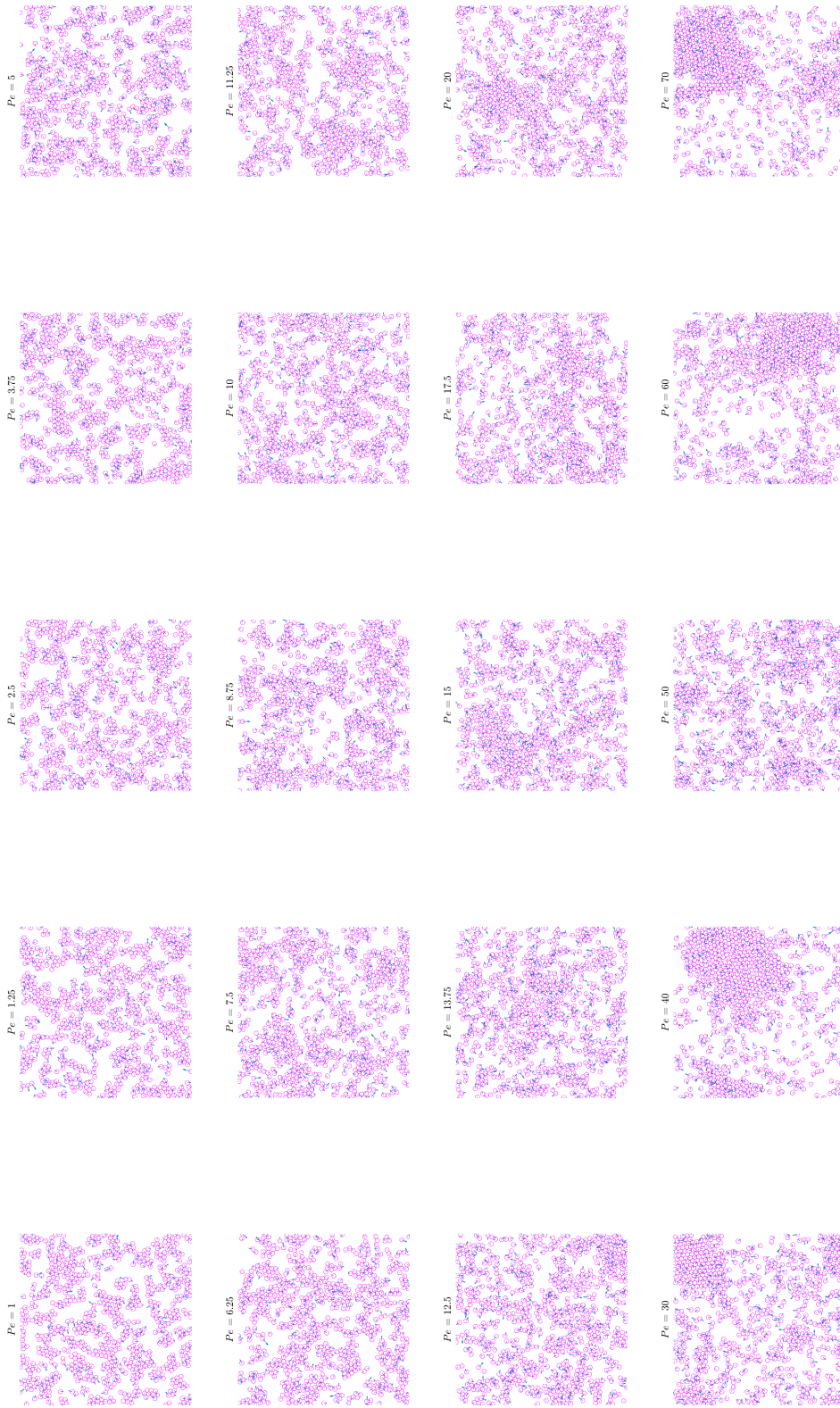


Figure 3.26: Particles configurations corresponding to an Attraction Strength = 0.000625, $\tilde{v}_f = 0.0005$ at t_f for several Péclet numbers.

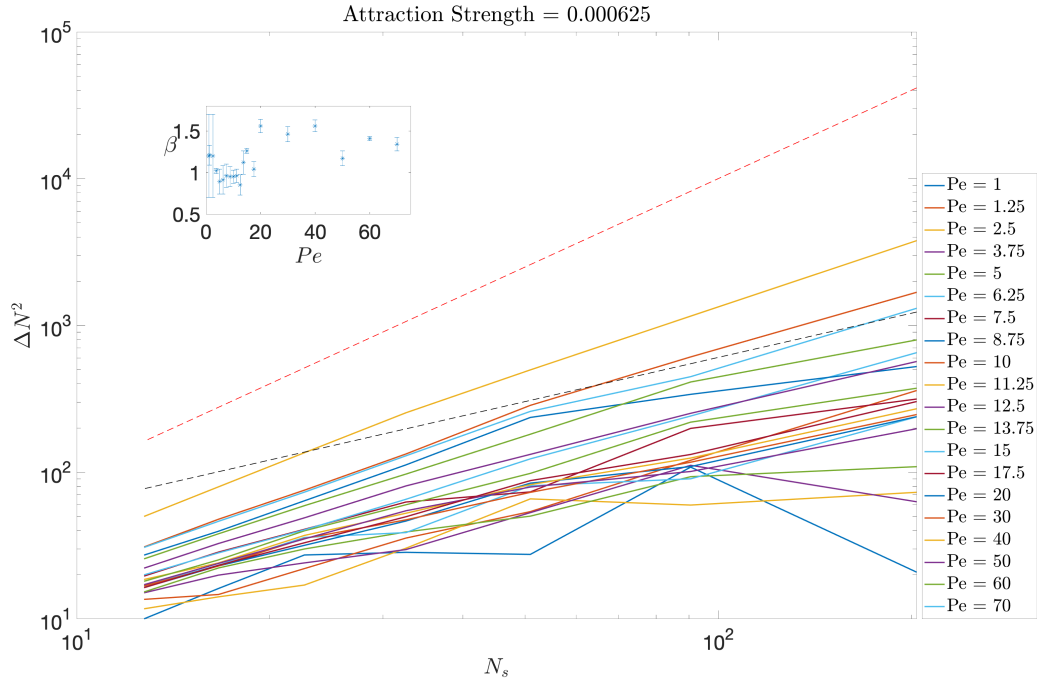


Figure 3.27: Number fluctuations for $\tilde{\nu}_r = 0.0005$ for various self-propulsion, for an Attraction Strength = 0.000625. The dashed lines correspond to slopes 1 (black) and 2 (red). Inset: the values of β obtained by the power-law fit $\Delta N^2(N_s) \sim N_s^\beta$ for the data at large N_s .

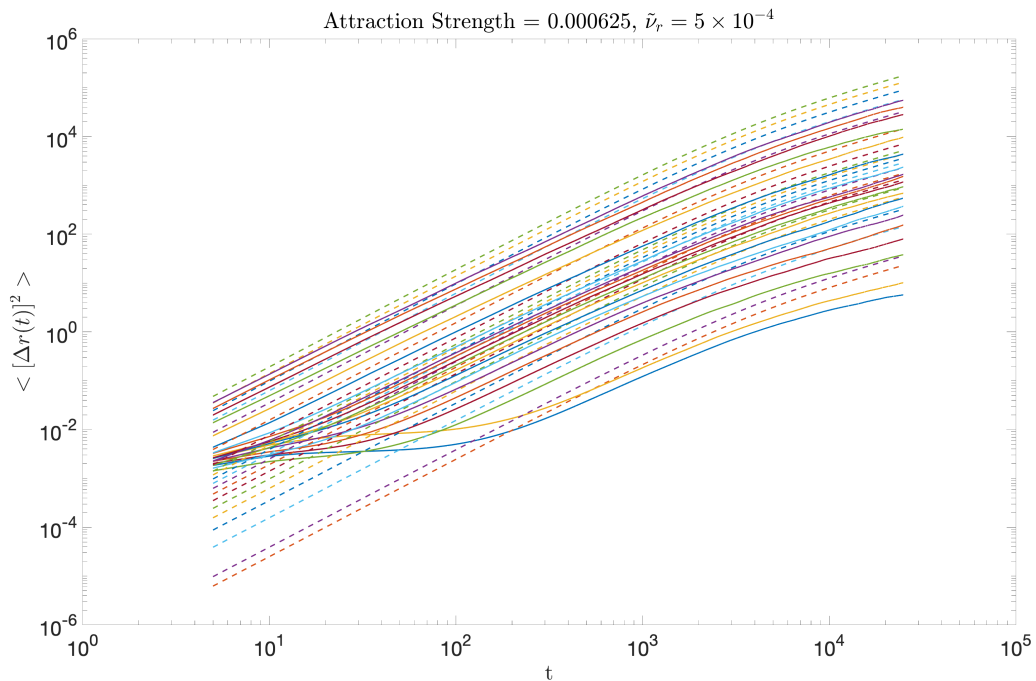


Figure 3.28: Mean square displacement for $\tilde{\nu}_r = 0.0005$ for various self-propulsion, for an Attraction Strength = 0.000625. The dashed lines correspond to the theoretical MSD that a single particle performs. At short time, the dashed lines correspond to slope of 2 (ballistic) and at large times, the dashed lines correspond to slope of 1 (diffusive)

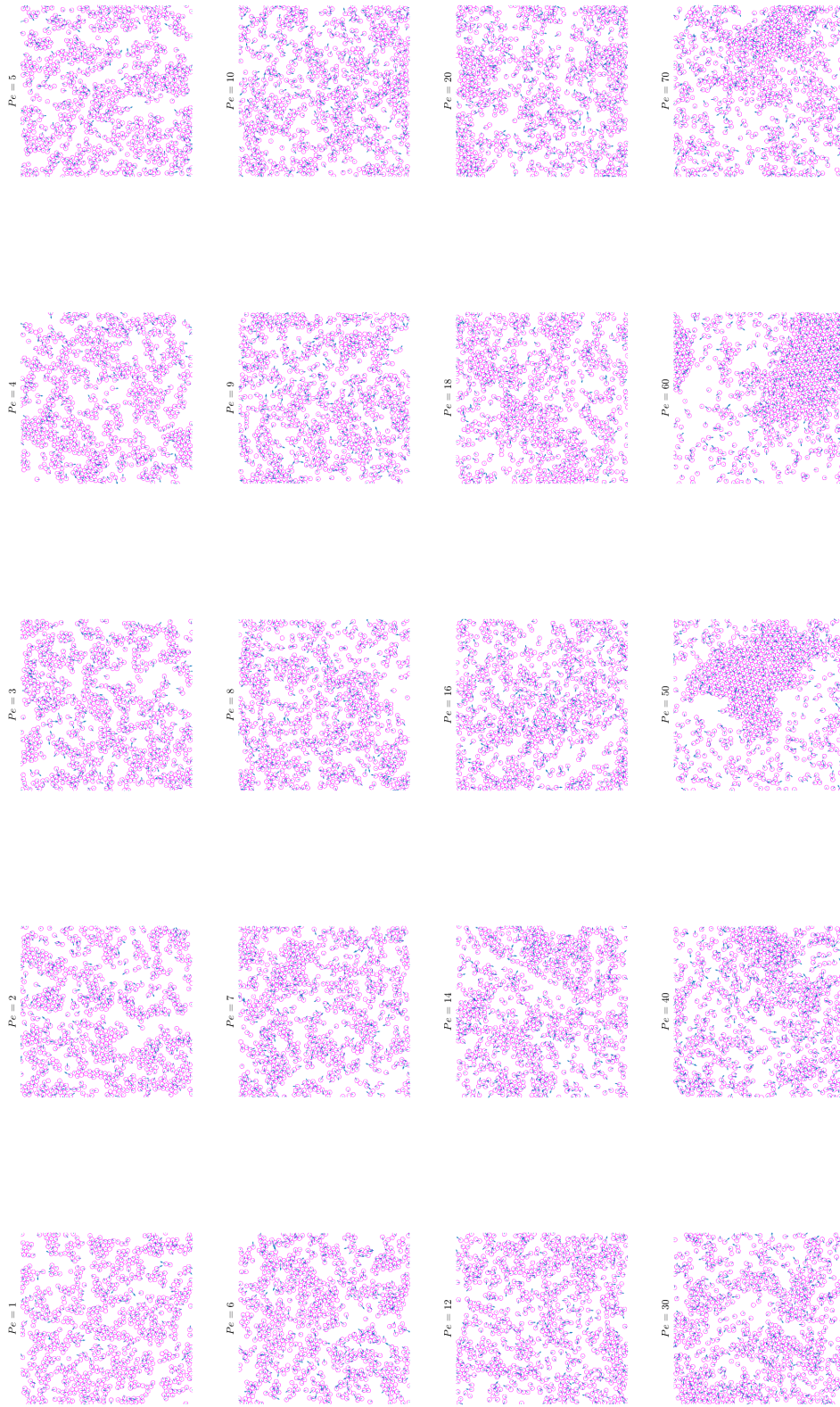


Figure 3.29: Particles configurations corresponding to an Attraction Strength = 0.0005, $\tilde{u}_r = 0.0005$, $\tilde{v}_r = 0.0005$ at t_f for several Péclet numbers.

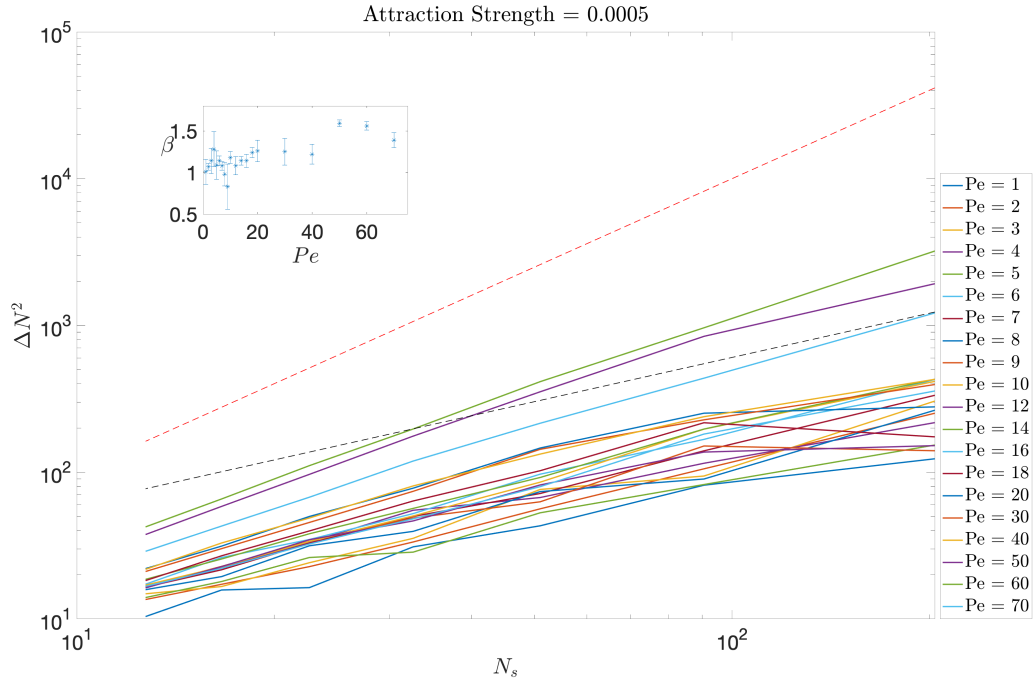


Figure 3.30: Number fluctuations for $\tilde{\nu}_r = 0.0005$ for various self-propulsion, for an Attraction Strength = 0.0005. The dashed lines correspond to slopes 1 (black) and 2 (red). Inset: the values of β obtained by the power-law fit $\Delta N^2(N_s) \sim N_s^\beta$ for the data at large N_s .

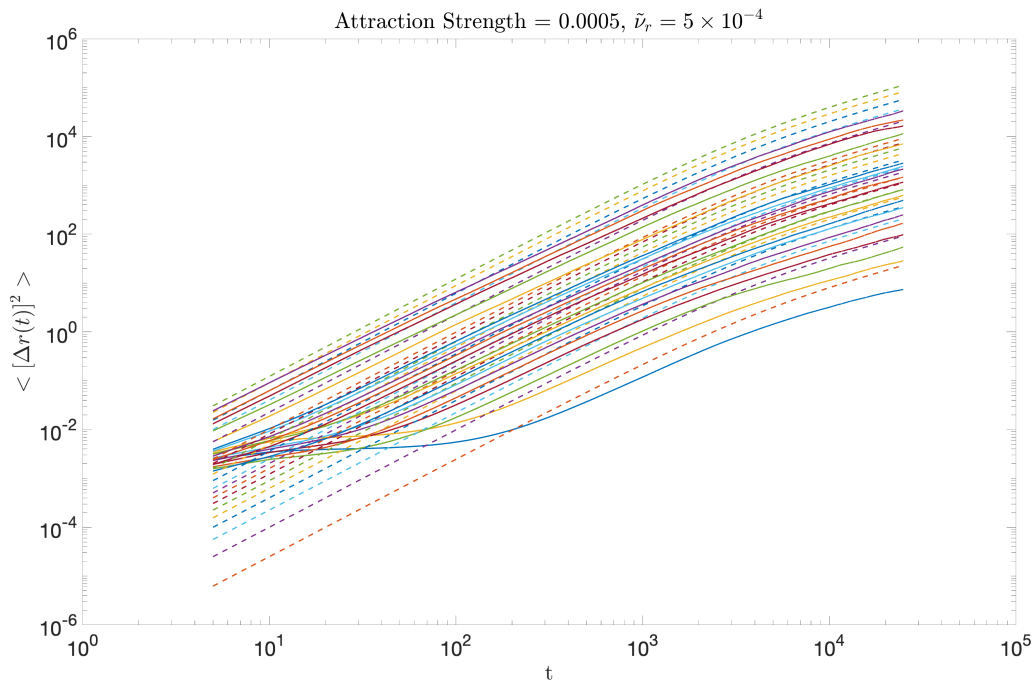


Figure 3.31: Mean square displacement for $\tilde{\nu}_r = 0.0005$ for various self-propulsion, for an Attraction Strength = 0.0005. The dashed lines correspond to the theoretical MSD that a single particle performs. At short time, the dashed lines correspond to slope of 2 (ballistic) and at large times, the dashed lines correspond to slope of 1 (diffusive)

Chapter 4

Pressure of Active Matter

If someone points out to you that your pet theory of the Universe is contradicted by experiment, well, these experimentalists do bungle things sometimes. But if your theory is found to be against the Second Law I can give you no hope; there is nothing for it but to collapse in deepest humiliation.

Sir Arthur Eddington

4.1 Introduction

Minimal models of active Brownian particles interacting through steric repulsion have been the subject of recent extensive numerical and analytical investigations. Such systems exhibit a rich phase diagram showing active phase separation in the absence of attractive interactions. Recent advances in characterizing the mechanical properties of the novel phases of active matter include a theoretical description of the active gas and its swim pressure. Theoretical efforts include describing this non-equilibrium system by a pressure equation of state. It is then useful to recall the definition of pressure in equilibrium systems. For a fluid in equilibrium [53], we can define the pressure as:

1. Mechanical description: force exerted by particles on walls of the container, which is the force per unit area
2. Thermodynamic description: pressure is the derivative of a free energy
3. Momentum flux definition, which originates from continuum mechanics as the pressure being the steady state flux of momentum. Pressure is then the trace of the hydrodynamic stress tensor of the fluid

In equilibrium systems, all of the above definitions of pressure are equivalent and hence pressure is a state function. Recent work on ABP with purely repulsive interactions show that the pressure is a state function for an active fluid [21, 47]. However, the pressure becomes wall dependent when active particles exert torques on the walls or on each other.

4.2 Methods

In the following, we highlight the pressure calculations found in the literature for purely repulsive self-propelled particles exhibiting MIPS. We study the active (swim) and passive (direct) pressure as function of density for two different potentials and for different set of parameters. The first potential is given by the linear force introduced in Chapter 2 using Eq. 2.21. For this model, we use the previously introduced definition of Pe as a dimensionless run length. However, for the model introduced in the following subsection, in order to better compare our pressure calculations to the results found in [11], we use their definition of Pe as

$$Pe = \frac{3v_0}{\sigma D_r} \quad (4.1)$$

Péclet number was defined historically as

$$Pe = \frac{v_0 \sigma}{D_t} \quad (4.2)$$

where D_t denotes translational diffusion with rotational diffusion given by

$$D_r = \frac{3D_t}{\sigma^2} \quad (4.3)$$

However, simulations of active particles interacting through pairwise additive forces showed that translational diffusion's effect on the phase diagram is insignificant. For this reason, there is an additional factor of 3 in the definition of Pe . Note that in this Chapter, we use two notations to denote the same parameter. Rotational diffusion $\tilde{\nu}_r \equiv D_r$ and self-propulsion $\tilde{v} \equiv v_0$.

4.2.1 Model: MIPS Revisited

We study the phase behavior of a two-dimensional system of N self-propelled particles, interacting via pairwise additive, Weeks-Chandler-Anderson (WCA) potential, with a cut-off at $r = 2^{1/6}$, beyond which the potential is set to zero. This is the Lennard-Jones (LJ) potential:

$$V(r) = 4\epsilon \left[\left(\frac{\sigma}{r} \right)^{12} - \left(\frac{\sigma}{r} \right)^6 \right] + \epsilon \quad (4.4)$$

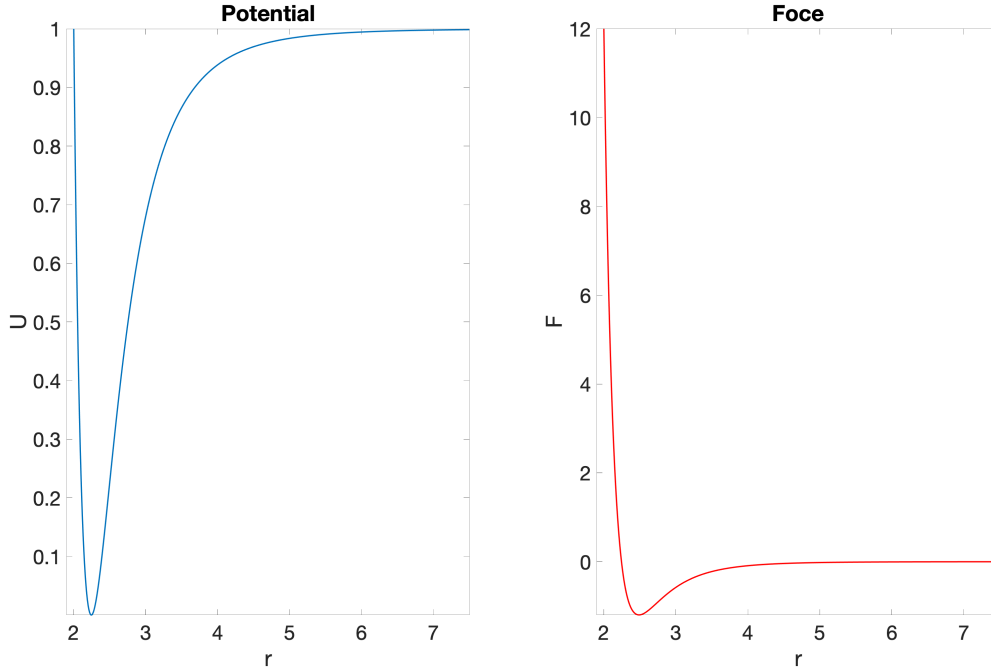


Figure 4.1: A plot of the potential and force of interaction given by LJ

Fig. 4.1 presents a plot of the potential and force, where σ defines the particle diameter, r is the center-to-center separation between two particles, and ϵ sets the strength of interaction. We denote the position of particle i by \mathbf{r}_i . The dynamics is overdamped and is governed according to the Langevin equations

$$\dot{\mathbf{r}}_i = -\mu \sum_j \nabla_i V(|\mathbf{r}_i - \mathbf{r}_j|) + \sqrt{2D_t} \boldsymbol{\xi}_i + v_0 \mathbf{u}_i \quad (4.5)$$

$$\dot{\theta}_i = \sqrt{2D_r} \eta_i \quad (4.6)$$

As introduced earlier in Chapter 3, v_0 denotes the self-propulsive speed, $\mathbf{u}_i = (\cos\theta_i, \sin\theta_i)$ indicates the direction of self-propulsion, and η_i . $\boldsymbol{\xi}_i$ are unit Gaussian white noises with zero mean and delta correlations in time. For simplicity, in our simulations we only include rotational diffusion

$$\langle \eta_i(t) \rangle = 0 \quad (4.7)$$

$$\langle \eta_i(t) \eta_j(t') \rangle = \delta_{ij} \delta(t - t') \quad (4.8)$$

We use the same dimensionless parameters used in Chapter 3. In our simulations, we set $\epsilon = 1$, $\mu = 1$, $\sigma = 1$, $D_r = 5 \times 10^{-4}$ (unless otherwise noted) and vary the packing fraction (or density) ρ and v_0 . In other words, we study the model as function of the Péclet number and packing fraction.

4.2.2 Hydrodynamic Description

In this section, we follow standard procedures available in the literature [11,47] to obtain a macroscopic description of the model through a coarse grain of the microscopic dynamics given by Eq. 4.9. Note that the dynamics of the solvent is not included in our description and by “hydrodynamic” we mean slowly varying dynamics in space and time. Using the

microscopic Eq. 4.9, we use $It\bar{o}$ calculus to write down the microscopic density of particles given by

$$\hat{\psi}(\mathbf{r}, \theta) = \sum_{i=1}^N \delta(\mathbf{r} - \mathbf{r}_i) \delta(\theta - \theta_i) \quad (4.9)$$

and write down a stochastic dynamical equation for the evolution of the density of particle at position \mathbf{r} with orientation θ as

$$\partial_t \hat{\psi} = -\nabla \cdot \left[v_0 \mathbf{u} \hat{\psi} + \hat{\mathbf{I}}^\theta - D_t \nabla \hat{\psi} + \sqrt{2D_t} \hat{\psi} \boldsymbol{\eta} \right] + \partial_\theta \left[D_r \partial_\theta \hat{\psi} + \sqrt{2D_r} \hat{\psi} \boldsymbol{\xi} \right] \quad (4.10)$$

where $\boldsymbol{\eta}$ and $\boldsymbol{\xi}$ are unit-variance 2-d vectors of Gaussian white noises. We define $\hat{\mathbf{I}}(\mathbf{r}, \theta)$ as

$$\hat{\mathbf{I}}(\mathbf{r}, \theta) = - \int d\mathbf{r}' \mu \nabla V(|\mathbf{r}' - \mathbf{r}|) \hat{\rho}(\mathbf{r}') \hat{\psi}(\mathbf{r}, \theta) \quad (4.11)$$

We define the zeroth, first, and second angular harmonics of the microscopic density $\hat{\psi}(\mathbf{r}, \theta)$, the fluctuating density

$$\hat{\rho}(\mathbf{r}) = \int d\theta \hat{\psi}(\mathbf{r}, \theta) \quad (4.12)$$

the orientation vector as

$$\hat{\mathbf{m}} = \int d\theta \mathbf{u} \hat{\psi}(\mathbf{r}, \theta) \quad (4.13)$$

and the nematic tensor as

$$\hat{\mathbb{Q}}(\mathbf{r}) = \int d\theta (\mathbf{u} : \mathbf{u} - \mathbb{1}/2) \hat{\psi}(\mathbf{r}, \theta) \quad (4.14)$$

where $\mathbb{1}$ is the identity matrix. We denote averages over noise realizations by brackets, we define $\rho(\mathbf{r}) = \langle \hat{\rho}(\mathbf{r}) \rangle$, $\mathbf{m} = \langle \hat{\mathbf{m}}(\mathbf{r}) \rangle$, and $\mathbb{Q}(\mathbf{r}) = \langle \hat{\mathbb{Q}}(\mathbf{r}) \rangle$.

Now we assume that our system is in a steady state. The time derivatives vanish. To obtain the dynamics of $\rho(\mathbf{r}, t)$, we integrate Eq. 4.10 over θ and perform an average over noise realizations, we find that

$$\partial_t \rho = -\nabla \cdot \mathbf{J}; \quad \mathbf{J} = v_0 \mathbf{m} + \mathbf{I}^{(0)} - D_t \nabla \rho \quad (4.15)$$

where \mathbf{J} is the particle current and $\mathbf{I}^{(0)}$ is given by

$$\mathbf{I}^{(0)} = \left\langle \int d\theta \hat{\mathbf{I}}^{(\theta)}(\mathbf{r}, \theta) \right\rangle = - \int d\mathbf{r}' \mu \nabla V(|\mathbf{r} - \mathbf{r}'|) \langle \hat{\rho}(\mathbf{r}) \hat{\rho}(\mathbf{r}') \rangle \quad (4.16)$$

The dynamics of \mathbf{m} is obtained by multiplying Eq. 4.10 by \mathbf{u} and integrating over θ . This gives, with a summation over repeated indices,

$$\partial_t m_\alpha = -\partial_\beta \left[v_0 \left(\mathbb{Q}_{\alpha\beta} + \frac{\rho \delta_{\alpha\beta}}{2} \right) + \mathbb{I}_{\alpha\beta}^{(1)} - D_t \partial_\beta m_\alpha \right] - D_r m_\alpha \quad (4.17)$$

where we have defined

$$\mathbb{I}_{\alpha\beta}^{(1)} = - \int d\mathbf{r}' \mu \nabla V(|\mathbf{r} - \mathbf{r}'|) \langle \hat{\rho}(\mathbf{r}') \hat{m}_\alpha(\mathbf{r}) \rangle \quad (4.18)$$

\mathbf{m} is a fast mode decaying at a rate D_r such that on time scales much larger than D_r^{-1} , we can assume that m_α relaxes locally to

$$m_\alpha = -\frac{1}{D_r} \partial_\beta \left[v_0 \left(\hat{\mathbb{Q}}_{\alpha\beta} + \frac{\rho \delta_{\alpha\beta}}{2} \right) + \mathbb{I}_{\alpha\beta}^{(1)} - D_t \partial_\beta m_\alpha \right] \quad (4.19)$$

Then we can write the current in Eq. 4.15 as

$$J_\alpha = -\left[D_t + \frac{v_0^2}{2D_r} \right] \partial_\alpha \rho - \frac{v_0}{D_r} \partial_\beta \mathbb{I}_{\alpha\beta}^{(1)} + I_\alpha^{(0)} - \frac{v_0^2}{D_r} \partial_\beta \mathbb{Q}_{\alpha\beta} + \frac{D_t v_0}{D_r} \partial_{\beta\beta} m_\alpha \quad (4.20)$$

We again rewrite the current in Eq. 4.20 as the divergence of a stress tensor

$$J_\alpha = \mu \partial_\beta \sigma_{\alpha\beta} \quad (4.21)$$

with

$$\sigma_{\alpha\beta} = -\left[\frac{D_t}{\mu} + \frac{v_0^2}{2\mu D_r} \right] \rho \delta_{\alpha\beta} - \frac{v_0}{\mu D_r} \mathbb{I}_{\alpha\beta}^{(1)} + \sigma_{\alpha\beta}^{IK} - \frac{v_0^2}{\mu D_r} \mathbb{Q}_{\alpha\beta} + \frac{D_t v_0}{\mu D_r} \partial_\beta m_\alpha \quad (4.22)$$

where we have written $I_\alpha^{(0)}$ as

$$I_\alpha^{(0)} = \mu \partial_\beta \sigma_{\alpha\beta}^{IK} \quad (4.23)$$

where $\sigma_{\alpha\beta}^{IK}$ is the Irving and Kirkwood expression for the stress tensor [54] given by

$$\sigma_{\alpha\beta}^{IK}(\mathbf{r}) = \frac{1}{2} \int d\mathbf{r}' \frac{(\mathbf{r} - \mathbf{r}')_\alpha (\mathbf{r} - \mathbf{r}')_\beta}{|\mathbf{r} - \mathbf{r}'|} \frac{dV(|\mathbf{r} - \mathbf{r}'|)}{d|\mathbf{r} - \mathbf{r}'|} \int_0^1 d\lambda \langle \hat{\rho}(\mathbf{r} + (1 - \lambda)\mathbf{r}') \hat{\rho}(\mathbf{r} - \lambda\mathbf{r}') \rangle \quad (4.24)$$

We now make a connection with the formalism derived previously in Chapter 2.

4.2.3 Generalized Pressure and Equation of State

The derived dynamics for ρ , with the current given by 4.23, should be compared to the generalized Cahn-Hilliard equation of Chapter 2 with the current driven by a generalized stress tensor as in Eq. 2.39. We see that our model of self-propelled particles interacting via pairwise forces correspond to the special case of $M/R = \mu$, the mobility. This is important for the mechanical interpretation of $\boldsymbol{\sigma}$. Imposing an external potential U on the particles lead to

$$\mathbf{J} = \mu \nabla \cdot \boldsymbol{\sigma} - \mu \rho \nabla U \quad (4.25)$$

Eq. 4.25 becomes a force balance in a flux free steady state with $\mathbf{J} = 0$. By integrating Eq. 4.25 from a point in the bulk to infinity, we find that the normal component of $\boldsymbol{\sigma}$ to be equal to the total force per unit area exerted on a boundary. It was verified that the normal component of $\boldsymbol{\sigma}$ exactly coincides in homogeneous phases with the equation of state found previously for the mechanical pressure of self-propelled particles interacting through pairwise forces [47]. Thus, generalized and mechanical pressure coincide for such systems and we write following the notation in Chapter 2

$$h \equiv -\sigma_{xx} = \frac{D_t}{\mu} \rho + P^A(x) + P^D(x) + \frac{v_0^2}{\mu D_r} \mathbb{Q}_{xx} - \frac{D_t v_0}{\mu D_r} \partial_x m_x \quad (4.26)$$

where we have defined, following [47], an ‘‘active’’ contribution to pressure P^A and a ‘‘direct’’ (passive) contribution part P^D as

$$P^A = \frac{v_0^2}{2\mu D_r} \rho + \frac{v_0}{\mu D_r} \mathbb{I}_{xx}^{(1)} \quad P^D = -\sigma_{xx}^{IK} \quad (4.27)$$

The value of the pressure in a homogeneous phase of density ρ_0 is given by

$$h[\rho(x) = \rho_0] \equiv h_0(\rho_0) = \rho_0 \frac{D_t}{\mu} + P_0^A + P_0^D \quad (4.28)$$

where P_0^A and P_0^D are the values taken by P^A and P^D in homogeneous phases of density ρ_0 . We can thus, in analogy with Eq. 2.42, to identify

$$h = h_0(\rho(x)) + h_1([\rho], x) \quad (4.29)$$

where h_1 is an exact expression containing gradients of all orders. It is given by

$$h_1 = P_1^A[\rho] + P_1^D[\rho] + \frac{v_0^2}{\mu D_r} \mathbb{Q}_{xx} - \frac{D_t v_0}{\mu D_r} \partial_x m_x \quad (4.30)$$

where $P_1^{A/D} \equiv P^{A/D} - P_0^{A/D}$ contains the interfacial contribution to the active and direct pressures. The interfacial terms m_x and \mathbb{Q}_{xx} vanish in disordered bulk phases.

4.3 Passive and Active Pressure

For our passive pressure calculation due to inter-particle interactions, we follow the algorithm found in [55] for calculating the pressure tensor from our simulations. Following Solon et. al. in [47], the exact expression for active pressure in a homogeneous system is given by:

$$\mu P_A^0(\rho) = \frac{v_0}{2D_r} v(\rho) \rho \quad (4.31)$$

where $v(\rho)$ is the single particle contribution to the active pressure. It is a density dependent swim velocity projected along the particle's orientation:

$$v(\rho) \equiv v_0 + \frac{2\mathbb{I}_{xx}}{\rho} = v_0 + \langle \mathbf{u}(\theta_i) \cdot \sum_{j \neq i} \mathbf{F}(\mathbf{r}_j - \mathbf{r}_i) \rangle = \langle \dot{\mathbf{r}}_i \cdot \mathbf{u}_i \rangle \quad (4.32)$$

In the following we simulate a system of $N = 815$ self-propelled particles, with periodic boundary conditions for various packing fractions given by

$$\phi = \frac{N\pi\sigma^2}{L^2} \quad (4.33)$$

We vary L in order to get the desired ϕ . We run our simulations for at least $50\tau_r$, where τ_r is the rotational relaxation time given by ν_r^{-1} . We vary our integration time step in such a way that it is much smaller than the self-propulsion v_0 . We average our data over different configurations in which the system is homogeneous.

4.3.1 Linear Force

Fig. 4.2 shows the passive pressure calculation at a fixed $v_0 = 0.2$ for two different rotational diffusion values $\tilde{\nu}_r = 0.02$ and $\tilde{\nu}_r = 0.01$ corresponding to $Pe = 10$ and $Pe = 20$, respectively. The graph shows that the passive pressure scales with self-propulsion. At low densities, the data points corresponding to two different ν_r collapse on the same curve. This is expected since at low densities the particles move ballistically with a

velocity proportional to v_0 . However, at higher densities, particles start bumping into each other. They will then move due to their self-propulsion v_0 and their inter-particle interaction. This is why at high densities, the passive pressure for two different $\tilde{\nu}_r$ does not necessarily scale in the same way.

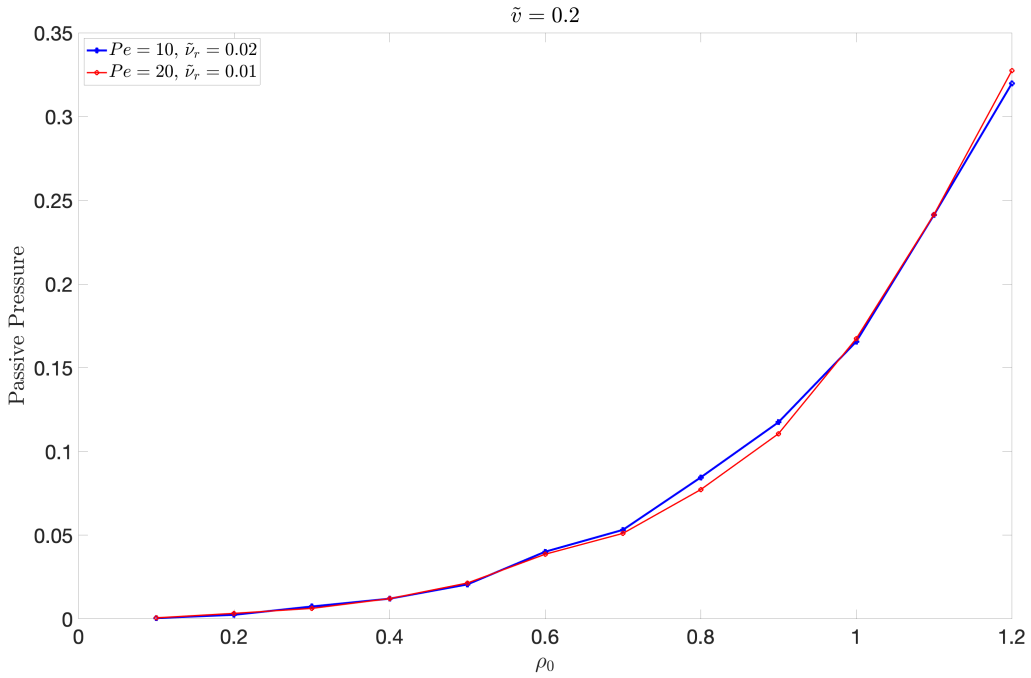


Figure 4.2: Passive pressure for a fixed self-propulsion $v_0 = 0.2$ for two different rotational diffusion values $\tilde{\nu}_r = 0.02$ and $\tilde{\nu}_r = 0.01$ corresponding to $Pe = 10$ and $Pe = 20$, respectively. Solid lines are guide for the eye.

Active pressure for a fixed rotational diffusion $\tilde{\nu}_r = 0.0005$ for $Pe = 20$ and $Pe = 40$ is shown in Fig. 4.3. At low densities, active pressure is an increasing function of density and it then starts decreasing at the onset of phase separation, for high enough densities ($\approx \rho_0 = 0.6$). It is evident from Eq. 4.27 that how active pressure scales depends on which parameter we fix and which parameter we vary. The slope of active pressure is $\propto \frac{v_0^2}{2\mu D_r}$. In this case the active pressure scales with $v_0 Pe$. In other words, in order to extrapolate P_0^A curve for $Pe = 40$ from P_0^A curve for $Pe = 20$, we would have to divide the latter by $(v_0 = 20)^2$ and multiply it by $(v_0 = 40)^2$.

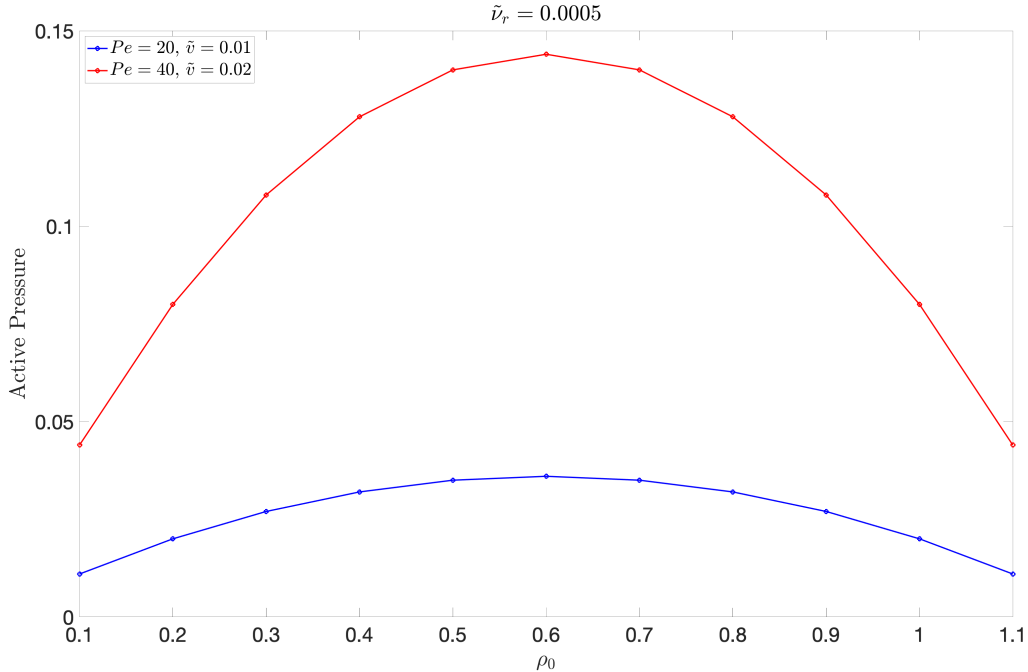


Figure 4.3: Active pressure at fixed $\tilde{\nu}_r = 0.0005$ for $v_0 = 0.01$ and $v_0 = 0.02$ corresponding to $Pe = 20$ and $Pe = 40$, respectively. Solid lines are guide for the eye.

4.3.2 Lennard-Jones Potential

Following [11], we fix $v_0 = 24$ and using the definition of Pe given by Eq. 4.1, we get $Dr = 1.8$ for $Pe = 40$. We calculate the active and passive contributions to pressure from simulations and add them to obtain the equation of state given by Eq. 4.28. Starting from our earlier statement about the slope of the active pressure, since we fixed self-propulsion, the active pressure in this case scales linearly with Pe . In other words, we can extrapolate the P_0^A curve for $Pe = 40$ from P_0^A curve for $Pe = 20$ by multiplying P_0^A curve for $Pe = 20$ by 2. By adding the passive and active pressure contributions to pressure, we obtain an equation of state given by $h_0(\rho_0)$, which develops an instability due to phase separation.

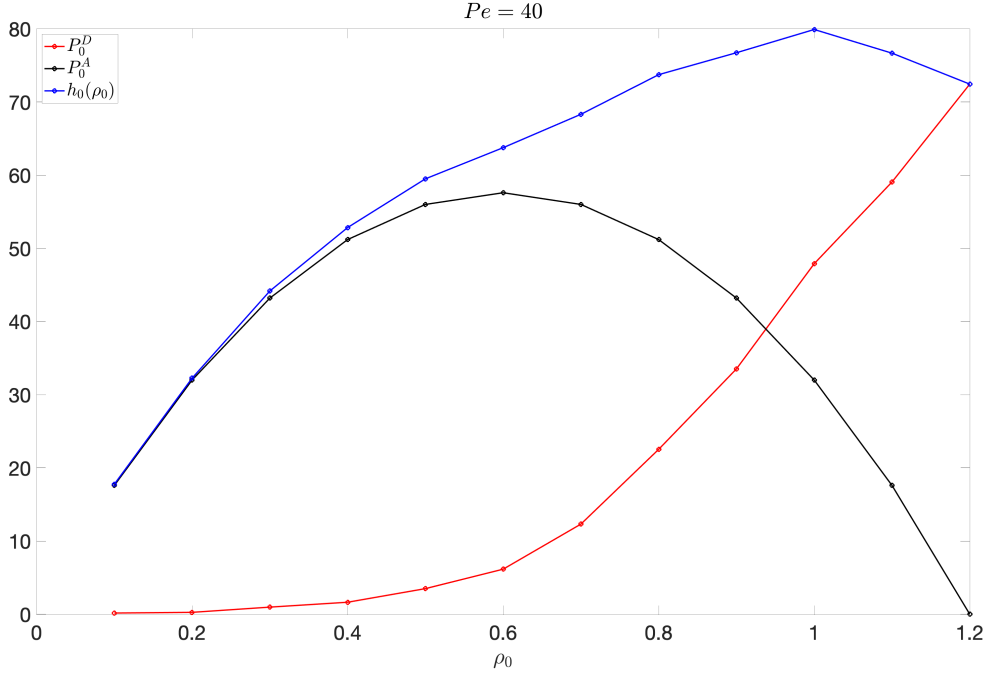


Figure 4.4: Construction of the equation of state. Active and passive pressure at a fixed $v_0 = 24$. Solid lines are guide for the eye.

4.3.3 Adding Attraction

Our attempts in characterizing the reentrant phase behavior of active particles using an equation of state were not successful. We initially started by calculating the direct pressure for particles interacting through attractive interactions by preparing our homogeneous system using repulsive positions, and then we only included attraction while calculating the direct pressure. However, the resulting direct pressure did not produce any non-monotonic behavior as we initially anticipated. Further attempts include trying to estimate the shape of the direct pressure using scaling arguments. In the previous subsection, we established that the direct pressure scales with self-propulsion in case of active particles with purely repulsive interactions. Given $P_0^D(\rho_0)$ for attractive active matter, in the case when strength of attraction is comparable to self-propulsion (as in the case of MIPS), $P_0^D(\rho_0) \propto v_0$ and this corresponds to the caging of particles in a cluster. However, when a particle is able to escape a cluster, the unstable part of $P_0^D(\rho_0)$ will not scale with v_0 . It will instead scale with \sim energy of attraction times ρ_0 . Thus, calculation of the direct pressure with attraction is not trivial.

Chapter 5

Conclusion

In order to study the collective behavior of living matter, we use active matter systems, made of self-driven units. Minimal model of active matter have been extensively studied analytically, numerically, and experimentally. Most of the numerical work found in the literature on active systems focus on purely repulsive interactions between active particles. Phase separation in the absence of attractive interactions is referred to as MIPS. The idea of MIPS is the following: self-propelled particles tend to accumulate where they move more slowly. This slow down creates a positive feedback which induced MIPS. The accumulation of active particles where they move more slowly lead to the formulation of density dependent propulsion speed: the speed of the active particles decreases as their local density increases. A step into adding complexity is including attractive interactions. We study two such models. One may intuitively think that including attraction in the potential will promote phase separation. However, phase separation may be suppressed depending on the activity level (self-propulsion). So self-propulsion can either enhance or suppress phase separation by either acting cooperatively or competing with inter-particle attractions. In this model, we vary the attraction strength and self-propulsion, simultaneously, in order to create a competition between the two parameters. In the second model, we fix the attraction strength to be much larger than self-propulsion. In this case, clustering is inevitable. We make use of this model to study the kinetics of cluster-cluster aggregation by predicting the time dependent growth exponent. Concerning the reentrant phase behavior, we had an unsuccessful attempt in characterizing this behavior by constructing a pressure equation of state.

Appendix A

Abbreviations

ABP	Active Brownian Particles
ATP	Adenosine Triphosphate
GNF	Giant Number Fluctuation
LB	Lattice Boltzmann
LJ	Lennard-Jones
MIPS	Motility Induced Phase Separation
MPCD	Multi-Particle Collision Dynamics
MSD	Mean Squared Displacement
ODE	Ordinary Differential Equation
WCA	Weeks-Chandler-Anderson

Bibliography

- [1] S. Ramaswamy and M. Rao, “Active-filament hydrodynamics: instabilities, boundary conditions and rheology,” *New Journal of Physics*, vol. 9, no. 11, p. 423, 2007.
- [2] C. Dombrowski, L. Cisneros, S. Chatkaew, R. E. Goldstein, and J. O. Kessler, “Self-concentration and large-scale coherence in bacterial dynamics,” *Physical review letters*, vol. 93, no. 9, p. 098103, 2004.
- [3] F. Ndlec, T. Surrey, A. C. Maggs, and S. Leibler, “Self-organization of microtubules and motors,” *Nature*, vol. 389, no. 6648, pp. 305–308, 1997.
- [4] E. Karsenti, F. Nédélec, and T. Surrey, “Modelling microtubule patterns,” *Nature cell biology*, vol. 8, no. 11, pp. 1204–1211, 2006.
- [5] V. Narayan, S. Ramaswamy, and N. Menon, “Long-lived giant number fluctuations in a swarming granular nematic,” *Science*, vol. 317, no. 5834, pp. 105–108, 2007.
- [6] I. D. Couzin, J. Krause, R. James, G. D. Ruxton, and N. R. Franks, “Collective memory and spatial sorting in animal groups,” *Journal of theoretical biology*, vol. 218, no. 1, pp. 1–12, 2002.
- [7] T. Vicsek, A. Czirók, E. Ben-Jacob, I. Cohen, and O. Shochet, “Novel type of phase transition in a system of self-driven particles,” *Physical review letters*, vol. 75, no. 6, p. 1226, 1995.
- [8] M. Ballerini, N. Cabibbo, R. Candelier, A. Cavagna, E. Cisbani, I. Giardina, V. Lecomte, A. Orlandi, G. Parisi, A. Procaccini, *et al.*, “Interaction ruling animal collective behavior depends on topological rather than metric distance: Evidence from a field study,” *Proceedings of the national academy of sciences*, vol. 105, no. 4, pp. 1232–1237, 2008.
- [9] C. Bechinger, R. Di Leonardo, H. Löwen, C. Reichhardt, G. Volpe, and G. Volpe, “Active particles in complex and crowded environments,” *Reviews of Modern Physics*, vol. 88, no. 4, p. 045006, 2016.
- [10] G. S. Redner, A. Baskaran, and M. F. Hagan, “Reentrant phase behavior in active colloids with attraction,” *Physical Review E*, vol. 88, no. 1, p. 012305, 2013.
- [11] A. P. Solon, J. Stenhammar, M. E. Cates, Y. Kafri, and J. Tailleur, “Generalized thermodynamics of motility-induced phase separation: phase equilibria, laplace pressure, and change of ensembles,” *New Journal of Physics*, vol. 20, no. 7, p. 075001, 2018.

- [12] A. Callegari and G. Volpe, “Numerical simulations of active brownian particles,” in *Flowing Matter*, pp. 211–238, Springer, 2019.
- [13] J. Blaschke, M. Maurer, K. Menon, A. Zöttl, and H. Stark, “Phase separation and coexistence of hydrodynamically interacting microswimmers,” *Soft matter*, vol. 12, no. 48, pp. 9821–9831, 2016.
- [14] J. de Graaf, H. Menke, A. J. Mathijssen, M. Fabritius, C. Holm, and T. N. Shendruk, “Lattice-boltzmann hydrodynamics of anisotropic active matter,” *The Journal of chemical physics*, vol. 144, no. 13, p. 134106, 2016.
- [15] R. M. Navarro and S. M. Fielding, “Clustering and phase behaviour of attractive active particles with hydrodynamics,” *Soft Matter*, vol. 11, no. 38, pp. 7525–7546, 2015.
- [16] B. Ten Hagen, R. Wittkowski, D. Takagi, F. Kümmel, C. Bechinger, and H. Löwen, “Can the self-propulsion of anisotropic microswimmers be described by using forces and torques?,” *Journal of Physics: Condensed Matter*, vol. 27, no. 19, p. 194110, 2015.
- [17] P. Langevin, “Sur la théorie du mouvement brownien,” *Compt. Rendus*, vol. 146, pp. 530–533, 1908.
- [18] E. Hauge and A. Martin-Löf, “Fluctuating hydrodynamics and brownian motion,” *Journal of Statistical Physics*, vol. 7, no. 3, pp. 259–281, 1973.
- [19] J. Elgeti, R. G. Winkler, and G. Gompper, “Physics of microswimmers—single particle motion and collective behavior: a review,” *Reports on progress in physics*, vol. 78, no. 5, p. 056601, 2015.
- [20] A. Czirók, E. Ben-Jacob, I. Cohen, and T. Vicsek, “Formation of complex bacterial colonies via self-generated vortices,” *Physical Review E*, vol. 54, no. 2, p. 1791, 1996.
- [21] X. Yang, M. L. Manning, and M. C. Marchetti, “Aggregation and segregation of confined active particles,” *Soft matter*, vol. 10, no. 34, pp. 6477–6484, 2014.
- [22] M. C. Marchetti, J.-F. Joanny, S. Ramaswamy, T. B. Liverpool, J. Prost, M. Rao, and R. A. Simha, “Hydrodynamics of soft active matter,” *Reviews of Modern Physics*, vol. 85, no. 3, p. 1143, 2013.
- [23] Y. Fily, S. Henkes, and M. C. Marchetti, “Freezing and phase separation of self-propelled disks,” *Soft matter*, vol. 10, no. 13, pp. 2132–2140, 2014.
- [24] Y. Fily and M. C. Marchetti, “Athermal phase separation of self-propelled particles with no alignment,” *Physical review letters*, vol. 108, no. 23, p. 235702, 2012.
- [25] A. P. Solon, J.-B. Caussin, D. Bartolo, H. Chaté, and J. Tailleur, “Pattern formation in flocking models: A hydrodynamic description,” *Physical Review E*, vol. 92, no. 6, p. 062111, 2015.
- [26] H. Chaté, F. Ginelli, G. Grégoire, F. Peruani, and F. Raynaud, “Modeling collective motion: variations on the vicsek model,” *The European Physical Journal B*, vol. 64, no. 3-4, pp. 451–456, 2008.

- [27] H. Chaté, F. Ginelli, G. Grégoire, and F. Raynaud, “Collective motion of self-propelled particles interacting without cohesion,” *Physical Review E*, vol. 77, no. 4, p. 046113, 2008.
- [28] A. Solon and J. Tailleur, “Revisiting the flocking transition using active spins,” *Physical review letters*, vol. 111, no. 7, p. 078101, 2013.
- [29] J.-B. Caussin, A. Solon, A. Peshkov, H. Chaté, T. Dauxois, J. Tailleur, V. Vitelli, and D. Bartolo, “Emergent spatial structures in flocking models: a dynamical system insight,” *Physical review letters*, vol. 112, no. 14, p. 148102, 2014.
- [30] J. Stenhammar, D. Marenduzzo, R. J. Allen, and M. E. Cates, “Phase behaviour of active brownian particles: the role of dimensionality,” *Soft matter*, vol. 10, no. 10, pp. 1489–1499, 2014.
- [31] M. E. Cates and J. Tailleur, “Motility-induced phase separation,” *Annu. Rev. Condens. Matter Phys.*, vol. 6, no. 1, pp. 219–244, 2015.
- [32] G. S. Redner, M. F. Hagan, and A. Baskaran, “Structure and dynamics of a phase-separating active colloidal fluid,” *Physical review letters*, vol. 110, no. 5, p. 055701, 2013.
- [33] J. Stenhammar, A. Tiribocchi, R. J. Allen, D. Marenduzzo, and M. E. Cates, “Continuum theory of phase separation kinetics for active brownian particles,” *Physical review letters*, vol. 111, no. 14, p. 145702, 2013.
- [34] R. Wittkowski, A. Tiribocchi, J. Stenhammar, R. J. Allen, D. Marenduzzo, and M. E. Cates, “Scalar φ 4 field theory for active-particle phase separation,” *Nature communications*, vol. 5, no. 1, pp. 1–9, 2014.
- [35] T. Speck, J. Bialké, A. M. Menzel, and H. Löwen, “Effective cahn-hilliard equation for the phase separation of active brownian particles,” *Physical Review Letters*, vol. 112, no. 21, p. 218304, 2014.
- [36] A. Suma, G. Gonnella, D. Marenduzzo, and E. Orlandini, “Motility-induced phase separation in an active dumbbell fluid,” *EPL (Europhysics Letters)*, vol. 108, no. 5, p. 56004, 2014.
- [37] S. Weitz, A. Deutsch, and F. Peruani, “Self-propelled rods exhibit a phase-separated state characterized by the presence of active stresses and the ejection of polar clusters,” *Physical Review E*, vol. 92, no. 1, p. 012322, 2015.
- [38] S. E. Ilse, C. Holm, and J. de Graaf, “Surface roughness stabilizes the clustering of self-propelled triangles,” *The Journal of chemical physics*, vol. 145, no. 13, p. 134904, 2016.
- [39] W. Greiner, L. Neise, and H. Stöcker, *Thermodynamics and statistical mechanics*. Springer Science & Business Media, 2012.
- [40] S. C. Takatori and J. F. Brady, “Towards a thermodynamics of active matter,” *Physical Review E*, vol. 91, no. 3, p. 032117, 2015.

- [41] U. M. B. Marconi and C. Maggi, “Towards a statistical mechanical theory of active fluids,” *Soft matter*, vol. 11, no. 45, pp. 8768–8781, 2015.
- [42] J. Bialké, J. T. Siebert, H. Löwen, and T. Speck, “Negative interfacial tension in phase-separated active brownian particles,” *Physical review letters*, vol. 115, no. 9, p. 098301, 2015.
- [43] T. Speck and R. L. Jack, “Ideal bulk pressure of active brownian particles,” *Physical Review E*, vol. 93, no. 6, p. 062605, 2016.
- [44] D. Loi, S. Mossa, and L. F. Cugliandolo, “Effective temperature of active matter,” *Physical Review E*, vol. 77, no. 5, p. 051111, 2008.
- [45] J. Palacci, C. Cottin-Bizonne, C. Ybert, and L. Bocquet, “Sedimentation and effective temperature of active colloidal suspensions,” *Physical Review Letters*, vol. 105, no. 8, p. 088304, 2010.
- [46] S. C. Takatori, W. Yan, and J. F. Brady, “Swim pressure: stress generation in active matter,” *Physical review letters*, vol. 113, no. 2, p. 028103, 2014.
- [47] A. P. Solon, J. Stenhammar, R. Wittkowski, M. Kardar, Y. Kafri, M. E. Cates, and J. Tailleur, “Pressure and phase equilibria in interacting active brownian spheres,” *Physical review letters*, vol. 114, no. 19, p. 198301, 2015.
- [48] J. Palacci, S. Sacanna, A. P. Steinberg, D. J. Pine, and P. M. Chaikin, “Living crystals of light-activated colloidal surfers,” *Science*, vol. 339, no. 6122, pp. 936–940, 2013.
- [49] D. Frenkel and B. Smit, *Understanding molecular simulation: from algorithms to applications*, vol. 1. Elsevier, 2001.
- [50] N. de Macedo Biniossek, H. Löwen, T. Voigtmann, and F. Smallenburg, “Static structure of active brownian hard disks,” *Journal of Physics: Condensed Matter*, vol. 30, no. 7, p. 074001, 2018.
- [51] F. Sciortino and P. Tartaglia, “Structure factor scaling during irreversible cluster-cluster aggregation,” *Physical review letters*, vol. 74, no. 2, p. 282, 1995.
- [52] P. M. Chaikin, T. C. Lubensky, and T. A. Witten, *Principles of condensed matter physics*, vol. 10. Cambridge university press Cambridge, 1995.
- [53] M. C. Marchetti, Y. Fily, S. Henkes, A. Patch, and D. Yllanes, “Minimal model of active colloids highlights the role of mechanical interactions in controlling the emergent behavior of active matter,” *Current Opinion in Colloid & Interface Science*, vol. 21, pp. 34–43, 2016.
- [54] J. Irving and J. G. Kirkwood, “The statistical mechanical theory of transport processes. iv. the equations of hydrodynamics,” *The Journal of chemical physics*, vol. 18, no. 6, pp. 817–829, 1950.
- [55] T. Nakamura, S. Kawamoto, and W. Shinoda, “Precise calculation of the local pressure tensor in cartesian and spherical coordinates in lammps,” *Computer Physics Communications*, vol. 190, pp. 120–128, 2015.